Electronic Thesis and Dissertation Repository

2-23-2018 2:00 PM

Augmented Reality Ultrasound Guidance in Anesthesiology

Golafsoun Ameri
The University of Western Ontario

Supervisor
Peters, Terry M.
The University of Western Ontario

Graduate Program in Biomedical Engineering
A thesis submitted in partial fulfillment of the requirements for the degree in Doctor of Philosophy
© Golafsoun Ameri 2018

Follow this and additional works at: https://ir.lib.uwo.ca/etd

🎯 Part of the Biomedical Commons, Biomedical Devices and Instrumentation Commons, and the Systems and Integrative Engineering Commons

Abstract

Real-time ultrasound has become a mainstay in many image-guided interventions and increasingly popular in several percutaneous procedures in anesthesiology. One of the main constraints of ultrasound-guided needle interventions is identifying and distinguishing the needle tip from needle shaft in the image. Augmented reality (AR) environments have been employed to address challenges surrounding surgical tool visualization, navigation, and positioning in many image-guided interventions. The motivation behind this work was to explore the feasibility and utility of such visualization techniques in anesthesiology to address some of the specific limitations of ultrasound-guided needle interventions. This thesis brings together the goals, guidelines, and best development practices of functional AR ultrasound image guidance (AR-UIG) systems, examines the general structure of such systems suitable for applications in anesthesiology, and provides a series of recommendations for their development. The main components of such systems, including ultrasound calibration and system interface design, as well as applications of AR-UIG systems for quantitative skill assessment, were also examined in this thesis.

The effects of ultrasound image reconstruction techniques, as well as phantom material and geometry on ultrasound calibration, were investigated. Ultrasound calibration error was reduced by 10% with synthetic transmit aperture imaging compared with B-mode ultrasound. Phantom properties were shown to have a significant effect on calibration error, which is a variable based on ultrasound beamforming techniques. This finding has the potential to alter how calibration phantoms are designed cognizant of the ultrasound imaging technique.

Performance of an AR-UIG guidance system tailored to central line insertions was evaluated in novice and expert user studies. While the system outperformed ultrasound-only guidance with novice users, it did not significantly affect the performance of experienced operators. Although the extensive experience of the users with ultrasound may have affected the results, certain aspects of the AR-UIG system contributed to the lackluster outcomes, which were analyzed via a thorough critique of the design decisions.

i

The application of an AR-UIG system in quantitative skill assessment was investigated, and the first quantitative analysis of needle tip localization error in ultrasound in a simulated central line procedure, performed by experienced operators, is presented. Most participants did not closely follow the needle tip in ultrasound, resulting in 42% unsuccessful needle placements and a 33% complication rate. Compared to successful trials, unsuccessful procedures featured a significantly greater (p=0.04) needle-tip to image-plane distance. Professional experience with ultrasound does not necessarily lead to expert level performance. Along with deliberate practice, quantitative skill assessment may reinforce clinical best practices in ultrasound-guided needle insertions.

Based on the development guidelines, an AR-UIG system was developed to address the challenges in ultrasound-guided epidural injections. For improved needle positioning, this system integrated A-mode ultrasound signal obtained from a transducer housed at the tip of the needle. Improved needle navigation was achieved via enhanced visualization of the needle in an AR environment, in which B-mode and A-mode ultrasound data were incorporated. The technical feasibility of the AR-UIG system was evaluated in a preliminary user study. The results suggested that the AR-UIG system has the potential to outperform ultrasound-only guidance.

Co-Authorship Statement

This thesis integrates several publications that are published, under review, or in preparation for submission. Details regarding the authors contributions to these manuscripts are provided below.

- Ameri, Golafsoun, John S. H. Baxter, Daniel Bainbridge, Terry M. Peters, and Elvis C. S. Chen. "Mixed reality ultrasound guidance system: a case study in system development and a cautionary tale." International Journal of Computer Assisted Radiology and Surgery (2017): 1-11.

  My contributions to this work included designing, implementing, performing the case study, as well as analyzing the data. Both J. S. H. Baxter and I contributed systemically to bringing together the goals, guidelines, and best development practices for augmented reality ultrasound guidance systems; providing a critique on the case study and a series of recommendations about the development of such systems; and drafting the manuscript. D. Bainbridge, the clinical collaborator, contributed to defining the clinical motivation for the study and recruiting participants. E. C. S. Chen contributed to the guidance system development used in the case study. The work was performed under the supervision of T. M. Peters and E. C. S. Chen. All authors helped in reviewing and editing the manuscript.

- Ameri, Golafsoun, John S. H. Baxter, A. Jonathan McLeod, Terry M. Peters, and Elvis C. S. Chen. "Effects of line fiducial parameters and beamforming on ultrasound calibration." Journal of Medical Imaging 4, no. 1 (2017): 015002-015002.

  My contributions to this work included designing and implementing the methods being evaluated; designing and performing the experiments; collecting and analyzing the data; and drafting the manuscript. J. S. H. Baxter and A. J. McLeod helped with data collection and data analysis. The work was performed under the supervision of T. M. Peters and E. C. S. Chen. All authors helped in reviewing and editing the manuscript.

- Ameri, Golafsoun, Daniel Bainbridge, Terry M. Peters, and Elvis C. S. Chen. "Quantitative analysis of needle navigation under ultrasound guidance in a simulated central line procedure." Ultrasound in medicine & biology (submitted)

  My contribution to this work included designing, implementing, performing the user study; designing and developing the phantom; analyzing the data and drafting the manuscript. D. Bainbridge, the clinical collaborator, contributed to defining the clinical motivation for the study and recruiting participants. E. C. S. Chen contributed to software development. The work was performed under the supervision of T. M. Peters and E. C. S. Chen. All authors contributed to formalizing the study design and evaluation metrics, as well as reviewing and editing the manuscript.

- Ameri, Golafsoun, Adam Rankin, John S.H. Baxter, Sugantha Ganapathy, Terry M. Peters, and Elvis C.S. Chen. "Development and evaluation of an augmented reality A-mode ultrasound guidance system for spinal anesthesia: preliminary results." (In preparation for submission to TBME)

  My contributions to this work included designing, developing, and implementing the methods being evaluated (including both hardware design and software development); designing and developing the phantom; designing, implementing, and performing an evaluation user study; collecting and analyzing the data; and drafting the manuscript. A. Rankin helped with software development. J. S. H. Baxter contributed to data analysis. S. Ganapathy, the clinical collaborator, contributed to defining the clinical motivation for the study. The work was performed under the supervision of T. M. Peters and E. C. S. Chen. All authors helped in reviewing and editing the manuscript.

Acknowledgments

My deepest gratitude goes to my supervisor and mentor, Dr. Terry Peters, for his guidance, deep insights, and continuous support throughout the course of this work. I am very grateful for all the incredible opportunities that he provided me with to explore my research interests and collaborate with industrial, academic, and clinical partners. I truly feel honoured to have had the opportunity to be part of his lab and to work with and learn from him, an experience that has incredibly enriched many aspects of my life.

I would like to thank Dr. Elvis Chen for his guidance, insights, and mentorship. I am truly grateful for his constructive feedback and assistance throughout this work. I would also like to thank Dr. James Lacefield, Dr. Purang Abolmaesumi, and Dr. Sugantha Ganapathy for their feedback and insights. Special thanks goes out to Dr. Daniel Bainbridge for sharing his clinical expertise and providing advice on multiple research projects. I would like to thank Dr. Tamie Poepping for giving me access to her lab equipment.

Special recognition goes out to Dr. Gerrard Guiraudon for his mentorship. I am very grateful for our long conversations about critical thinking, ethics, passion, and commitment, the impact of which extends well beyond my academic training.

I would like to extend my thanks to everyone in the VASST lab. It has truly been a privilege to work with and learn from such a talented, supportive, and collaborative team. I would like to express my sincere gratitude to John Moore for his expertise, honest feedback, and help with rapid prototyping and trouble-shooting many of the technical and practical problems that I faced during the course of this work.

I would like to extend my sincere gratitude to a multitude of colleagues and friends who have supported me in my research and life beyond research, especially, John Baxter, Ali Khan, Danny Gelman, Jon Lau, Adam Rankin, Jonathan McLeod, Uditha Jayarathne, and Wes Hodges.

Many thanks to my parents and sisters for their unconditional support and love.

Contents

List of Figures

List of Tables

List of Abbreviations

2D	Two-dimensional
3D	Three-dimensional
4D	Four-dimensional
ANOVA	Analysis of variance
AR	Augmented reality
AR-UIG	Augmented reality ultrasound image guidance
ASICP	Anisotropically scaled iterative closest point
CA	Carotid artery
CI	Confidence interval
CT	Computed tomography
CVC	Central venous cannulation
DoF	Degrees-of-freedom
FLE	Fiducial localization error
FRE	Fiducial registration error
FWHM	Full width at half maximum
HMD	Head-mounted display
ICP	Iterative closest point
IJV	Internal jugular vein
LF	Ligamentum flavum
LOR	Loss-of-resistance
MRI	Magnetic resonance imaging
NASA-TLX	NASA task load index
OR	Operating room
PCI	Peripheral component interconnect
PVA	Polyvinyl alcohol
PVA-C	Polyvinyl alcohol cryogel
QA	Quality assurance
REB	Research ethics board
RF	Radio frequency
SAI	Synthetic aperture imaging
SCM	Sternocleidomastoid muscle
STA	Synthetic transmit aperture
STD	Standard deviation
TRE	Target registration error

Chapter 1

Introduction

Anesthesiology encompasses a broad array of procedures for total patient care before, during, and after surgery and it is essential to the practice of modern medicine. In addition, outside the operating room, anesthesiologists monitor, sedate, and provide anesthesia for various procedures, including endoscopy, electroconvulsive therapy, and cardiac catheterization [148]. Some of the most common procedures performed by an anesthesiologist include cardiovascular and non-cardiovascular monitoring, anesthesia delivery and management, as well as chronic and perioperative pain management. A large number of these procedures involve percutaneous techniques, mainly for local anesthesia delivery or catheterization.

The general structure of needle interventions in anesthesiology includes targeting, needle navigation, positioning, and validation of the needle position. The goal of the targeting step is to localize the anatomy of interest, which is traditionally achieved using anatomical landmarks. Most recently, different types of medical imaging have been used to provide preoperative or intraoperative image guidance for target localization. Once the location of the target is identified, during the navigation step, the needle is advanced toward the target tissue. Finally, at the positioning step, the needle tip is placed inside the target anatomy. Depending on the procedure, the correct position of the needle may be validated using haptic feedback during needle positioning, return of fluid, or medical imaging. This thesis concerns two of the most common

and yet challenging needle interventions in anesthesiology, namely central line placement and epidural injections. An overview of these procedures is provided in the following sections.

1.1   Common Needle Interventions in Anesthesia

1.1.1   Central Line Placement

Background

Central venous catheterization is a fundamental component of patient care performed predominantly in intensive care units and operating rooms, with over five million procedures performed annually in the United States alone [133]. The most common technique for accessing the central venous system is through the internal jugular vein (IJV), known as the central line procedure [3].

Common indications for central line placement, especially in cancer and critically ill cardiac patients, include hemodynamic monitoring, haemodialysis, administration of drugs, fluid therapy, infusion of caustic drugs and total parenteral nutrition, aspiration of air emboli, insertion of transcutaneous pacing leads, and gaining venous access in patients with poor peripheral veins [29, 130, 148, 155, 164]. Contraindications include coagulopathy and the presence of tumors or clots that could be dislodged during cannulation [148]. In addition, the number of sites available for catheterization could be reduced due to the presence of other central catheters or pacemakers [148].

The preferred access site for central line placement is the right IJV as it allows for easy access and provides a straight course to the superior vena cava [3, 8]. The IJV is rather superficial, usually at a depth of 1 to 1.5 cm below the skin [52]. It is often located proximal to the carotid artery (CA) in the lateral and anterior direction (Figure 1.1) [52].

The most common technique for cannulating the IJV is the Seldinger technique [8], in which a needle is placed in the IJV, and a guidewire is advanced through it. The needle is
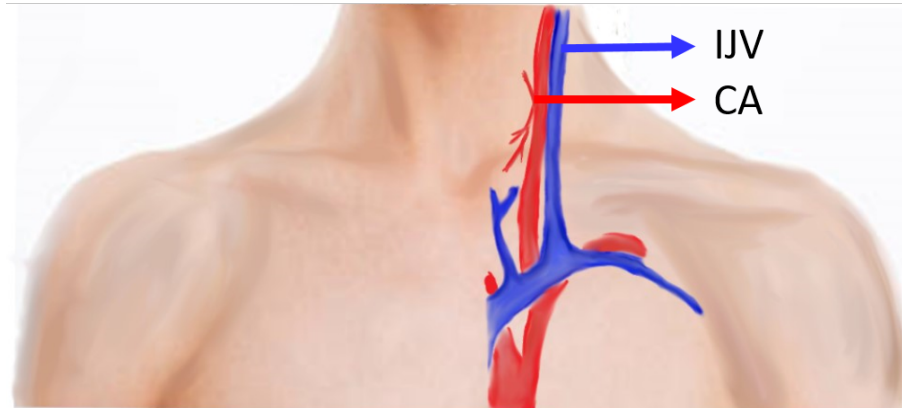
Figure 1.1: The internal jugular vein (IJV) is often positioned in intimate contact and laterally and anteriorly to the carotid artery (CA).

then removed, and a catheter inserted over the guidewire. To facilitate needle and catheter placement, several maneuvers are used to distend the IJV [130]. One technique is to position the patient with the head lower than the pelvis, i.e. the Trendelenburg position. In this position, the IJV is distended through the gravitational pooling of blood, creating a larger target for venipuncture [8]. Another technique is the Valsalva maneuver, in which the patient is asked to breathe with the glottis closed, resulting in increased blood pressure in the IJV and distension of the vein [52, 56]. The final position of the catheter is often validated with a post-procedural chest X-ray [8].

Challenges and Complications

The overall complication rate associated with central venous cannulations is as high as 15% [133]. Apart from infectious (5%-26%) and thrombotic (2%-26%) complications [103], mechanical complications, such as hematoma (0.1%-2.2%) and pneumothorax (0.1%-0.2%), could occur during IJV cannulations [133]. The reported failure rate to access the IJV ranges from 7% to 19.4% depending on the experience of the operator [52]. The most feared procedure-related complication is CA puncture, which can lead to catastrophic events including hematoma, hemorrhage, pseudoaneurysm, stroke, or death [21, 215, 148]. The rate of CA puncture during central line procedures ranges from 6.3-9.4% depending on the clinician's experience [133].
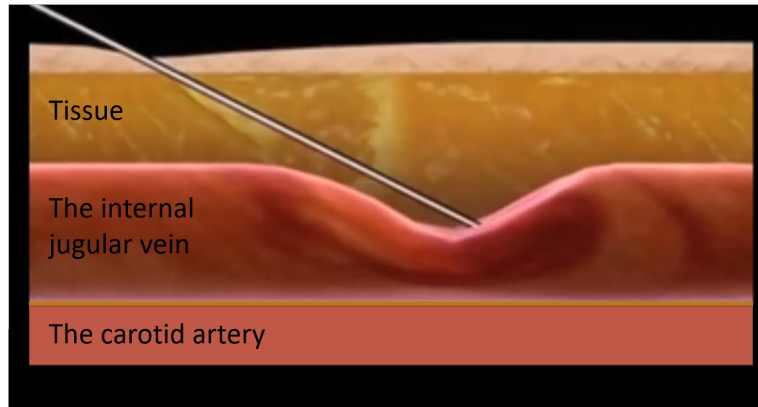
Figure 1.2: The IJV is highly compressible. As a result, the needle tip could press the anterior wall of the IJV down prior to puncturing the vein. This could result in inadvertent puncturing of the posterior wall of the IJV and the adjacent CA. Adapted from [82].

Inadvertent CA puncture can occur either directly or after the needle traverses the IJV [159]. Moreover, due to compressibility of the IJV, the needle sometimes does not immediately puncture the vein, but instead presses down upon the anterior vein wall, bringing the needle tip close to the posterior wall, Figure 1.2. This can result in traversing the posterior wall of the IJV and puncturing the CA.

1.1.2 Epidural Anesthesia

Background

Spinal anesthesia is one of the most important procedures in pain management. There has been a growing interest in research, education, and training to improve spinal anesthesia and analgesia as the annual cost of pain ($635 billion) in the United States was greater than that of heart disease, cancer, and diabetes [77]. In spinal anesthesia and pain management, epidural injections are the most commonly performed intervention for alleviating back and neck pain or for analgesic purposes in surgery and labour [182]. The growing interest in epidural injections resulted in a 130% increase in injections from 2000 to 2011, with over 8.9 million procedures performed in 2010 in the United States alone [60]. The total health care cost attributed to this
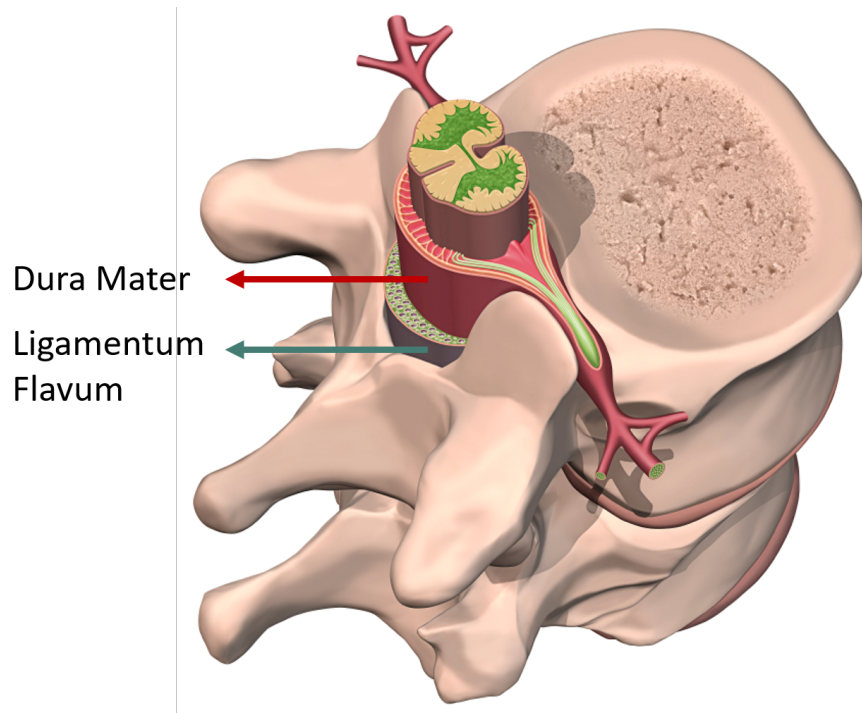
Figure 1.3: The epidural space is a potential space between the ligamentum flavum and dura mater within the spinal canal. Adapted from [1].

procedure in 2011 was \$23 billion, 231% more than in 2002 [6].

The main indications for epidural anesthesia are for surgical anesthesia, obstetric analgesia, post-operative pain control, and chronic pain management [148]. Epidurals can be used as a single-shot technique or with a catheter that allows intermittent or continuous drug administration. Epidural anesthesia may also be performed as an adjunct to general anesthesia [204]. Major contraindications to epidural anesthesia include patient refusal, coagulopathy, and sepsis [148, 204]. Other relative contraindications include elevated intracranial pressure, severe aortic or mitral stenosis, and severe left ventricular outflow obstruction [148].

An epidural block can be performed at the lumbar, thoracic, or cervical spinal level. The epidural space is a potential anatomic space between the ligamentum flavum (LF), a dense connective tissue covering the interlaminar spaces, and the dura mater, the outer most layer of the thecal sac surrounding the spinal cord, shown in Figure 1.3, [41]. Access into the vertebral canal and the epidural space can be achieved via the intervertebral foramina and the
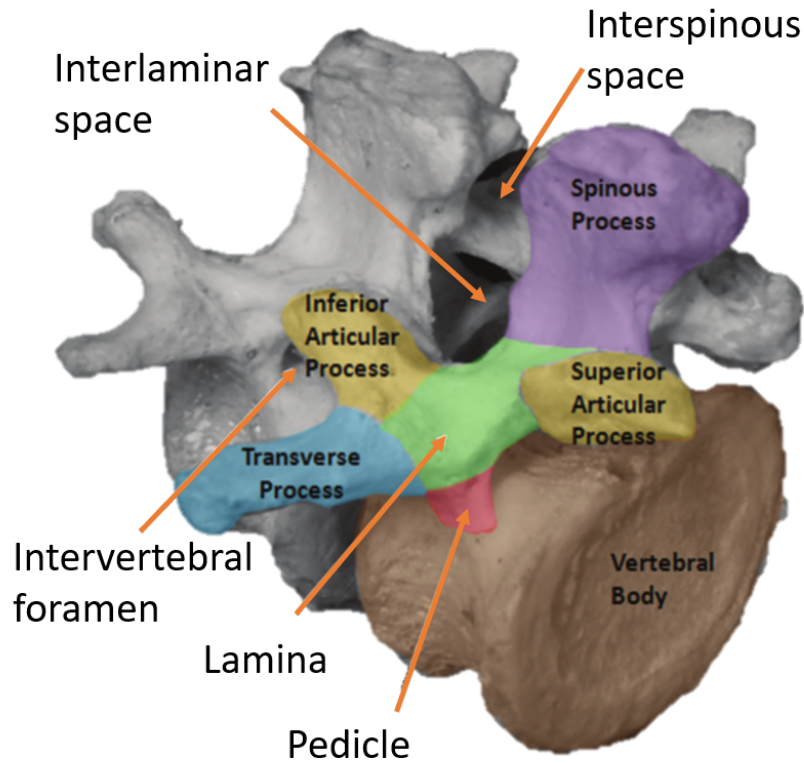
Figure 1.4: The posterior view of adjacent lumbar vertebrae. Adapted from [41].

interlaminar spaces (Figure 1.4). Epidural anesthesia and analgesia is most often performed in the lumbar region, and the epidural space is accessed via the interlaminar spaces. Because the spinal cord typically terminates at the L1 level, the common interlaminar spaces used for epidural anesthesia are the L3-L4 and L4-L5, providing an extra measure of safety in performing the block [148].

The catheterization technique used in epidural anesthesia is the "catheter through needle" technique [148]. Catheter placement allows for longitudinal drug delivery via the catheter. Once the epidural needle is placed inside the epidural space, a catheter is introduced through the needle and then the needle is removed.

Challenges and Complications

Although widely applied, epidural injection remains as one of the most challenging tasks an anesthesiologist performs, particularly if the spinal anatomy is altered or obscured by factors including obesity, spinal deformities such as scoliosis, or previous spine surgery [168].

The major complications accompanying interlaminar epidural injections are due to accidental dural puncture, with an incidence of 1-3% and 3-5% in the hands of experienced and novice operators, respectively [74]. Accidental dural punctures could lead to both temporary and irreversible permanent complications such as chronic headaches, epidural hematoma, or neurologic injury [168]. The frequency of post dural puncture headaches could be as high as 80%, with 28% exhibiting chronic headaches. While the incident rate of epidural hematoma and spinal cord injury is less than 1 in 100,000 cases, these are considered as the most catastrophic complications in epidural anesthesia [168].

An inaccurate assessment of the location of intervertebral spaces can also lead to unintended intracord injection resulting in spinal cord injury and permanent neurologic sequelae [168]. Challenges in placing the needle in the epidural space can result in multiple needle passes [51]. Multiple insertion attempts are an independent predictor of complications such as inadvertent dural puncture, vascular puncture, and epidural hematoma [41, 168].

Such complications, not only impose a significant risk and discomfort on the patient, but also introduce additional costs to the health care system as a result of extending the procedure time and requiring further medical procedures to alleviate the complications. The cost of epidural complications exceeds $1.5 billion annually in the United States alone. [1]

1.2   Needle Placement Without Image Guidance

Needle interventions in anesthesia are traditionally performed without any form of image guidance. In the absence of image guidance, anesthesiologists need to rely on their knowledge of

---

[1]http://rivannamedical.com/clinical-need/

anatomy and several haptic or visual cues for needle placement, depending on the procedure.

One of the most common methods for identifying the target and insertion site is the land-mark guidance technique. Anatomical landmarks can be identified visually or by palpation, and they may provide coarse-grained guidance for targeting and navigation. In many anesthe-siology procedures, needle navigation and positioning relies on the haptic feedback, providing relatively subtle, fine-grained, and continuous guidance. Multiple methods are used to validate the final needle position at the target site, depending on the intervention. For example, return of fluid, such as blood or cerebral spinal fluid, could be an indicator of the needle placement at the target. Such methods are also course grained and not continuous, i.e. they provide only a binary assessment on whether the needle tip is at the target or not. Despite their widespread application, landmark-based techniques cannot take into account all anatomical variations or abnormalities, which could result in misidentification of the target and needle position, leading to adverse outcomes [46].

An overview of non-imaging guidance techniques in central line placement and epidural injections is provided in the following sections.

1.2.1 Needle Placement Without Image Guidance in Central Line Proce-dures

One of the most challenging aspects of central line insertion lies in successful differentiation between the vein or pulmonary apex and the carotid artery [8]. Traditionally, the IJV is iden-tified using external anatomical landmarks and the needle is inserted blindly. The surface anatomical landmark used to identify the position of the IJV is a triangle formed by the sternal head of the sternocleidomastoid muscle (SCM), clavicular head of the SCM, and the clavicle, known as the Sedillot's triangle, as shown in Figure 1.5. The IJV is often posterior to the apex of the Sedillot's triangle. If the triangle is not accentuated, it is identified via palpation [8]. The carotid pulse is also identified by palpation to locate the CA. Once the IJV and CA are identi-fied, the needle is inserted at the apex of this triangle in a sagittal plane immediately lateral to
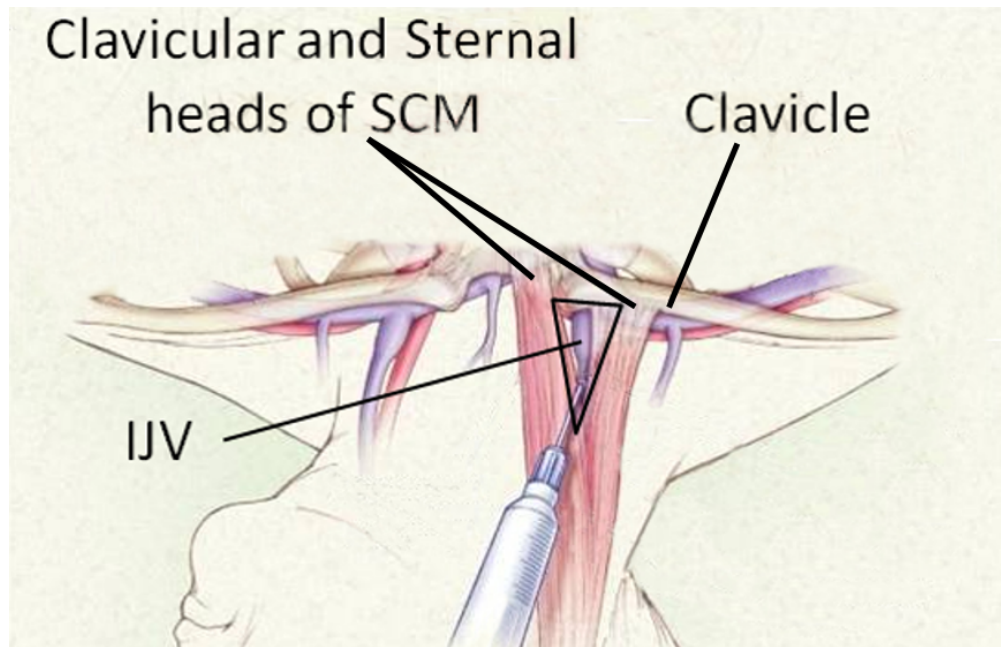
Figure 1.5: External landmarks used to identify the IJV. The needle is inserted at the apex of a triangle formed by the sternal head of the sternocleidomastoid muscle (SCM), clavicular head of the SCM, and the clavicle. Note that the operator usually stands by the head of the patient. Adapted from [133].

the carotid pulse, at an angle of 45° off a coronal plane [8]. Once the needle is placed in the IJV, aspiration of venous blood is used as a validation of the vein's location. Due to compliance of the IJV, perforation of the vein does not result in a sufficiently strong haptic feedback for validation. Anatomical variations and an aberrant anatomical position of the IJV make correct identification of the IJV and CA challenging even in the hands of experienced operators, leading to adverse outcomes [52]. Although the IJV is often positioned anterolaterally to the CA (71% of cases), it may be positioned directly anterior, lateral, and in rare cases, medial to the CA [8].

During needle navigation, the insertion depth of the needle is used to infer the relevant distance between the needle tip and the IJV. If the IJV is not accessed at a needle depth of 1-1.5 cm from the cutaneous surface, it is likely that the needle has pressed on the anterior wall of the IJV, collapsing the lumen and allowing transluminal passage of the needle through the IJV's posterior wall, [8]. This could result in CA puncture especially if the CA is positioned

directly posterior to the IJV, an anatomical aberration with an incidence of 26% [8].

1.2.2 Needle Placement Without Image Guidance in Epidural Injections

Traditionally, anatomical landmark guided techniques are used to identify both the target spinal level and the epidural space for epidural injections [46]. The spinal level and insertion site are often identified via palpation of the surface anatomical landmarks. One common palpation technique relies on first identifying the iliac crests and then counting up the vertebral levels. Other techniques include counting down from C7 or finding the vertebra that is attached to the twelfth rib [174]. However, the surface anatomical landmarks may be difficult to palpate, especially in patients with spinal disorders, obesity, or edema [46, 168]. Anatomical-based guidance frequently leads to incorrect identification of a given lumbar interspace, with an incidence of 70-71% [26, 46, 74]. The quality of anatomical landmarks are affected by age, abnormal spinal anatomy, and brevilineal biotype, which could contribute to multiple needle passes [51]. Another disadvantages of anatomical landmark guidance is that technical difficulties, such as an inadequate insertion angle, cannot be predicted in advance. An inadequate insertion angle could lead to vertebral contact, full needle retraction and redirection, and multiple attempts, resulting in pain and discomfort to the patient and an increased chance of failed epidural analgesia.

The most popular method for detecting the epidural space is the loss-of-resistance (LOR) technique [217]. LOR is considered a blind technique in which the interventionalist applies constant pressure to the plunger of the syringe, often filled with saline, as the needle is advanced through the body [217]. Once the needle passes through the LF into the epidural space, a loss of resistance to pressure is felt at the plunger of the syringe indicating that the needle tip is in the epidural space [148]. Despite the wide use of the LOR technique, the intensity of LOR varies among patients and sometimes is not felt at all, which can mislead both novice and experienced anesthesiologists. In addition, there is a steep learning curve associated with this technique, with a success rate of 80% after 90 attempts [166]. The LOR technique has been associated

with complications, including dural puncture or more significantly neurological deficits as a result of unintentional spinal cord trauma [217].

1.3 Needle Placement Under Ultrasound Image Guidance

Once considered exclusive to radiology and cardiology, applications of ultrasound imaging now extend over multiple disciplines [129]. With the introduction of transesophageal echocardiography, ultrasound entered anesthesiology in the 1980s as an intraoperative imaging modality for cardiac surgery [179]. With the improvement of its quality and accessibility, B-mode ultrasound imaging now plays an ever increasing role as a point-of-care modality in anesthesiology [129]. One of the emerging applications of ultrasound in anesthesiology is providing image guidance for several percutaneous procedures for vascular access and regional anesthesia [7, 41]. Ultrasound has revolutionized some of the procedures in regional anesthesia, such as peripheral nerve blockade [41] and has become increasingly popular for performing neuraxial blockade [148].

Ultrasound guidance is often used in tandem with traditional, non-imaging techniques and its addition offers several advantages, especially for targeting and navigation. Not only does ultrasound imaging enable direct visualization of the target prior to needle insertion, but it also provides continuous visual feedback during the procedure to localize the needle with respect to the target as it is advanced in tissue. Ultrasound guidance is particularly valuable for overcoming challenges faced in identifying the target anatomy in patients with poorly palpable landmarks [148, 179]. While ultrasound improves procedure outcomes, reduces procedure time, and increases patient safety in several procedures, ultrasound image interpretation remains a challenging and user-dependent task. Moreover, adopting ultrasound guidance requires additional skills, which complicate training, and hardware, which increases procedure cost.

Ultrasound guidance may be used preoperatively or intraoperatively. Preoperative ultrasound can facilitate localization of the target anatomy and identifying any anatomical aber-
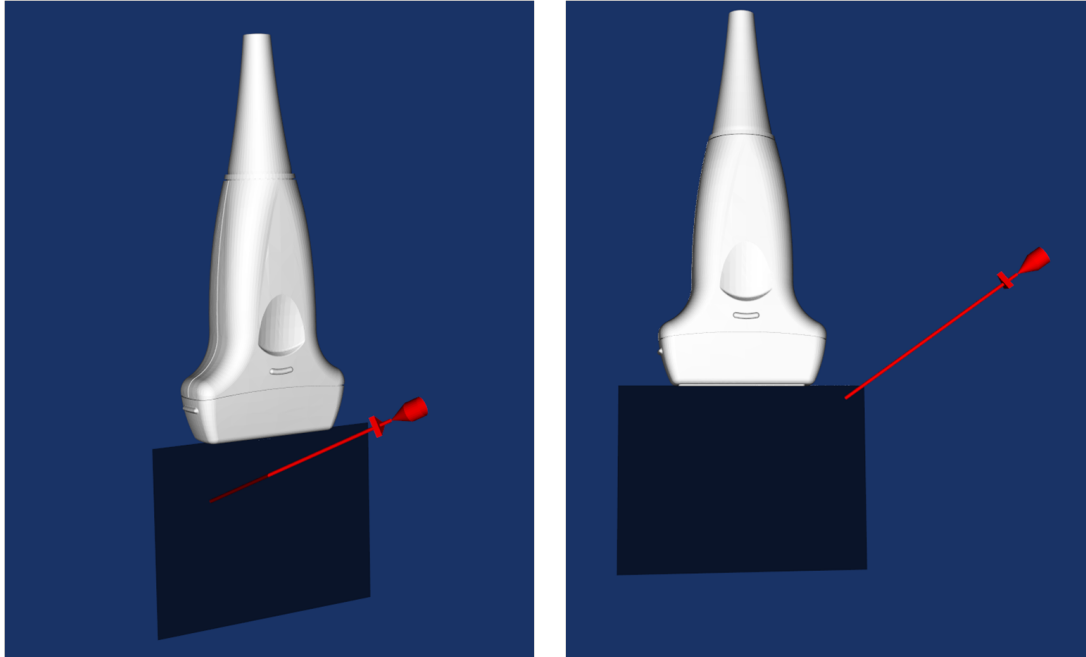
Figure 1.6: The out-of-plane (left) and in-plane (right) techniques are the most common methods used for visualizing the needle in ultrasound-guided procedures during needle insertion and navigation.

ration prior to needle insertion. Real-time ultrasound has also been used intraoperatively to provide image guidance during needle navigation and placement at the target [7, 41]. Depending on the needle intervention, two different real-time ultrasound guidance techniques are used for needle insertion and navigation, as shown in Figure 1.6. In the first technique, the needle is inserted through the image plane, along the short axis of the probe. This approach is known as the out-of-plane technique. In this visualization, the needle's cross section appears in the ultrasound image, as a bright spot. In this technique, the needle tip and shaft have the same visualization in ultrasound, and difficulties in distinguishing one from the other leads to uncertainties regarding the needle tip position and penetration depth. In the second approach, the needle is inserted within the ultrasound image plane along the long axis of the probe. This approach is known as the in-plane technique and allows full visualization of the needle tip and shaft in the ultrasound image. The main challenge in this technique is keeping the needle within the relatively thin image plane. Therefore, with a slight movement of the ultrasound

probe or the needle, the needle can get out of the image plane and not appear in the image. Visualization of the needle in the technique could also be challenging at steep insertion angles due to specular reflection.

Applications of B-mode ultrasound guidance for central line insertions and epidural injections are provided in the following sections.

1.3.1   Ultrasound Guidance in Central Line Procedures

The value of real-time ultrasound guidance over traditional landmark techniques for central venous cannulation (CVC) of the IJV is well established [29, 115, 133]. Real-time ultrasound guidance enables direct evaluation of the vein position and diameter, and also allows visualization of the needle tip as it is advanced through the tissue. As the IJV and CA are superficial structures, they are easily visible and identifiable in ultrasound. The pulsation of the CA and the dilation of the IJV in the Trendelenburg position can be visualized in ultrasound. Ultrasound guidance increases patient safety and improves procedure outcomes in IJV cannulations [186]. The Agency for Healthcare Quality and Research in the United States and the National Institute for Health and Care Excellence in the United Kingdom have endorsed real-time ultrasound guidance in central venous catheterizations as a key safety measure, improving procedure outcomes and increasing patient safety [53, 100, 115, 133, 186, 201, 206]. Ultrasound guidance reduces the rate of mechanical, infectious, and thrombotic complications in central line insertions by 57% [7]. The procedure failure rate is also reduced with ultrasound guidance by 86% [7]. This increased procedural success with ultrasound guidance decreases the expenses associated with the treatment of complications, which compensates for the cost of ultrasound equipment [7].

Despite the achieved successes with ultrasound, ultrasound-guided IJV cannulations are not infallible. Adverse events still occur, with an incidence of up to 20% [201] and this procedure remains a significant cause of morbidity and mortality [21, 124, 143]. Although some patients may be predisposed to complications, the physicians expertise level in using real-time ultra-

sound guidance is a major contributing factor to procedure outcomes [3]. The main factor that makes real-time ultrasound guidance challenging, even in the hands of experienced operators, pertains to the technique used for providing image guidance. The preferred ultrasound mode for the IJV cannulation is the transverse approach, where the cross-section of the IJV and CA are seen in the ultrasound image and the needle is inserted out-of-plane into the vein [186]. However, the needle tip and shaft both appear as bright spots in the ultrasound image, leading to difficulties in distinguishing one from the other. Uncertainty surrounding the exact location of the needle tip under real-time ultrasound is associated with inadvertent arterial, posterior IJV, and pleura punctures [20, 215, 218].

1.3.2 Ultrasound Guidance in Epidural Injections

While the feasibility of neuraxial ultrasound imaging was reported in the early 1980's [47, 48], it was not until the early 2000s that the role of ultrasound for performing neuraxial blockades, including epidural anesthesia, became widely established in the clinic [83, 84, 85].

Ultrasound was first used as only a preoperative guidance technique to identify the spinal level of interest and the entry angle, and the needle placement would still be performed blindly. Ultrasound imaging improves correct vertebral level identification compared to anatomical landmark. Furness *et al.* [74] showed that the spinal level was marked correctly in 70% of cases, compared to 30% with palpation. Pre-procedural ultrasound guidance technique significantly reduced the number of needle passes [83, 85, 208] and increased the first-pass success rate to 75%, compared to 20% with landmark guidance [84]. These improvements were observed in both patients with normal surface landmarks and those at risk of difficult insertion due to obesity, scoliosis, or previous spine surgery [168].

There has been an increasing interest in using ultrasound guidance, especially in challenging cases, for needle navigation and positioning in the epidural space to improve precision, accuracy, and safety of needle placement in epidural injections [24]. One of the challenges with real-time ultrasound guidance is that access to the epidural space is limited by narrow

interlaminar spaces, constraining the placement of the ultrasound transducer and the needle. Real-time ultrasound imaging of the epidural space is often achieved using the paramedian sagittal oblique technique. In this technique, the beam is first oriented in the sagittal plane of the spine lateral to the midline and then tilted and aimed toward the median sagittal plane, allowing the acoustic beam to reach the epidural space through the narrow interlaminar opening [41]. This orientation ensures that the incident ultrasound signal entered the spinal canal through the widest part of the interlaminar space [107]. Once the epidural space or the interlaminar opening is identified in the ultrasound image, the needle is then inserted in-plane, providing a visualization of the needle length in its entirety[107].

Needle placement in the epidural space remains challenging even under ultrasound guidance. Deep anatomical structures, such as the LF and dura, are not always identifiable in B-mode ultrasound images due to acoustic shadowing and attenuation, especially in obese patients. Needle visibility is also poor due to specular reflections, encountered at the steep insertion angles. In addition, the use of ultrasound for guidance in epidural injections has been limited by the cost of the equipment, the steep learning curve necessary to accurately interpret images and maintain needle visibility within the image plane, and the displaced sense of hand-eye coordination [32, 41]. As a result of these challenges, real-time ultrasound guidance has not been widely adopted for everyday practice in the performance of epidural injections [24, 41]. Real-time ultrasound image guidance in neuraxial blockade remains experimental at this time and the anatomical landmark guidance techniques remain the gold-standard for epidural injections [168].

1.4   New Trends in Image-Guided Needle Interventions

A variety of technologies have been developed to address the challenges in targeting, navigation, and positioning in image-guided surgery and therapy. Several of these technologies have been employed, resulting in improvements in percutaneous procedures in anesthesiology. In

this section, an overview of some of the promising state-of-the art technologies in ultrasound-guided needle interventions is provided.

1.4.1   3D/4D Ultrasound

Currently, ultrasound guidance for needle interventions in anesthesiology is provided using 2D B-mode ultrasound. Most recently, applications of 3D/4D ultrasound imaging for needle guidance in anesthesiology procedures have been explored in an effort to address challenges in keeping the needle tip in the image plane [187].

Using conventional 2D probes, 3D ultrasound images can be reconstructed from a 3D dataset obtained from scanning the probe, either mechanically or freehand. 3D ultrasound can be rendered as a volume or visualized as 2D images in multiple planes, i.e. multiplanar. Multiple retrospective studies investigated the application of 3D ultrasound for evaluation of the anatomy of the nerve [106], observing the spread of the anesthetic agent after injection in sciatic and median nerve blockade [131, 144], and to evaluate the position of nerve block catheters [42]. In a case study using a mechanically steered ultrasound probe, a radial nerve block was performed successfully with multiplanar 3D ultrasound [70]. One of the downsides of mechanically steered probes is that they are bulky and limit maneuverability.

Real-time 3D imaging is referred to as 4D ultrasound and requires specialized ultrasound probes known as matrix array probes. These probes are smaller than mechanically steered probes and use electronic beam steering, which allows faster frame rates and achieving 4D ultrasound imaging. Bi-plane ultrasound is a common mode of visualization using matrix probes. In this visualization mode, ultrasound images along the short and long axis of the probe are shown side-by-side. Applications of bi-plane ultrasound imaging for cannulating the IJV have been investigated, showing promising results [72]. In a case study, the short-axis view was used to identify the CA and IJV. The needle was inserted in-plane in the long axis view, and its cross-section was shown simultaneously in the short axis view. The first study of 4D ultrasound in anesthesiology was for peripheral nerve block performance [64] followed

by a feasibility study for epidural catheter insertion [14]. An advantage of using the matrix probe, as reported in these studies, was the ability to manipulate the image and visualization planes without the need for repositioning the probe. However, compared to conventional 2D ultrasound, the in-plane visibility of the needle was inferior with 4D ultrasound.

Despite the advances in the hardware and image reconstruction techniques, 3D/4D ultrasound imaging suffers from lower resolution and frame rate compared to 2D ultrasound, and thus limited its use in needle interventions [14, 72, 78]. Additional limitation is due to increased difficulties in the interpretation of 3D ultrasound images [78]. While 3D/4D ultrasound imaging provides simultaneous visualization of multiple views, assessment of its value for needle guidance requires further investigation [78].

1.4.2 Incorporating Preoperative Images

Incorporation of medical images from multiple imaging modalities can provide diagnostic information to an extent beyond the sum of the individual modalities [214]. In the context of ultrasound-guided interventions in anesthesiology, depending on the anatomy of interest, ultrasound may not provide sufficient information about the target anatomy. For example, in epidural injections, acoustic shadowing prevents visualization of the anatomical structures underneath the bone. To overcome such limitations, medical images from other modalities that do not suffer from the same limitations, such as computed tomography (CT) or magnetic resonance imaging (MRI), can be incorporated in the guidance system [152]. Correct alignment of these preoperative images with intraoperative ultrasound images enhances anatomical information in ultrasound that would not be visible otherwise. Registration of ultrasound to preoperative CT images for several percutaneous procedures have been explored extensively [79, 120, 214, 219]. Several commercial systems have also incorporated preoperative CT or MRI into their ultrasound guidance systems, including Ultraguide (Haifa, Israel), Biosound Esaote (Genoa, Italy), and Hitachi Medical (Tokyo, Japan). However, preoperative images may not be acquired for reasons of cost, access, patient contraindications, or exposure to radiation. To circumvent this

challenge, the application of statistical shape models has been investigated as a surrogate for preoperative imaging. For example, statistical shape models of the spine derived from a population of CT scans have been developed and registered to ultrasound images in patients outside of that population [27, 109]. This technique enhances ultrasound image interpretation of the vertebra. However, it has not been shown to improve epidural space localization in ultrasound and may not perform adequately in patients with severe pathology, which may not be properly represented in the statistical shape model's population. The value of this technique in a clinical setting remains to be evaluated.

1.4.3   Augmented Reality Ultrasound Guidance Systems

One of the emerging technologies in image-guided interventions is *augmented reality* (AR), which allows the integration of supplemental information with the real-world environment [125]. AR is best described as part of the general concept of reality-virtuality continuum as defined by Milgram [142]. One end of this continuum includes environments consisting solely of real objects, and the opposite end defines environments consisting solely of virtual objects (Figure 1.7) [142]. Moving from the real environment towards the virtual environment on this continuum, AR encompasses environments where the emphasis is on the real environment while providing local virtuality [142]. Augmented virtuality, on the other hand, defines scenes that are dominated by a virtual environment, in which real elements appear as add-ons [142]. The spectrum ranging from AR to augmented virtuality is known as mixed reality [142].

In image-guided interventions, AR is a visualization paradigm that enhances images with virtual, computer-generated graphics [169]. This visualization aims to to address some of the shortcomings of traditional image guidance techniques and alleviate clinical challenges arising from incomplete visualization of the entire surgical field during minimally invasive procedures [125]. AR guidance systems aim to complement the surgeon's conventional visualization by displaying information from multiple sources in one common frame of reference [170]. Examples of additional information that is often used to augment the real surgical scene includes
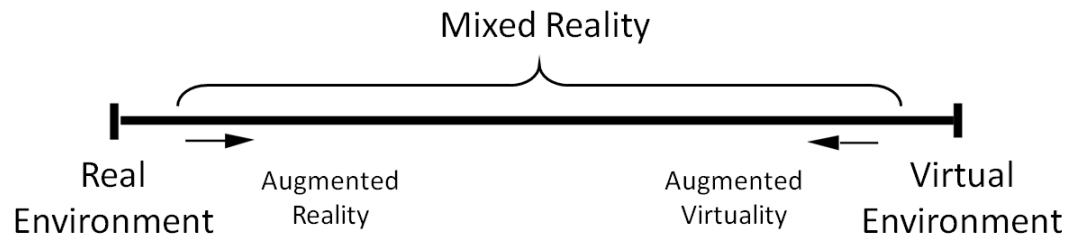
Figure 1.7: A representation of the reality-virtuality continuum. Adapted from [142].

spatial tracking of surgical tools, preoperative and intraoperative images, and virtual models of anatomical structures. In the context of AR guidance systems, real-time images or videos of the surgical scene may constitute the real part of the AR environment. However, the fuzzy boundaries between different mixed reality environments on the reality-virtuality continuum have led to the use of different terminology by the users of such tools. In this thesis, the term AR is used to refer to such a broad family of guidance systems in order to serve two main goals: (1) being accessible to a wide audience and (2) capturing the broad spectrum of AR guidance systems.

Applications of AR in image-guided surgery were first investigated for neurosurgery in 1985 to display preoperative CT images into an operating microscope [175]. However, it was not until 1995 that the first augmented stereo microscope was developed offering enhanced depth perception [58]. Since then, many AR guidance systems have been developed to augment intraoperative images and videos with additional information for a number of surgical applications including neurosurgery, laparoscopy, otolaryngology, and orthopedics [80, 108, 184]. AR environments have also been integrated in several ultrasound-guided procedures, such as needle biopsies, for providing enhanced visualization of the surgical scene and the needle [73, 177, 184].

The main components of AR guidance systems include tracking technology, ultrasound calibration, and a display, as described below.

Tracking technologies:

The AR guidance systems are made possible with the integration of tracking technology to localize and track surgical tools, intraoperative images, and the patient. The most common tracking technologies in image-guided interventions are optical and magnetic. The choice of one technology over another depends on the application and the environment in which it is used. Optical tracking provides a larger working area and higher accuracy compared to magnetic tracking. However, it requires a clear line-of-sight between the tracking device and the instrument to be tracked. Magnetic tracking, on the other hand, does not require a clear line-of-sight and can be more easily integrated into different surgical procedures. Magnetic sensors can be placed close to the tip of surgical instruments to provide higher tracking accuracy even when inserted in the body. A major drawback of magnetic tracking is that its accuracy can potentially be compromised by the presence of conductive and ferromagnetic materials [169].

Ultrasound calibration:

In the case of ultrasound-guided procedures, a fundamental criterion for the integration of ultrasound images in AR environments is ultrasound calibration, the process whereby image locations from a tracked ultrasound probe are related to the pose information of the probe's tracking sensor. More specifically, ultrasound calibration is the process of calculating the transformation (rotation, translation, and scaling) between the image plane and the origin of the tracking sensor mounted on the ultrasound probe. Accuracy of ultrasound calibration fundamentally affects the total accuracy of the interventional guidance system [92].

Display technologies:

Advances in display technologies have enabled integration of virtual and real environments in different ways. The broad categories of display techniques include external monitors, head-mounted displays (HMDs), semitransparent screens, and direct image projections on the patient [86]. In AR ultrasound guidance (AR-UIG) systems, ultrasound images are commonly augmented with computer-generated objects displayed directly on the scanner's monitor. In optical see-through HMDs, the ultrasound image, as well as virtual objects, can be overlaid directly onto the users view of the real world. In video see-through HMDs, a video feed of

the real environments is augmented. However, the real-world environment could be replaced with real-time medical images, such as ultrasound imaging. This mode of visualization is often referred to as virtual reality as opposed to augmented reality. Virtual objects can also be displayed on semitransparent screens, known as augmented windows, which can be placed directly over the surgical site allowing visualization of the real environment underneath. Most recently, direct projection of virtual objects onto the patient has been explored in neurosurgery using a standard projector [15].

AR Guidance Systems for Needle Interventions

Several AR guidance systems have been developed to address the challenges with needle tip visualization in ultrasound-guided needle interventions, as described below.

Sonic flashlight:

This guidance system, enables *in-situ* visualization of ultrasound images to overcome challenges with hand-eye coordination during ultrasound-guided procedures [193]. This technique combines a flat-panel monitor with a half-silvered mirror, positioned in such a way that ultrasound images on the monitor are reflected onto the see-through mirror. The ultrasound image, therefore, appears superimposed onto the patient. The superimposed ultrasound images are calibrated to represent the actual size of the anatomy being imaged. This visualization technique can be applied using B-mode ultrasound or tomographic ultrasound images obtained from matrix probes [192, 193]. A comparison of this technique against conventional ultrasound guidance for performing vascular access in a phantom study showed improved procedure time with the Sonic Flashlight system [31]. After a promising feasibility study on a cadaver [31], the Sonic Flashlight was compared against conventional ultrasound for providing image guidance for venous access in a small clinical study. No significant difference was found between the systems in terms of number of attempts and success rate of the first attempt [212]. The main advantage of this technique is that the virtual image is fixed in space, independent of the observer's viewpoint [43]. One of the limitations of this visualization is that the superimposed

ultrasound images must be scaled to have the same size as the anatomy of interest, in order to be superimposed correctly. As a result, the size of the superimposed image may be smaller than the conventional ultrasound image shown on the scanner, which may lead to ambiguity in image interpretation [212]. Nevertheless, such *in-situ* visualization of ultrasound images improves accuracy of perceived target depth and perceptually directed action [192].

SonixGPS (BK Ultrasound, Analogic, MA, USA):

SonixGPS is a navigation platform that integrates magnetic tracking and real-time ultrasound imaging for ultrasound-guided needle interventions [154]. This guidance system uses proprietary needles which are designed to house a reusable tracking sensor. The sensor element is contained within a disposable needle stylet that can be inserted in the introducer needle. The ultrasound probe is also tracked magnetically. A transmitter/receiver unit placed close to the intervention site tracks the position of the needle and ultrasound probe sensors. Virtual models displaying both current and predicted needle tip positions are overlaid on the 2D ultrasound image [154]. Application of the SonixGPS has been investigated in a few preliminary studies for performing simulated nerve blocks, vascular punctures, and spinal punctures [136, 183, 185]. Kopac *et al.* [114] evaluated the performance of the SonixGPS navigation system against ultrasound-only guidance in a phantom study simulating a vascular access procedure. No significant difference was observed between the two systems in terms of procedure time and number of attempts. The performance of 2D ultrasound, bi-plane ultrasound, and SonixGPS for needle placement in the epidural space was recently evaluated in a phantom study [138]. The SonixGPS system outperformed other modalities in terms of operator comfort, number of attempts, needle redirections, and bone contacts [138]. However, there were no significant differences between SonixGPS and the other two modalities in terms of needle tip and shaft visibility and procedure time [138]. The application of SonixGPS in spinal anesthesia was investigated in a few case reports [25, 220]. Although real-time guidance with the SonixGPS system was feasible, complications still occurred [25]. The SonixGPS is more effective in the out-of-plane approach compared to the in-plane technique. While clinical evidence

demonstrating patient benefits with SonixGPS is rare, the greatest potential for this navigation system may lie in education and training [187].

Clear Guide One (Clear Guide Medical, MD, USA):

Clear Guide One is a commercial system that uses a stereo camera for needle pose estimation for ultrasound-guided needle navigation. The stereo camera is mounted on the ultrasound probe and is used to track a needle with a tracking pattern marked onto its shaft, with an overall accuracy of 3.3 ± 2.3 mm [194]. To localize the needle tip, first the visible part of the needle is detected in the stereo images and the insertion depth calculated based on the detectable portion of the tracking pattern. The position of the needle tip is then calculated knowing the geometrical relationship between the sub-pattern and the needle tip. The location of the needle tip and its predicted path are overlaid on the ultrasound image using virtual, computer-generated graphics. This system has received clearance for clinical use in the United States, Canada, and Europe. However, clinical trials investigating any effect on procedure outcomes with this system have not been performed. One of the main disadvantages of this needle tracking system is that it does not account for needle deflection in tissue as the needle tip position estimation relies on a rigid model of the needle. The accuracy of needle tip detection is limited at larger depths. Moreover, the addition of a bulky stereo camera on an ultrasound probe is not ergonomically ideal considering the effects of ultrasound probe handle balance on work-related injuries, such as musculoskeletal disorders [163].

eZGuide (eZono, AG, Germany):

eZGuide is a passive magnetic tracking system developed for needle guidance. An array of magnetic sensors, which can detect nearby magnetic fields, is integrated in the ultrasound probe used for this guidance system. This system can track magnetized needles in the vicinity of the ultrasound transducer without using an active magnetic field generator [137]. The tracking information is used to display the position of the needle with respect to the surface of the ultrasound probe, next to the ultrasound image on the screen. A virtual representation of the needle trajectory and calculated needle tip intersection with the image plane are overlaid on the

ultrasound image. In a preliminary study, needle placement in a phantom was improved with the eZono guidance system, compared with ultrasound-only guidance, in terms of time and the success rate of the first attempt [137]. This improvement was observed only in the out-of-plane approach and not the in-plane technique [137]. While this technology eliminates the need for an external magnetic field generator, it requires specially designed ultrasound transducers. The needle also demagnetizes over time, which may affect its detectability by the tracking system. In terms of visualization, one of the main concerns with this technology is that the needle path is overlaid on the 2D ultrasound image even in the out-of-plane approach, in which the needle goes through the image plane. This visualization could result in ambiguity, which may mislead the interventionalist. In addition, the accuracy of needle localization at larger depths may be limited by the lower strength and wider spread of the magnetic field from the magnetization of the needle when placed at farther distances from the sensors in the probe [95].

Similar guidance systems that use a magnetized needle and specialized ultrasound probe have been developed by Axotrack (Soma Access Systems, SC, USA) [65] and General Electric (WI, USA) [101]. The Axotrack is cleared for human use in the United States by the Food and Drug Administration. In both systems, the predicted needle trajectory is displayed on the ultrasound image to facilitate needle tip positioning. While these guidance systems have shown promising results in preliminary studies, they require the use of specialized probes. Large clinical studies are needed to determine the value of this technology.

Overall, AR guidance systems aim to provide clinicians with an intuitive visualization of the surgical scene and complement their conventional visualization with computer graphics generated based on multiple sources of information. One of the main motivations behind using AR environments for image guidance is their ability to overcome difficulties related to hand-eye coordination [119]. Despite the benefits of visualizing multiple datasets simultaneously, it may lead to the display of extraneous information adding to the cognitive load of the interventionalist, causing distraction and inattentional blindness [86]. Other significant challenges to AR guidance systems include registration error, impaired depth perception, and additional

hardware and cost [86, 169]. Despite the encouraging results with some of the developed AR guidance systems, they have not been integrated in anesthesiology applications due to these challenges.

1.5 Thesis Outline

This thesis investigates the general research question of how to develop functional AR guidance systems for applications in central line and epidural injections. This question is addressed both as a whole, drawing conclusions from the literature, and also more specifically, taking into account different components of a functional AR system, from ultrasound calibration to the AR environment design considerations. A short summary of each chapter is provided as follows.

1.5.1 Goals and Guidelines of Augmented Reality Guidance Systems

The growing popularity and maturity of augmented reality has led to a series of informal guidelines to facilitate development of new systems. However, the goals of augmented reality image guidance systems and the guidelines for their development have not been thoroughly discussed. The purpose of this chapter is to identify the goals, guidelines, and best development practices in the context of AR ultrasound guidance systems.

1.5.2 Effects of Line Fiducial Parameters and Beamforming on Ultrasound Calibration

In this chapter, the effects of ultrasound image reconstruction technique, as well as phantom material and geometry, on ultrasound calibration were investigated. In terms of ultrasound image reconstruction, application of synthetic aperture imaging in ultrasound calibration was investigated. Synthetic aperture imaging is an image reconstruction technique that provides dynamic focusing, resulting in high resolution throughout the entire image. It was shown that

the calibration error was reduced by 10% with synthetic aperture imaging compared to conventional B-mode ultrasound. In addition, an evaluation of a variety of calibration phantoms with different geometrical and material properties was performed, these properties being shown to have a significant effect on calibration error, which is variable based on ultrasound beamforming techniques.

1.5.3 Augmented Reality Ultrasound Guidance System for Central Line Insertions

The overall objective of this chapter was twofold: to evaluate and critically examine an AR-UIG system tailored to central line procedures, which was developed following the guidelines described in this thesis, and to investigate the application of an AR environment for post-procedural performance analysis for central line insertions.

Compared to conventional ultrasound guidance, in a phantom study with novice operators, the AR system significantly reduced the intervention time and normalized needle path length suggesting that the use of such a system may make the procedure easier for the interventionalist (N = 36, $p \leq 0.05$). However, a similar study did not show a significant difference on the performance of expert operators using the AR-UIG system or ultrasound-only guidance. Specific design decisions made for the development of the AR system were critically examined to highlight the limitations of the system and direct further improvement of the AR system. In addition, applications of tracking technologies and AR environments for post-procedural skill assessment was investigated as a secondary objective of the expert user study.

1.5.4 Augmented Reality Ultrasound Guidance System for Epidural Injections

The purpose of this chapter was to design, develop, and evaluate an AR-UIG system tailored to epidural injections. As mentioned earlier, poor needle visibility in ultrasound, difficulties in

localizing the LF and dura with respect to the needle tip in ultrasound due to attenuation and bone shadowing limit the application of B-mode ultrasound guidance in the epidural space. To better identify the epidural space, a single-element ultrasound transducer was housed at the tip of a hypodermic tube, which could be inserted inside an introducer needle. The A-mode signal can be used to identify tissue layers, such as the LF and dura, as the needle tip is advanced towards them. This chapter explores the integration of A-mode and B-mode ultrasound in an AR environment for epidural injections. The technical feasibility and utility of the AR-UIG was evaluated in a preliminary novice user study.

1.5.5   Conclusions

This chapter summarizes the contributions of this thesis along with a discussion on the interplay between AR guidance systems and advanced training systems regarding their common considerations, constraints, and effects on quality assurance for training and clinical performance. The future direction of the particular research projects discussed in this thesis as well as the field as a whole are also discussed in this chapter.

Chapter 2

Goals, Guidelines, and Best Practices: Augmented Reality Ultrasound Guidance Systems

This chapter is adapted from the following manuscript:

- Ameri, Golafsoun, John S. H. Baxter, Daniel Bainbridge, Terry M. Peters, and Elvis C. S. Chen. "Mixed reality ultrasound guidance system: a case study in system development and a cautionary tale." *International Journal of Computer Assisted Radiology and Surgery* (2017): 1-11.

2.1   Introduction

Ultrasound imaging, due to its portability, low-cost, and accessibility, has received a high degree of interest as an intraoperative modality in image-guided interventions. These advantages make ultrasound a key component of point-of-care imaging in a variety of applications such as central and peripheral vascular access, thoracentesis, paracentesis, arthrocentesis, regional anesthesia, incision and drainage of abscesses, localization and removal of foreign bodies, lum-

bar puncture, biopsies, and other procedures [146]. In addition, ultrasound is employed in a number of surgical applications, such as neurosurgery [30, 207] and cardiac surgery [94, 162], to provide image guidance.

However, ultrasound has a distinct disadvantage in terms of interpretability, requiring advanced education and training for different procedures. To address this difficulty and the visualization challenges due to the limited field of view of the interventional scene, many state-of-the-art systems in ultrasound-guided interventions have implemented some form of augmented reality (AR) environment by placing the ultrasound image in a more complete surgical context. The term AR has been used both formally and informally to encompass a broad spectrum of mixed reality on the reality-virtuality continuum [142, 209]. In these contexts, ultrasound images may constitute the real part of the AR scene, where additional information can be added in order to complement the clinicians conventional field of view [223]. This information may contain the location of surgical instruments, critical anatomy, other imaging modalities, both pre-operative and intra-operative [170, 184].

The versatility of the AR paradigm has allowed for its integration into a variety of ultrasound-guided interventions. For example, in neurosurgical navigation, several AR ultrasound image guidance (AR-UIG) systems, such as the SonoWand Invite system (Trondheim, Norway) [96, 189], are already available on the market as clinically approved devices. In cardiac electrophysiology, CARTO (Biosense Webster Ltd, Israel) is a navigation system used for the treatment of patients with cardiac arrhythmia in which intra-cardiac ultrasound images, information from multiple sensors, and the position of the RF ablation catheter are integrated with a virtual environment [111, 172]. In addition, several AR-UIG systems have been proposed for other cardiac interventions, such as mitral [59, 127, 147] and aortic valve repair [49]. The use of AR-UIG systems in tandem with robotic and mechatronic assistance have been used in cancer diagnosis through ultrasound-guided biopsy [9, 10] and in cancer therapy through targeted brachytherapy [213].

Despite many successes with the integration of AR environments in many image-guided

procedures and the extensive work in this area, there is a lack of clear goals, guidelines, and best practices for the development of such systems. However, other communities that use similar tools, such as software engineering and game-based training, have a history of development best practices and guidelines that support the use of these tools [19, 57, 195, 221].

2.1.1   Contributions

This chapter provides a comprehensive overview of the goals, guidelines, and best development practices for AR-UIG systems that take into account the nuances of medical software development. The result is a series of recommendations about the development of such systems that reflect the particular context and constraints of augmented reality systems and image-guided interventions, providing a loose framework for development with:

1. Goals around which to justify and elucidate system requirements and evaluation approaches;

2. Guidelines around which to justify design decisions that heuristically (although not consistently and unambiguously) encourage identifiable goals; and

3. Best practices to direct and inform the development process itself.

2.2   Goals of Augmented Reality

The goals of an AR guidance system can be defined as properties of the system that are unambiguously desirable. These goals are unambiguous in that, although they may involve trade-offs between one another and may be prioritized differently across clinical centres and applications, they reflect fundamentally desirable properties of the system regardless of how they are implemented. AR-UIG systems have many goals including:

- *Addressing currently unmet clinical needs*: One of the most clear goals of an AR guidance system is to provide a solution to a valid clinical limitation [169]. For a guidance

system to be adopted in the clinic, it must add value and improve the targeted intervention. Maintaining a favourable cost-benefit analysis is imperative for the successful adoption of an AR guidance system in the clinic. Consequently, it is not sufficient to improve on a currently satisfied need as such marginal improvements are unlikely to warrant the cost of replacing existing systems or modifying existing workflows.

- *High accuracy and patient safety*: Ensuring high performance accuracy is a crucial goal for any AR-UIG system. Note that the definition of accuracy from the engineering and clinical perspectives may be different, and an AR-UIG system should meet the requirements for both aspects. From the engineering perspective, accuracy may be defined as the "degree to which a measurement is true or correct" [81]. The overall AR-UIG system accuracy is dependent on the accuracy of its integrating components [97]. Examples of such components include: anatomical modeling, registration, and tracking. High accuracy of each component is integral in providing an image guidance system with high overall accuracy. From a clinical perspective, accuracy may be defined as "the maximum error that can be tolerated during an intervention without compromising the effect of the therapy or leading to non-negligibly increased risks to the patient" [126]. Overall, accuracy of an AR guidance system fundamentally affects patient safety, which is of utmost priority of any intervention.

- *Low initial and recurring costs*: The cost-effectiveness of an image guidance system plays an important role in its adoption in the clinic [90]. Adoption of a new image guidance technique comes at the cost of training and, in some cases, extended operating room (OR) cost [141]. Therefore, similar to any image guidance technique, it is important that the initial and recurring cost of an AR-UIG system would not significantly add to the cost of adopting and maintaining the technology. Note that what is considered adequately low cost varies depending on the procedure and clinical need being filled, as well as the region in which the procedure is performed and its healthcare payment approach.

- *Minimal intrusion on clinical workflow*: An impactful AR guidance system must fit into the clinical environment and provide an efficient workflow [184]. This is one of the main hurdles for developing a clinically meaningful AR system [184]. Workflow refers to not only all the steps that the interventionalist takes to perform a procedure, but also other aspects of the procedure such as pre-operative imaging, wait times, OR accessibility, and sterilization. The underlying emphasis of this goal pertains to how accessibility of a system is outside of cost.

- *Low cognitive impositions on the clinical user*: An AR guidance system should not impose a significant cognitive load on the user clinician or result in cognitive overload. Cognitive overload can severely degrade the performance of the clinician. Primary causes of cognitive overload include: (1) too much information supply, (2) too much information demand, and (3) frequent multitasking or interruption [113]. It is imperative to the success of an AR guidance system that it does not overwhelm the user with too much information. Reducing the complexity of the system and ensuring ease-of-use are critical to lowering cognitive load imposed on the user, reducing training required to interact with the system, and intrusion on clinical workflow [169].

The extent to which any particular system or design decision affects a particular goal is not immediately predictable, making goals effective at justifying evaluation metrics or approaches, but not design decisions directly.

2.3 Guidelines in Augmented Reality Ultrasonic Guidance System Development

While the goals of an AR-UIG are unambiguous and are undeniably desirable, how can these systems be implemented to promote these goals? Modern AR-UIG systems are commonly developed along the lines of a user-centric approach. Using this paradigm, particular guidelines

are used as surrogates for the goals themselves, which can later be measured. The idea behind these guidelines is to direct implementation at an abstract level, rather than to evaluate the end-product. Common guidelines for AR-UIG systems include:

- *Minimalism*: Reducing the complexity of the user interface, to limit the cognitive load inherent in its use, has long been a guideline for developing all varieties of user interfaces, not limited exclusively to medical interventions or AR [147, 170]. The philosophy underlying minimalism is to limit the space of a user's options to correct ones and eliminate distractions within the system itself.

- *Minimize mental transformations*: One of the more complex mental tasks performed in an image-guided intervention is transforming information such as location and direction between different coordinate systems [2]. One way to achieve this is to present all surgical tools, images, and targets in a single, unified reference coordinate system, a goal that can be accomplished if the imaging modality is tracked relative to instruments and their surrounding context [170, 184]. An example of mental transformation is when the clinician toggles between different views of the surgical scene, such as those acquired by different imaging modalities or two different views acquired from the same modality. An example of a design decision that aims to minimize mental transformation is *in-situ* visualization, in which the clinician's view of the surgical scene is augmented with all the visualized information.

- *Plug-and-play*: One key hurdle to the incorporation of AR systems into the clinic is the issue of workflow intrusion. The concept behind a plug-and-play system is to minimize workflow intrusion and the additional time required to employ the system, as well as the additional cost of new equipment. The ideal AR system would involve minimal hardware and interact with a wide variety of available ultrasound scanners [10, 213]. Modularity is critical in creating plug-and-play systems, ideally interpreting any external hardware as interchangeable modules.

- *Minimal operating room footprint*: Creating a physically compact system with a minimal OR footprint allows for more ready integration into the clinical workflow. This involves not only minimizing the use of expensive components (to restrain costs) [125] but also inexpensive hardware such as keyboards that require additional personnel or sterilization [125, 170].

- *Similarity to previous systems*: As the goal is to design systems immediately usable in clinic, there are a number of psychological and regulatory hurdles that could be overcome by encouraging a high degree of similarity to previous systems. This similarity lowers the barriers to adoption by the clinical community, by taking advantage of their former experience and training [170].

- *High ultrasound visibility*: The ideal AR environment would allow the clinical user to view the area of interest necessary for performing the intervention, while simultaneously being aware of, but undistracted by, surrounding anatomy [170]. One recommended mechanism to achieve this is to provide a high degree of visibility to the ultrasound image, minimizing occlusion and promoting a direct view of the ultrasound image plane.

- *Transparency to the clinician*: AR systems should be designed to be transparent to the clinical user, so that errors, such as mis-registration or loss of tracking, can be easily identified and corrected [170].

- *Representative of reality*: Widgets in an AR system should be visually representative of real-life, i.e. the virtual representation of surgical instruments should resemble the actual devices, so that the cognitive load required to identify and interact with virtual components in the surgical scene is minimized. Similarly, when employing AR techniques to portray images within the body, the paradigm should be to represent the image as if it were viewed on a physical plane inside the body accessed via a "window" rather than simply superimposing the image on the surface of the patient [2, 17].

These guidelines often ensure higher degrees of intuitivity and ease-of-use, while minimizing regulatory issues and workflow intrusion and thus have directed the development of many AR-UIG systems. But they are not without their difficulties and ambiguities. Although many of these principles support others, many appear to be mutually contradictory and determining the balance between them prior to extensive development and evaluation may be difficult to impossible. They, nevertheless, provide a language for justifying design decisions which can facilitate development. That is, two developers may disagree on the effect a particular design decision has on a particular goal, but both can more readily agree on the guideline motivating said decision.

2.4 Best Practices

This chapter brings together the goals and development guidelines for AR-UIG systems. While the goals of an AR-UIG system are clear and unequivocal, the development guidelines are less explicit, and the degree to which they are adhered is at the discretion of the developer. Nonetheless, the guidelines are necessary to boot-strap the development process of an AR-UIG system and can readily bring development into the ball-park of the optimal system, even if they alone cannot guarantee optimality. Note that these elements should be incorporated into a development process, which itself is subject to several best practices. Further discussion on multiple aspects of these best practices is provided below.

2.4.1 Regulation

Similar to medical devices, the life cycle of the development of medical software needs to meet certain regulatory requirements in order to obtain Health Canada or Food and Drug Administration approval for clinical trials and use in the clinic [196]. The software life cycle refers to the software development, risk management, problem resolution, and maintenance processes. The international standard International Electrotechnical Commission (IEC) 62304 [102], devel-

oped in 2006, provides a framework of life cycle processes with activities and tasks necessary for the safe design and maintenance of medical device software. The goal of this standard is to enhance the reliability of the software by requiring detail and rigor in the design, testing, and verification of the software and ultimately improve the safety of medical device software for clinical use. IEC 62304 applies not only to the development, but also the maintenance, of medical device software. This standard complies with other standards, including Quality Management Systems as described in International Organization for Standardization (ISO) 13485 and Risk Management Process as described in ISO 14971.

As part of best practices of AR-UIG system development for clinical use, the developer should bear in mind the requirements of IEC 62304. This includes (1) defining the intended use of the software, (2) demonstrating that the software fulfills those intentions, (3) demonstrate that the software does not cause any unacceptable risks. Adherence to this standard encourages developers to adopt rigorous processes and documentation for elements of requirements elicitation and product quality assurance prior to commencing implementation. The degree to which this limits the flexibility of the development process is an open question [45, 134, 135, 165, 178, 180, 181].

2.4.2 Clinical Input

Development of an effective and valuable guidance system cannot be achieved without the input of the clinical users. It is essential that the clinical need is outlined and the desired guidance system described by clinical experts prior to the design and development of an AR-UIG system.

Clinicians should also be consulted to identify the environmental and practical limitations that need to be accounted for during the design of a guidance system. One of the main challenges is finding a balance between what the clinician envisions for the guidance system and what is technically and economically feasible. As a result, the importance of maintaining an open dialogue and thorough communication with the intended users cannot be overstated. However, the developers should be wary of developing an over-engineered system if clini-

cians over-describe the clinical problem or under-engineered when insufficient information is provided. Moreover, clinicians with different levels of expertise and experience may view a clinical problem differently and envision a different solution. Therefore, it is important not only to seek the input of clinicians, but to also elucidate alternatives, evaluate the system, and collect feedback with as many clinicians as possible.

2.4.3 Iterative and Small-Scale Evaluation

The importance of intermediate, small-scale evaluation with the intended clinical population cannot be over-estimated. Although, during the development phase, design decisions may seem obvious and inherently justified, there is no substitute for evaluation with clinical users. Incremental evaluation which interrogates each design decision can better determine its effect on particular goals as well as unearth special cases and considerations that can radically change the system for the better.

In a larger software development community, this methodology is widely known and used under the moniker of *agile development*. There has been some discussion regarding the implementation of agile development practices in medical software, although several medical device standards, such as IEC 62304 on medical device software life cycle processes [45], favour more traditional development processes [180, 181]. Discussion regarding the place of agile development in the medical and pharmaceutical industries has been divided. Authors such as Rottier and Rodrigues [178] favour agile development and have detailed some of the challenges of using agile development with respect to these medical software standards especially with respect to changing user requirements. Authors against, such as Paulk [165], emphasize issues with merging agile development with the strict regulatory documentation requirements. Recently, McHugh *et al.* [134, 135] have investigated the actual and perceived barriers to agile development in medical software, but in an application-agnostic approach that captures neither the unique developmental, technical, and user challenges of image-guided interventions, nor AR visualization, which we attempted to capture in the description of common guidelines in

AR-UIG development.

2.4.4   Trade-off Between Standardization and Versatility

As a developer of a medical system, one must accept a certain fundamental choice between standardization and versatility. Often there is a high degree of variability in the approaches taken by clinicians, especially if trained at different institutions, to perform a procedure. Either a system must support this variability and be versatile to fundamental variations in how the procedure is performed, or its use must be standardized and the standards explicitly stated in order to remove these variations. This must be a conscious and communicated decision of the design team and not an ad-hoc consideration. Given a specific procedure, the choice between standardization and versatility should either be explicitly planned for in the initial discussion with the clinical user, or discovered during iterative evaluation.

2.4.5   Multi-use System Design

Navigation and positioning should be recognized and thought of as different uses of the guidance system. Developers must bear in mind that image-guided interventions are composed of multiple tasks. Therefore, a guidance system aimed to guide the entire set of procedures is going to be fundamentally multi-use.

In addition, a guidance system has multiple parts that can be configured to accomplish different aspects of an image-guided procedure ranging from training to quality assurance (QA).

Training is an important part of an image-guided procedure. Configuring a guidance system to provide a training platform is particularly important as any guidance system requires training before being used in practice. Also, keeping training as similar to the guidance system as possible is desirable. Therefore, making the system itself suitable for training would potentially be beneficial, because the clinicians would have more experience with the system itself and would not be subject to minute differences between the training and clinical system that would cause undue distraction or cognitive load. One example could be configuring the guidance

system to allow integration of synthetic images and models for training purposes. This may eliminate the need for physical phantoms, making the training platform more affordable and accessible.

Moreover, there is no standardized training for many image-guided interventions and performance is assessed subjectively and by observation. An image guidance system may be configured to provide quantitative skill assessment for QA. One simple way for QA could be providing a procedure replay capability achieved by simply recording the tracking information of the tracked intra-operative images and surgical tools (for post-hoc QA). Addition of a replay capability allows a retrospective quantitative analysis and assessment. Such simple and small additions can lead to new capabilities of the system while keeping the core system intact.

The potential use of an image guidance system for multiple tasks, other than surgical guidance, may not be clear to the collaborating clinicians and not come up in initial discussions. As developers have a better grasp of the capabilities of the technology and guidance system being developed, they may need to envision and design additional functionalities for their guidance system first and then further refine the design and assess the usefulness of such functionalities via consulting with clinicians.

2.5   Conclusion

There is currently a need for the image-guided surgery community to discuss, enumerate and describe the goals of AR guidance systems as well as the guidelines and best practices for their development. This chapter has tried to address this by producing a list of guidelines that have appeared multiple times in the literature. Ultimately, a more complete description taking into account a higher diversity of perspectives through discussion in the AR-UIG community may create a more comprehensive and usable framework with common terminology.

The success of an AR-UIG system ultimately relies on the successful identification and balancing of competing guidelines in each design decision directed by best practices in devel-

opment. In this sense, one size does not fit all. At all stages of design, it is important to identify and focus on the specific features that address limitations of current standard of care, and also to acknowledge that experienced practitioners of a procedure may perceive technological intrusion into their domain in a negative light.

Chapter 3

Effects of Line Fiducial Parameters and Beamforming on Ultrasound Calibration

This chapter is adapted from the following manuscripts:

- Ameri, Golafsoun, John S. H. Baxter, A. Jonathan McLeod, Terry M. Peters, and Elvis C. S. Chen. "Effects of line fiducial parameters and beamforming on ultrasound calibration." *Journal of Medical Imaging* 4, no. 1 (2017): 015002-015002.

- Ameri, Golafsoun, A. Jonathan McLeod, John S. H. Baxter, Elvis C. S. Chen, and Terry M. Peters. "Line fiducial material and thickness considerations for ultrasound calibration." In *SPIE Medical Imaging*, pp. 941529-941529. International Society for Optics and Photonics, 2015.

- Ameri, Golafsoun, John S. H. Baxter, A. Jonathan McLeod, Uditha L. Jayaranthe, Elvis C. S. Chen, and Terry M. Peters. "Synthetic aperture imaging in ultrasound calibration." In *SPIE Medical Imaging*, pp. 90361I-90361I. International Society for Optics and Photonics, 2014.

41

3.1   Introduction

A fundamental criterion for the integration of ultrasound images in augmented reality (AR) environments is ultrasound calibration, the process whereby images from a tracked ultrasound probe are placed in the context of the tracker, i.e. a common frame of reference (Figure 3.1). More specifically, ultrasound calibration is the process of calculating the transformation (rotation, translation, and scaling) between the image plane and the origin of the sensor mounted on the ultrasound probe, Figure 3.1.
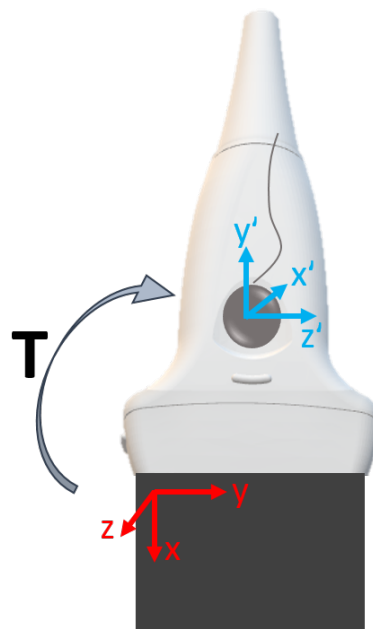
Figure 3.1: Ultrasound calibration is the process of calculating the transformation (T) between the coordinate frame of the image plane (illustrated in red) and that of the tracking sensor mounted on the ultrasound probe (illustrated in blue).

Commonly, ultrasound calibration is performed by capturing ultrasound images of a tracked, calibration phantom with a known geometry at various depths and phantom poses. Then, the phantom features, i.e. fiducials, are segmented in the images. Knowing the physical location of the fiducials and the ultrasound probe in tracker space and the location of the fiducials in the ultrasound image space, the transformation between the ultrasound image and the probe sensor can be calculated. Many different ultrasound probe calibration techniques using a variety of

phantom geometries have been proposed over the years, one of the most common of which is a Z-bar calibration technique, using taut wires in a Z shape as fiducials. This technique has the advantage of low cost phantoms [211] and a fully automatic pipeline developed and available in the open-source PLUS library [38]. Alternative proposed ultrasound calibration methods take advantage of the properties of different geometries, which are not immediately representable as points in the ultrasound image. Wall calibration [171], for example, uses a single highly reflective plane, which, seen in cross-section, becomes a line. The main advantage of this approach is that segmentation of a line has properties that make it more robust. Other volume-based methods, such as the rooftop phantom [36], have been used to provide similar orientation information in 3D ultrasound calibration. Phantomless calibration has also been of increasing interest as surgical tools or needles could be used in lieu of a dedicated calibration phantom [110]. These tools are often modeled as lines, or points in a cross-sectional view, similar to the wires in the Z-bar phantom.

Regardless of the calibration phantom type, the basis of ultrasound calibration is the accurate and rapid segmentation of fiducials. The imaging and segmentation steps of an ultrasound calibration pipeline traditionally rely on conventional B-mode imaging, where highly reflective materials such as taut wires are commonly used as fiducials. Due to ringing effects, specular reflection, beam width, and low resolution outside the focal region, such fiducials appear to be spread wide and/or blurred in ultrasound images [93], making their localization in the ultrasound image a challenging task. For example, Figure 3.2 shows ultrasound images of braided nylon wire fiducials of 0.3 mm in diameter placed within and out of the focal region of the image, with the foci at 7.0 and 7.5 cm in both cases. These fiducials, even when in focus, appear spread out and much larger than their actual size in the ultrasound image, making their accurate segmentation prone to error. Inaccuracies in fiducial localization can result in calibration error, which ultimately decreases the accuracy of image-guided interventions.

To overcome the challenges, we have investigated the effects of ultrasound image beamforming and reconstruction [4], as well as phantom material and geometry [5], on fiducial ap-
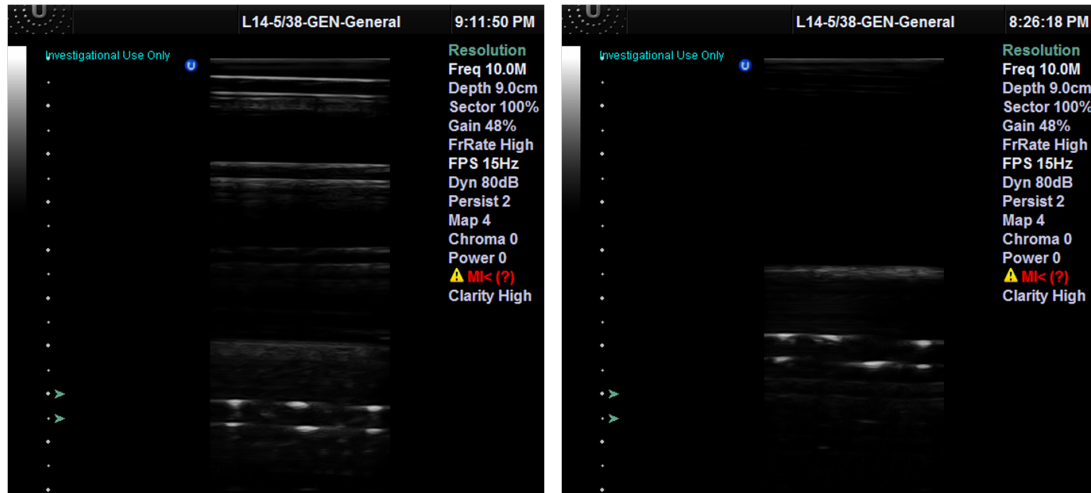
Figure 3.2: B-mode images of two nylon Z fiducials, that are 5 mm apart, placed in focus (on the left) and out of focus (on the right) of the ultrasound image. Focal depths are indicated by arrows in the images.

pearance and localization in ultrasound images and ultimately, ultrasound calibration accuracy. To improve ultrasound image quality of the fiducials, synthetic aperture imaging (SAI) was used. SAI is a focusing technique, providing dynamic focusing and high resolution throughout the entire image, which could lead to improved fiducial localization and subsequently calibration accuracy. In addition, since hypoechoic materials with acoustic properties similar to tissue produce fewer ringing effects in ultrasound images, it is expected that fiducials made out of such materials would be more easily segmented in these images, leading to increased ultrasound calibration accuracy.

3.1.1 Objectives

The purpose of this chapter is to investigate the effects that ultrasound image beamforming technique, phantom geometry, and material acoustic properties play in ultrasound calibration and what effect these factors have on overall ultrasound calibration accuracy. By quantifying these effects, ultrasound calibration for image-guided interventions can be optimized appropriately according to the beamforming technique and calibration phantom design.

3.1.2 Contributions

The contributions of this chapter are summarized as follows:

1. This work introduces and evaluates the use of synthetic aperture imaging in existing Z-bar calibration. This technique improves ultrasound calibration by reducing fiducial localization error, fiducial registration error, and target registration error.

2. Ultrasound calibration phantom design considerations cognizant of the image reconstruction and beamforming technique are introduced and analyzed. An evaluation of a variety of calibration phantoms with different geometrical and material properties for ultrasound calibration is performed. The effects of these phantom properties on ultrasound calibration are investigated under different ultrasound beamforming techniques.

3.2 Ultrasound Calibration

3.2.1 Error in Ultrasound Calibration

A common approach to ultrasound calibration is to image a phantom or set of fiducials with a known geometry and formulate a marker-based registration problem relating the known geometry to the image through a coordinate transformation. This registration accuracy and ultimately the calibration accuracy is affected by a number of factors including the fiducial localization accuracy, fiducial configuration, and the number of fiducials used [68, 69]. As ultrasound calibration is inherently a registration problem, [140] the metrics used for evaluating ultrasound calibration accuracy are the same as those used for registration processes, namely, the fiducial localization error (FLE), fiducial registration error (FRE), and target registration error (TRE) [37, 69].

The FLE is defined as the distance of the localized fiducial in the ultrasound image from the fiducial's true position in the image space. However, the true position of the fiducial in the

image is "forever unknown" [69]. As a result, in practice, true position of a fiducial is estimated as the mean location of fiducials identified in all the segmented images.

FRE is the root-mean-square distance between homologous fiducials after registration. The expected value of FRE depends on the number of fiducials used and the expected square value of FLE [69]. Fitzpatrick *et al.* [69] have shown that FRE is not a reliable predictor of registration accuracy. An error that is more of concern in ultrasound calibration is the TRE, which is a more direct measure of registration error [67].

TRE is defined as the distance between homologous points, other than the fiducials used for the registration process, after registration has been performed. TRE is strongly dependent on the fiducial configuration and the position of the measurement points with respect to registration fiducials [69]. Therefore, to reduce TRE in ultrasound calibration, the fiducials should be placed throughout the entire field of view.

Although targets can be separate objects in practice, a surrogate metric, the leave-one-out TRE, is often used. Given a set of N imaged fiducials, X, with known locations, Y, the leave-one-out TRE can be calculated as:

$$TRE_{Leave-one-out} = \frac{1}{N} \sum_{i=1}^{N} \|Y_i - T_{\neg i}(X_i)\| , \tag{3.1}$$

where $T_{\neg i}(\cdot)$ is a calibration algorithm minimizing the FRE for the fiducial set $X \setminus \{X_i\}$, that is, all fiducials except the $i^t h$. In this work, the leave-one-out TRE is used to evaluate and compare the calibration error in the proposed calibration techniques.

3.2.2 Rigid and Anisotropic-Scaled Calibration Transformations

Often, the transformation between the known geometry and calibration images is rigid, consisting only of rotation and translation. In order to specify a transformation, corresponding points between the geometry and its representation in the image must be known. In the case of Z-bar calibration [44], these correspondences can be approximated quickly allowing for the

calibration transformation to be formulated as an Orthogonal Procrustes problem and solved analytically [91, 188].

If point-to-point correspondences are not known *a priori*, the Iterative Closest Point (ICP) algorithm [16] can be used to simultaneously find these correspondences and the rigid transformation. ICP is a generic algorithm, independent of shape representation, that iteratively performs a correspondence and a transformation operation until a stable solution is obtained. The correspondence operation establishes a one-to-one correspondence between the measurement point-set and the model point-set using the shortest Euclidean distance, and the transformation operation finds the optimal rigid-body transform using a closed-form, least-squares method [91, 188]. In general, ICP converges monotonically, but requires a fairly reasonable initialization in order to reach a global minimum.

We used anisotropically scaled ICP (ASICP) proposed by Chen *et al.* [34] to solve for the ultrasound calibration transform. This method improves the accuracy of ultrasound calibration by solving for anisotropic pixel scaling in addition to translation and rotation. Deviations of the speed of sound from 1540 m/s (the speed assumed by most scanners) can result in anisotropic pixel scaling when using a linear array probe. These effects are particularly significant when performing ultrasound calibration in a room temperature water bath [140].

Similar to traditional ICP, ASICP converges monotonically [34]. However, this increased flexibility has its disadvantages as a larger number of fiducials or images must be acquired to accurately determine the additional scaling parameters [35]. That is, although anisotropically scaled calibration is guaranteed to have a lower FRE than rigid calibration, with fewer than seven calibration images, anisotropic-scaled calibration can result in a higher TRE [35].

3.2.3 Synthetic Aperture Imaging (SAI)

SAI techniques, originally conceived for radar systems, have been investigated in medical ultrasound imaging since the beginning of the 1990's [99]. SAI provides dynamic focusing and improves resolution throughout the image via post-processed beamforming, which in turn im-

proves ultrasound image quality. Unlike traditional B-mode imaging, where transmit focal regions are predefined and fixed, SAI achieves focusing during both transmit and receive mode on every image point. Therefore, SAI allows for higher resolution and interpretability throughout the entire image, rather than only at pre-specified foci. SAI has shown superior image quality in breast [112], liver [23], and abdominal ultrasound imaging [88] due to increased resolution.

There are multiple methods for performing synthetic aperture beamforming. In the modified synthetic transmit aperture (STA) algorithm [200], employed in this work, each element in the probe array transmits sequentially in an isolated manner. After each transmit, every crystal is used to receive echoes. The acquired complete dataset allows both dynamic transmit and receive focusing to be achieved, retroactively. Image reconstruction, then, is performed in two stages. In the first stage, an image is reconstructed after each transmit. As a result the number of images reconstructed is equal to the number of transmissions, i.e. the number of elements in the array. Image reconstruction is performed using the delay-and-sum technique [99]. Coherent summation is performed by finding the geometric distance between the transmitting element to the image point and back to the receiving element, resulting in dynamic receive focusing. In STA, the angular directivity function, $f(\theta)$, of the transducer element is incorporated as weights in the delay-and-sum stage [200]. $f(\theta)$ describes the radiation pattern of the transducer element and can be calculated using the far-field approximation for the narrow-strip transducer element by [190]:

$$f(\theta) = \frac{sin(\pi d/\lambda sin\theta)}{\pi d/\lambda sin\theta} cos\theta, \tag{3.2}$$

where d is the element width and λ is the wavelength. $f(\theta)$ is calculated for both the transmit and receive elements. During transmission, θ is the angle between the transmit element's surface normal and a virtual line connecting the element's center to the image point, Figure 3.3a. In receive, θ is defined as the angle between the receive element's surface normal and a virtual
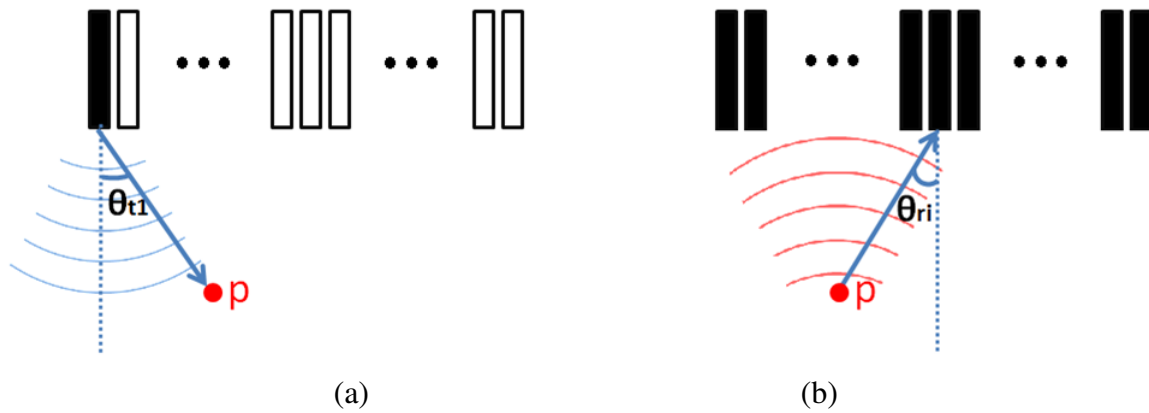
Figure 3.3: (a) The first transmit element's directivity angle, θ_{t1}, for the image point P. (b) The ith receive element's directivity angle, θ_{ri}, for the image point P.

line connecting the receive element's center to the image point, Figure 3.3b.

Due to the finite size of a single transducer element, its acoustic radiation pattern is not spherical and instead is angularly dependent [190]. Therefore, images reconstructed in the first stage, referred to as low resolution images, have appreciable signal only over a limited field of view. In the second stage, the low resolution images are added together and a high resolution image is obtained [99]. As a result, focusing in both transmit and receive is achieved (Figure 3.4).

Segmentation of these STA images is greatly simplified due to the increased resolution, particularly for small features, such as echoes of wires in a calibration phantom. In the past, calibration has been restricted to conventional B-mode images. By performing calibration on STA images rather than B-mode images, higher accuracy segmentation of the wire fiducials is possible.

3.3 Effect of Imaging Type on Ultrasound Calibration

Here, the performance of STA on Z-bar calibration accuracy is compared to that of conventional B-mode imaging. High resolution STA images are expected to facilitate fiducial localization in the image, allowing for more accurate calibration of ultrasound probes.
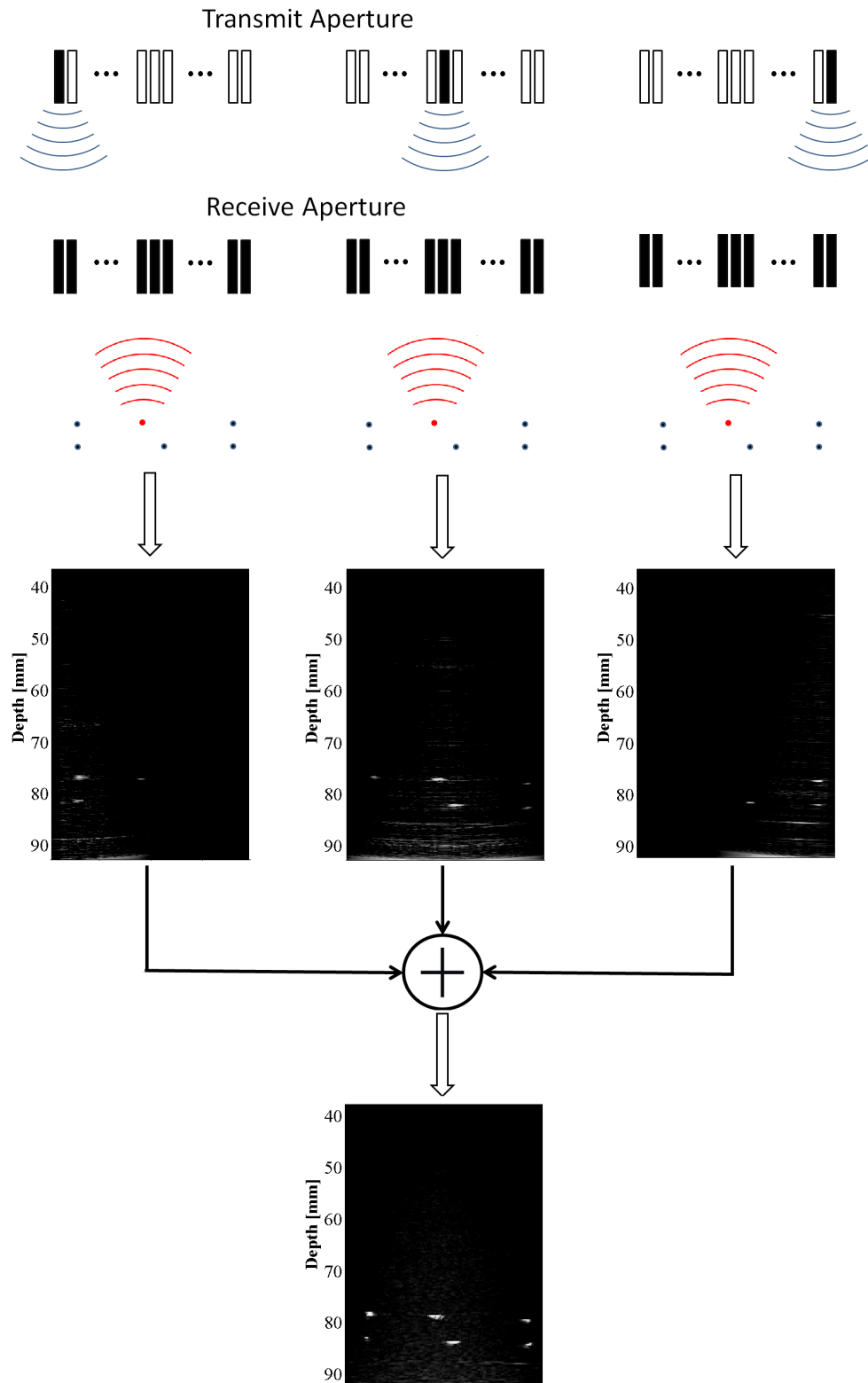
Figure 3.4: Modified synthetic transmit aperture imaging. A high resolution image is obtained in the second stage by adding images reconstructed in the first stage.
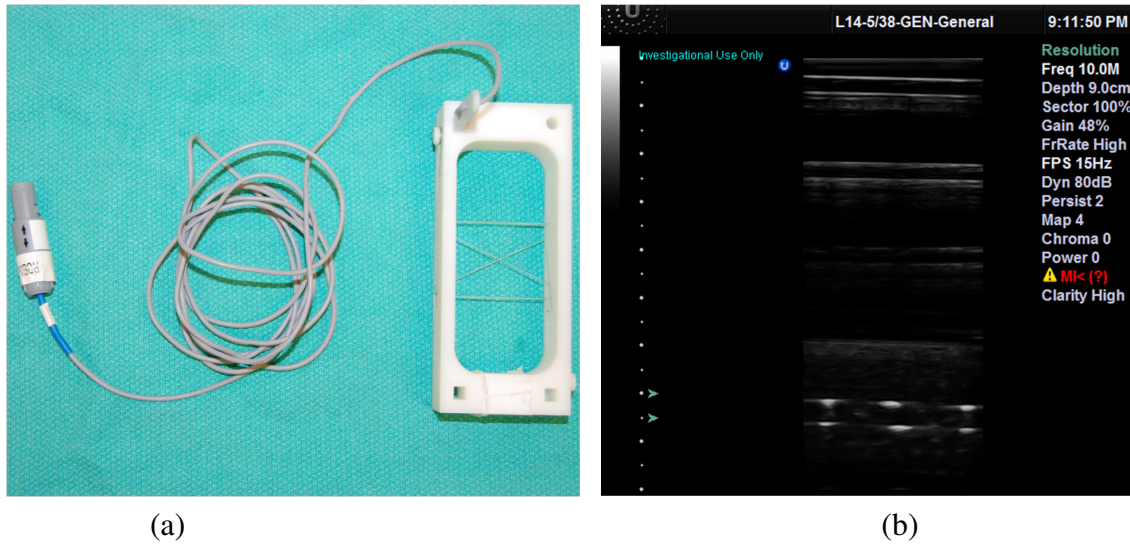
Figure 3.5: (a) Z-bar calibration phantom, (b) Corresponding B-mode image.

3.3.1   Z-Bar Ultrasound Calibration

The basis of Z-bar calibration [44] is the calibration phantom, which consists of two parallel plates a known distance apart with a grid of holes milled perpendicular to the faces of the plates. Wires, acting as line fiducials, are then threaded through the two plates to form a series of Z-shaped configurations. A magnetic tracker is rigidly affixed to the calibration phantom. These collinear line fiducials produce identifiable echoes in the ultrasound images. In the experiment presented in this section, the Z-bar phantom designed by the PERK lab[1], known as the fCal phantom [121], was used. The tracked fCal phantom and its ultrasound image are shown in Figure 3.5.

All of the line fiducials are localized in the ultrasound images. Because of the Z-shaped configuration, the intersections of the ultrasound image plane with the diagonal fiducials can be calculated based on similar triangles [38]. Using the tracking information, these points are transformed into probe coordinates and registered with their corresponding pixel locations in the ultrasound image, yielding a calibration transform relating the ultrasound image to the tracking sensor rigidly fixed to the probe.

---

[1]http://perk.cs.queensu.ca

Figure 3.6: Experimental calibration setup comprising a magnetic tracking system, tracked ultrasound probe, tracked Z-bar calibration phantom, and plastic supports.

3.3.2 Experimental Setup

The calibration experiment consists of a SonixRP ultrasound scanner and L14-5 linear array probe, with an element pitch of 0.30 mm (BK Ultrasound, Analogic, MA, USA), Z-bar calibration phantom, and an Aurora Magnetic Tracking System (Northern Digital Inc, Waterloo, Canada) arranged as shown in Figure 3.6. Both the ultrasound probe and calibration phantom are fixed in place using plastic supports to remove relative motion and are magnetically tracked, using 6-degrees-of-freedom (DoF) magnetic sensors, allowing for their tracking coordinates to be captured simultaneously with image acquisition. The root-mean-square error of the position and orientation measurements of the tracking system using a 6-DoF sensor is 0.48 mm and 0.30°, respectively.[2] The Z-bar calibration phantom included two opposite 40-mm wide Z-shaped line fiducial configurations 5 mm apart in the depth direction.

The ultrasound imaging settings for the calibration process are chosen to provide the highest resolution possible and cover the imaging depth that is intended for the image-guided pro-

[2]http://www.ndigital.com/medical/products/aurora/

cedure. In this study, the highest ultrasound frequency provided by the scanner for the linear array, 10 MHz, was used to acquire the highest resolution B-mode ultrasound images of the phantom. The image depth was set to 9 cm, the largest possible value at the chosen frequency. As ultrasound image quality is often compromised at larger depths, largely due to attenuation, choosing a large depth would ensure a challenging ultrasound calibration task. Two focal zones were chosen for B-mode imaging, at approximately 7.0 and 7.5 cm, as shown in Figure 3.5, to improve image resolution especially at larger depths.

Calibration experiments were performed at an imaging depth of 9 cm with the calibration phantom placed 6-9 cm from the probe. This experiment involved acquiring 9 images using both B-mode and STA imaging with the probe and calibration phantom physically secured to ensure correspondence between the images in each mode. The beamforming for STA imaging was performed using the Texo SDK (BK Ultrasound, Analogic, MA, USA), and the raw RF data were acquired using the SonixDAQ (BK Ultrasound, Analogic, MA, USA). The same centre frequency, i.e. 10 MHz, as that used for B-mode imaging was also used for STA imaging. The sampling frequency was set to 40 MHz. STA images were then reconstructed from the raw RF data, using an approximation of the speed of sound in water at room temperature, 1480 m/s [18]. The line fiducials intersect the imaging plane at 6 locations, producing hyperintensities. Both STA and B-mode images were segmented by 6 users, all familiar with ultrasound imaging and segmentation. The image segmentation was performed twice in each imaging mode by each user with the images displayed in a randomized order to minimize learning and fatigue effects. An anisotropic Orthogonal Procrustes solution based on singular value decomposition [188] was then performed to find the relationship between the tracking coordinates and segmented line fiducials.

3.3.3 Results

Qualitatively, compared to the B-mode images, STA produced much more readily interpretable ultrasound images of the Z-bar calibration phantom, with the line fiducials being clearer and
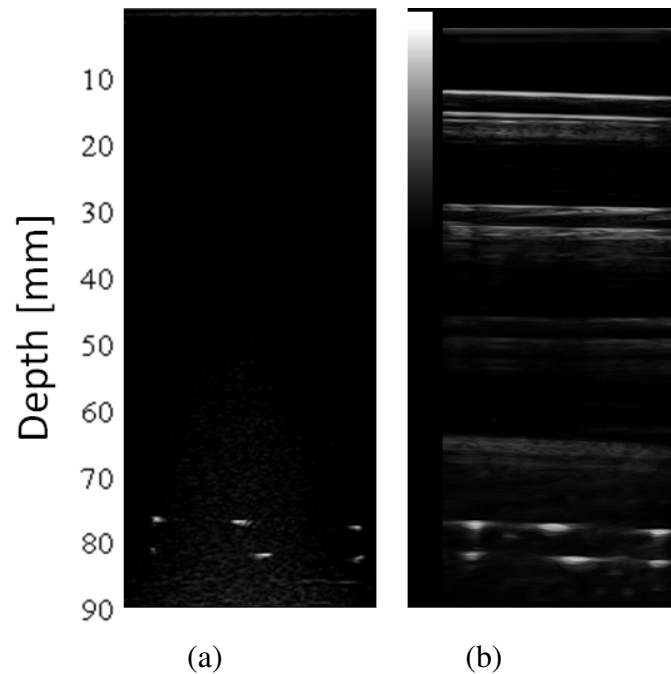
Figure 3.7: The (a) STA and (b) corresponding B-mode image of the Z-bar phantom.

easier to visually localize, as demonstrated in Figure 3.7. STA imaging also reduced the number and severity of artifacts in the images, such as the reflections off the bottom of the water bath.

For evaluation purposes, the mean fiducial location identified by all participants was used as the estimate of the true physical location, assuming the localization follows a normal distribution without bias. The FLE was then calculated for each user. The mean absolute error was 0.15 mm and 0.21 mm for STA and B-mode, respectively. STA resulted in a 29% improvement in FLE in comparison to conventional B-mode imaging. For the sake of comparison, the axial and lateral dimension of a pixel in the B-mode image were 0.175 mm and 0.176 mm, respectively. Calibration accuracy was determined by measuring both the FRE and the leave-one-out TRE. When these segmented fiducials were used for calibration, the resulting FRE also improved from 1.56 mm to 1.42 mm, i.e. an improvement of 9%, with STA. The resulting mean leave-one-out TRE improved from 2.00 mm to 1.80 mm, corresponding to a 10% improvement with STI. These values are recorded in Table 3.1.

Table 3.1: Calibration Error

	STA			B-mode		
	FLE (mm)	FRE (mm)	TRE$_{Leave-one-out}$ (mm)	FLE (mm)	FRE (mm)	TRE$_{Leave-one-out}$ (mm)
	0.14	1.36	1.74	0.20	1.67	2.15
	0.14	1.34	1.67	0.23	1.60	2.02
	0.14	1.37	1.74	0.16	1.78	2.31
	0.25	1.64	2.07	0.29	1.46	1.88
	0.14	1.44	1.82	0.20	1.40	1.78
	0.16	1.45	1.84	0.24	1.46	1.90
	0.16	1.43	1.83	0.21	1.50	1.89
	0.11	1.34	1.68	0.15	1.58	1.97
	0.12	1.36	1.76	0.21	1.67	2.16
	0.20	1.52	1.89	0.24	1.71	2.24
	0.13	1.42	1.80	0.15	1.41	1.84
	0.13	1.35	1.72	0.21	1.47	1.87
MEAN	0.15	1.42	1.80	0.21	1.56	2.00
STD	0.04	0.09	0.11	0.04	0.13	0.18

The paired t-test was used to determine statistical significance. The improvements in FLE, FRE, and leave-one-out TRE are all statistically significant ($p < 0.01$). It is important to note that the error due to magnetic tracking is a major contributor to the calibration error. As a result, the large improvement in line fiducial localization translated into a more modest, but still significant, improvement in the final calibration accuracy.

3.4 Effects of Phantom Material and Geometric Properties on Ultrasound Calibration

There is considerable uncertainty regarding the localization of the centroid of wire fiducials [38]. As shown in Figure 3.2, wire fiducials appear larger than their true size and/or blurred in B-mode ultrasound images, especially, when placed at an oblique angle with the image plane or outside the focal region of the transducer. Such elongated echoes in the image are not repre-

sentative of the true cross-section of the line fiducials with the image plane. As a result, the true intersection of the ultrasound beam's mid-plane with these line fiducials is not robustly identifiable, which decreases segmentation accuracy.

While changing the gain and dynamic range of the B-mode image could improve the image quality, not all the artifacts can be eliminated, and fiducial localization remains a challenging task. For the same gain and dynamic range settings, fiducials with lower echogenicity lessen the impact of the aforementioned artifacts in ultrasound, such as the comet-tail artifact and spreading at oblique angles. In this section, the effect of such materials on ultrasound calibration accuracy is investigated.

3.4.1 Phantomless Ultrasound Calibration

The phantomless calibration technique [110] has the advantage of using tracked surgical tools, such as a needle or a stylus, in lieu of a dedicated phantom to perform calibration. Ultrasound phantomless calibration can be formulated as a point-to-line registration problem [37], which was solved using the ASICP algorithm mentioned in section 3.2.2. An added benefit of this approach is that in any image, only a single calibration object needs to be identified, which simplifies the process of automatic segmentation by eliminating any correspondence problems. Also, this framework allows using a calibration phantom that can be modeled as a line or cylinder, similar to a surgical tool. This facilitates integration of different materials in the phantom construction.

As with Z-bar calibration, these phantoms and the ultrasound probe are tracked using a magnetic tracking system (Aurora, Northern Digital, Canada). The ultrasound probe is calibrated through the acquisition of at least three images showing a cross-section of the calibration object. However, a larger number of images (7-12) were acquired to ensure a higher accuracy calibration representative of clinical use. The phantoms used in this study and automated segmentation procedures are explained in the following sections.
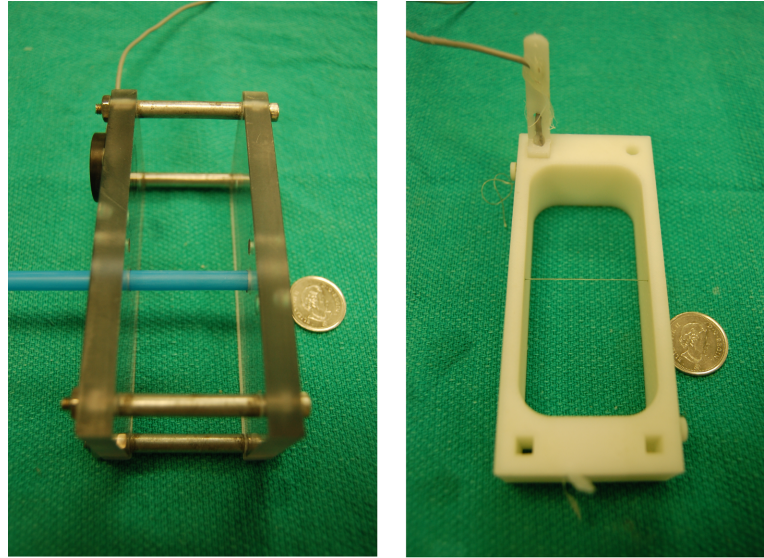
Figure 3.8: The phantom frame on the left was used to hold straws and PVA-C tubes. The fCal phantom is shown on the right, where braided wire was threaded through the holes of this frame.

3.4.2 Phantom Material

In this study, calibration phantoms were modeled as hollow plastic straws of different diameters, 7 and 3 mm, or solid tubes. The material used for making hypoechoic solid tubes was polyvinyl alcohol cryogel (PVA-C), a well known tissue-mimicking material in ultrasound imaging [197]. These phantoms were made by pouring PVA-C into molds, specifically plastic straws with two different diameters, and then subjecting them to three freeze-thaw cycles. The phantoms were then fixed in a tracked frame. For comparison purposes, a braided nylon wire phantom, with a diameter of 0.3 mm, was used as a line fiducial. The braided wire was placed in an fCal phantom [121]. Photos of the phantoms are shown in Figure 3.8. In our experience, braided wires have better visibility in ultrasound images compared to smooth wires. Both plastic straws and PVA-C tubes are less reflective than wire fiducials traditionally used in ultrasound calibration. Conventional B-mode and STA images of these phantoms are shown in Figure 3.9.
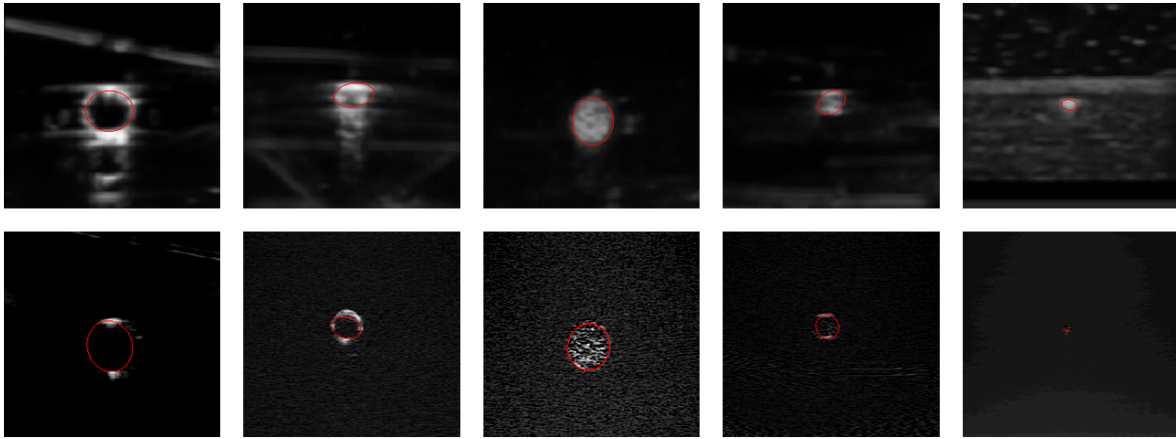
Figure 3.9: Automatically segmented fiducials in conventional B-mode (top row) and STA (bottom row) images. Phantoms from left to right: plastic straw (7 mm in diameter), small plastic straw (3 mm in diameter), large PVA-C tube, small PVA-C tube, and braided wire (0.3 mm in diameter).

3.4.3   Object Segmentation From Ultrasound Images

In this work, automatic segmentation of a user defined region of interest was used to localize the centroid of the phantoms. The cross-sectional views of the phantoms used are ellipsoidal, the eccentricity of the ellipse varying with the angle of insonation relative to the orientation of the object. Therefore, the automatic segmentation process used involved automatic detection of a best-fit ellipse. The first step of the segmentation is edge detection, where thresholding based on Otsu's method [161] was used to binarize the B-mode image. Morphological operations were performed to thin and smooth the binary images so that the edges could be extracted. For STA images, with high resolution and thin edges of the fiducials in the image, the edge detection was performed using a Canny edge detector [28]. The second step of the segmentation was ellipse fitting, where Simonovsky's MATLAB implementation[3] was employed. First, two points on the edge mask were chosen and defined as the major axis. The minor axis was then determined through the Hough transform. The algorithm iterated over all pairs subject to reasonable exclusion criteria, such as bounds on the major axis length, and the final ellipses were constrained to meet criteria such as bounds on the eccentricity. Segmented fiducials in

---

[3]http://www.mathworks.com/matlabcentral/fileexchange/289

both conventional B-mode and STA images are displayed in Figure 3.9.

3.4.4 Experimental Setup

The phantom and ultrasound probe were held stationary in a water bath. Ultrasound images of the phantoms and the raw RF data were acquired using a SonixRP ultrasound scanner and the SonixDAQ. The ultrasound probe and phantom were tracked using an Aurora tracking system. For every phantom position, first, the tracking information of the ultrasound probe and the phantom were recorded. Next the B-mode image with a fixed focus (at 5.47 cm) was acquired directly from the scanner. Finally, STA beamforming and image reconstruction were performed as described in section 3.3.2.

3.4.5 Results

Over all, B-mode displayed better visibility of large phantoms, due to reduced interference from shadowing, blurring, and ringing effects along object boundaries. STA images displayed fewer of these artifacts with higher resolution and improved interpretability of small phantoms. However, most of the STA images suffered from low contrast and signal-to-noise ratio (SNR) because of reflections from the sides of the phantom frame and low transmit power, as only one transducer element is used to transmit at a time.

Quantitatively, each calibration resulted in a visual alignment of the cross-section of the target and the ultrasound image, as shown in Figure 3.10. For evaluation purposes, calibration accuracy was determined by measuring the leave-one-out TRE. These values are recorded in Table 3.2.

For statistical analysis, first, multifactorial ANOVA was used to determine the significance of three factors in the experiment. The first factor (I) is the imaging type, either B-mode or STA. The second factor (M) is the phantom material, either a PVA-C tube or a hollow straw. The third factor (T) was the diameter of the phantom, either large (7 mm) or small (3 mm). The results are summarized in Table 3.3 with an asterisk (*) indicating significant findings, i.e.

Figure 3.10: Visual representation of the straw phantom registered to the ultrasound image after calibration.

$p < 0.05$. Then, an unpaired t-test was performed to compare the braided wire fiducial with the phantom and imaging type that gave the lowest calibration error with statistical significance based on the ANOVA test.

Table 3.2: Ultrasound calibration error using different phantoms in both B-mode and STA images

Phantom	Imaging Technique	Mean TRE$_{Leave-one-out}$ (mm)	Standard Deviation (mm)
Large Straw	B-mode	0.70	0.85
	STA	1.95	0.95
Small Straw	B-mode	1.63	0.77
	STA	0.79	0.64
Large PVA-C Tube	B-mode	0.70	0.48
	STA	0.96	0.63
Small PVA-C Tube	B-mode	1.20	0.83
	STA	0.56	0.39
Braided Wire	B-mode	1.22	0.77
	STA	0.98	0.60

Table 3.3: Multivariate ANOVA

Factor	Sum Sq.	d.f.	Mean Sq.	F	p
I	0.81	1	0.81	1.56	0.22
M	2.67	1	2.66	5.15	0.03*
T	0.03	1	0.03	0.06	0.82
$I \star M$	2.16	1	2.16	4.19	0.04*
$I \star T$	2.35	1	2.35	4.56	0.04*
$M \star T$	0.001	1	0.001	0	0.96
Error	36.65	71			
Total	48.04	77			

The resulting model from ANOVA only showing significant components ($p < 0.05$) is:

$$TRE_{Leave-one-out} = c + f(M) + g(I, M) + h(I, T) + \epsilon, \tag{3.3}$$

where:

$$c = 1.11 \text{ mm} \qquad g(I, M) = \begin{cases} 0.25mm, & if\ I = \text{Bmode and } M = \text{PVA-C} \\ 0.25mm, & if\ I = \text{STA and } M = \text{Straw} \\ -0.25mm, & if\ I = \text{Bmode and } M = \text{Straw} \\ -0.25mm, & if\ I = \text{STA and } M = \text{PVA-C} \end{cases}$$

$$f(M) = \begin{cases} 0.25mm, & if\ M = \text{Straw} \\ -0.25mm, & if\ M = \text{PVA-C} \end{cases} \qquad h(I, T) = \begin{cases} 0.23mm, & if\ I = \text{Bmode and } T = \text{Small} \\ 0.23mm, & if\ I = \text{STA and } T = \text{Large} \\ -0.23mm, & if\ I = \text{Bmode and } T = \text{Large} \\ -0.23mm, & if\ I = \text{STA and } T = \text{Small} \end{cases}$$

ANOVA analysis indicates that all three factors had some influence on the resulting leave-one-out TRE either directly or through interaction. The ultrasound image type showed significant interaction effects with both factors regarding phantom construction. This analysis shows that the lowest error with statistical significance is associated with SAI using a thin PVA-C tube, as it corresponds with decreased error in each function, $f(M)$, $g(I, M)$, and $h(I, T)$. Thus, the calibration error obtained with a thin PVA-C tube and SAI was compared to that obtained with the braided wire line fiducial in STA. The result of an unpaired t-test strongly suggest that the smaller PVA-C tube in STA imaging improved calibration accuracy compared to the braided wire in STA imaging, but this was not statistically significant due to the relatively low sample size ($p = 0.06$).

The results showed that calibration error based on conventional B-mode imaging was reduced for larger diameter phantoms, due to a more accurate segmentation of the centroid of the fiducials. For smaller phantoms, shadowing effects and blurring of the fiducials resulted in less accurate automatic segmentation of the centroids, which led to higher calibration error. With

STA, segmentation of the smaller phantoms was improved. However, segmentation of larger objects in STA did not improve compared to B-mode imaging. In all cases, calibration error from a wire phantom, which is commonly used, was higher than larger phantoms with lower echogenicity.

In order to decrease ultrasound calibration error, we recommend using STA and small PVA-C tubes. If only B-mode ultrasound is available, we recommend the use of a large straw over the conventional braided wire, for its accessibility in addition to improved calibration accuracy.

3.5   Discussion and Future Directions

We have shown that the optimal phantom construction, both in terms of size and material acoustic properties, is dependent on the ultrasound reconstruction and beamforming algorithms. The purpose of ultrasound calibration is to find the transformation between the coordinate system of the tracking sensor attached to the probe and that of the image plane. It is important to note that the location of the image plane with respect to the probe, or a sensor attached to it, is independent of ultrasound beamforming. Therefore, the ultrasound beamforming technique used for ultrasound calibration is not required to be the same as the imaging mode used for a clinical procedure following ultrasound calibration. As a result, for the purpose of ultrasound calibration, an ultrasound beamforming that provides a high resolution image of the phantom should be acquired in order to reduce FLE, improving the overall calibration accuracy. As more advanced ultrasound beamforming techniques, such as SAI, become available, we can only expect that the considerations in calibration phantom design remain and that there will not be a single calibration phantom that performs optimally for all techniques.

This chapter evaluated the performance of STA in ultrasound calibration with different phantom materials and geometries. STA allows dynamic focusing leading to higher resolution images and improved interpretation compared to conventional B-mode imaging. The improved localization capability improves the accuracy achievable in ultrasound calibration. However,

one of the limitations of this work is the specific SAI technique used, i.e. STA, as it has a low transmit power, due to transmission from a single element of the array transducer, limiting its applicability in calibration at large depths in which the SNR and contrast are poor. These issues could be overcome by employing other SAI techniques, such as multi-element SAI [105] and synthetic aperture sequential beamforming [116], where multiple elements are used for transmission, ensuring sufficient transmitted energy especially at larger depths. Coded excitation can also be used to improve the SNR in SAI [40, 76, 160]. Other advanced ultrasound beamforming techniques such as coherent plane-wave imaging also provide a higher SNR compared to STA [145]. Although SAI techniques are currently limited in clinical settings, open-architecture ultrasound scanners including SonixTouch (BK Ultrasound, Analogic, MA, USA) and ECUBE (Alpinion, WA, USA) have been developed allowing for customized beam-forming, and a number of commercial medical ultrasound manufacturers, such as Siemens [22], Philips [202], and Zonare [153], have recently incorporated similar advanced imaging modes in their ultrasound scanners.

Most ultrasound calibration procedures, such as those employed in this study are performed in water using a highly reflective calibration phantom [140]. Therefore, image speckle is not of major concern in the choice of ultrasound beamforming and processing. However, in the case of *in-situ* calibration, where calibration is performed inside the surgical scene [62], additional aspects of image quality aside from resolution become important. For example, speckle reduction techniques, such as SAI compounding [87], may improve fiducial localization. In addition, SA tissue harmonic imaging has also been shown to improve image quality [89]. The impact of these techniques for *in-situ* calibration and their impact on FLE and TRE need future investigation. Moreover, SAI in tissue is susceptible to motion and phase aberration artifacts, caused by spatial variations of the speed of sound in tissue, which may lead to errors in focusing calculations in SAI and deteriorate image quality [71]. The effects of different techniques for target displacement estimation [117] and the correction of motion [75, 99, 205] and phase aberration [104] in SAI for *in-situ* calibration need further investigation.

While 3D ultrasound calibration has been performed for B-mode imaging [36], doing so with SAI is hindered by the limited access to raw RF data from 3D probes and to customized beamforming. However, while such limitations are being addressed, 3D SA images can be reconstructed using 2D probes [157, 173]. Current commercial 3D ultrasound scanners are optimized for acceptable imaging frame rates as opposed to depth and resolution, which are of higher interest in ultrasound calibration. Barring these difficulties, 3D probe calibration may be constructed from the combination of bi-plane calibrations [62].

This work can be extended in a number of ways. First, the phantom materials evaluated in this paper have been constrained to braided wire, plastic straws, and PVA-C tubes. In the future, the range of phantom materials can be extended to include materials used specifically in certain calibration frameworks. For example, in the phantomless calibration technique [110], the calibration phantom can be replaced by the surgical tool, which is often metallic. It would be valuable to evaluate the performance of advanced ultrasound beamforming techniques, such as SAI, on ultrasound calibration using such materials. Second, this paper focused largely on the use of cylindrical or line phantoms, which form the majority of ultrasound calibration procedures [140]. However, there has been an increasing interest in different phantom geometries for calibration including single-wall phantoms [171], which may show similar performance differences based on material type and image reconstruction strategy. Lastly, another area of future work will be incorporating TRE prediction models with the proposed phantoms. TRE prediction models are important in guiding how calibration has been performed. Early point-to-point TRE prediction models, such as that developed by Fitzpatrick *et al.* [68, 69], have seen increasing generality in terms of imaging characteristics, incorporating anistotropic [216] and heteroscedastic [50] FLE. Spatial stiffness based models have been developed for point-to-point [128] and recently point-to-line [37] TRE prediction, which can be directly applied to the phantom geometries examined in this paper.

3.6   Conclusions

Accurate ultrasound calibration is a fundamental step for inclusion of ultrasound as a real-time modality for use in many image-guided interventions. With increased availability of a diverse array of ultrasound beamforming techniques, it is important to consider phantom material and geometry in designing optimal calibration procedures. Using conventional B-mode imaging, it was shown that calibration can be improved by using large diameter phantoms, compared to smaller diameter plastic straws, PVA-C tubes, or wire fiducials, due to improved fiducial localization. With SAI on the other hand, smaller diameter phantoms with lower echogenicity, i.e. small PVA-C tubes, resulted in better ultrasound calibration overall. In the case of a Z-bar calibration, STA significantly reduced the FLE, FRE, and TRE compared to B-mode imaging. This study of the effects of calibration phantom material and thickness has the potential to alter how calibration phantoms are designed cognizant of the image reconstruction and beamforming technique.

Chapter 4

Augmented Reality Ultrasound Guidance System for Central Line Insertions

This chapter is adapted from the following manuscripts:

- Ameri, Golafsoun, John S. H. Baxter, A. Jonathan McLeod, Terry M. Peters, and Elvis C. S. Chen. "Augmented Reality Ultrasound Guidance for Central Line Procedures: Preliminary Results." In Workshop on Augmented Environments for Computer-Assisted Interventions, pp. 11-20. Springer International Publishing, 2015.

- Ameri, Golafsoun, John S. H. Baxter, Daniel Bainbridge, Terry M. Peters, and Elvis C. S. Chen. "Mixed reality ultrasound guidance system: a case study in system development and a cautionary tale." *International Journal of Computer Assisted Radiology and Surgery* (2017): 1-11.

- Ameri, Golafsoun, Daniel Bainbridge, Terry M. Peters, and Elvis C. S. Chen. "Quantitative analysis of needle navigation under ultrasound guidance in a simulated central line procedure." *Ultrasound in medicine & biology* (submitted)

4.1   Introduction

Accessing the central venous system, commonly achieved via the internal jugular vein (IJV), is a fundamental component of patient care [3, 133]. Real-time ultrasound guidance is a key safety measure in central venous cannulation (CVC), improving procedure outcomes and increasing patient safety [53, 100, 115, 133, 186, 201, 206]. However, adverse events still occur, with an incidence of up to 20% [201], and imperfect CVCs remain a significant cause of morbidity and mortality [21, 124, 143]. Although some patients may be predisposed to complications, the physicians expertise level in using real-time ultrasound guidance is a major contributing factor to procedure outcomes [201]. The main challenge of ultrasound guidance in IJV cannulation, when the needle is inserted out-of-plane with ultrasound [186], arises from difficulties in distinguishing the needle tip from its shaft and keeping the needle tip in the image plane. Uncertainties surrounding the exact location of the needle tip, when employing real-time ultrasound for guidance, are associated with inadvertent arterial, posterior IJV, and pleural punctures [20].

It is widely believed that the routine use of ultrasound leads to the acquisition of expertise required for safe IJV cannulation [215]. However, studies in the field of expert performance demonstrate only a weak relationship between repetition and superior performance [61]. Furthermore, the rate at which the needle tip is inaccurately localized and tracked in ultrasound is underestimated, as CVC-related complications are self-reported [201], skewing risk factor analysis. In addition, it has not been established whether the difficulty in identifying and maintaining the needle tip in the image is dominated by an inherent inability of ultrasound guidance to identify the tip, or the operators technique and experience.

In short, the most critical contributing factors to the outcome of an ultrasound-guided central line procedure include needle tip visualization during the procedure and the expertise level of the clinician to use ultrasound guidance effectively. To address the challenges in needle tip visualization in ultrasound in central line procedures, an augmented reality ultrasound image guidance (AR-UIG) system was developed following the guidelines described in Section 2.3.

Multiple studies were carried out to evaluate the AR-UIG system and also to further investigate operator factors. The first study was designed to evaluate the system against conventional ultrasound guidance with novice operators. The second study involved expert operators and was designed to investigate multiple research questions. One of the objectives of the second study was to quantify the distance between the needle tip and ultrasound image plane, in conventional ultrasound guidance trials. This distance serves as a metric quantifying how effectively ultrasound guidance is used by experience operators to keep the needle in the image place during navigation and positioning. The other objective of the expert user study was to compare the performance of the AR-UIG system against conventional B-mode ultrasound guidance.

The remainder of this chapter is organized as follows. The design decisions for the development of the AR-UIG are discussed in section 4.2. The details of the novice user study and its results are discussed in Section 4.3. The expert user study, exploring multiple research questions, is presented in Section 4.4. This chapter also provides a critique of the design decisions made for the development of the AR-UIG system to guide further development and improvement of the guidance system. Discussion and future directions are presented in Section 4.5.

4.1.1 Contributions

1. This work provides a critique of the design decisions made for an AR-UIG system, that were based on the development guidelines described in Section 2.3. First of its kind, this work sets an example of how the guidelines can be used to bring design and development into the ballpark of an optimal AR-UIG system, and yet why the developers should keep a wary eye in development of such systems regardless of how well justified the design decisions may be.

2. In this work, an AR-UIG system, tailored to central line insertions, was evaluated against conventional ultrasound-only guidance in a novice user study using a custom-made phantom modeling a simplified central line access.

3. Evaluation of the AR-UIG system with expert operators was performed using a custom-made phantom. The phantom for this study was designed to model a challenging needle placement task for central venous access to ensure that experienced operators would not rely on their knowledge of the anatomy, and instead use ultrasound guidance for needle navigation and positioning.

4. This work introduces a novel technique for providing quantitative skill assessment for simulated central line insertions. Assessment of experienced operators' performance showed that the needle tip was not followed in ultrasound during needle insertion and placement. This finding emphasized that, without deliberate practice, great professional experience does not necessarily result in expert level performance. The proposed quantitative skill assessment technique has the potential to improve not only training and assessment, but also provide the means for deliberate practice for needle placement in the IJV. The application of this technique can be extended to other needle interventions.

4.2   Design and Development of the AR-UIG System

4.2.1   System Design

Hardware

The AR-UIG system comprised an ultrasound scanner (SonixTouch, Ultrasonix, Analogic Corp., USA) and a magnetic tracking system (Aurora, NDI, Canada). The scanner's built-in computer was used as the platform for the guidance system software with no additional computational resources being required. The magnetic field generator of the tracking system could be attached to the ultrasound scanner using an articulated arm (Fisso, Swiss) to facilitate its positioning close to the surgical scene. For tracking purposes, one Aurora 6-degrees-of-freedom (DoF) magnetic sensor was attached to a linear ultrasound probe (L14-5, Ultrasonix, Analogic Corp., USA) and another integrated into the hub of a standard surgical needle via a
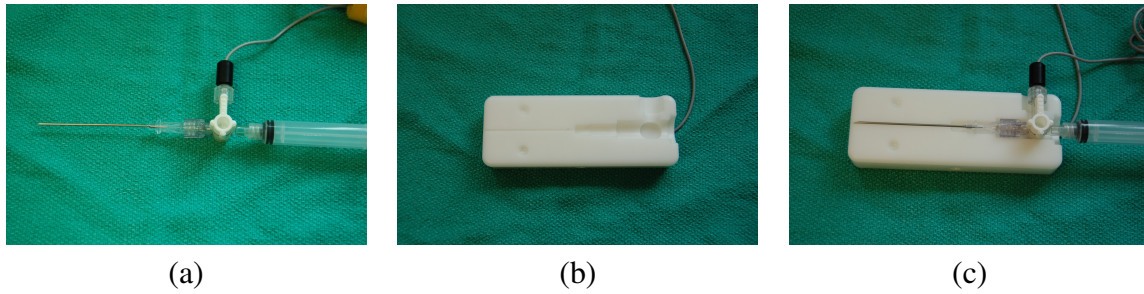
Figure 4.1: (a) The tracked surgical needle and (b) calibration widget used in the AR-UIG system. (c) To perform needle calibration, the needle is placed in the calibration widget.

T-connector, as shown in Figure 4.1a.

Calibration and Registration

Ultrasound calibration, i.e. the transformation between the coordinate system of the ultrasound image and ultrasound probe's tracking sensor, was performed using a point to line registration algorithm [37]. To calibrate the needle, a custom calibration widget was designed, Figure 4.1b, comprising a 6-DoF magnetic sensor, the negative imprint of the tracked needle assembly, and a set of hemispherical divots at known locations. This structure was registered to the global coordinate system of the magnetic tracking system using the known divot locations as fiducials [91]. When the needle was placed into the widget, Figure 4.1c, the spatial relationship between the needle and widget sensor specified the needle calibration. The ultrasound probe and needle were both calibrated prior to the intervention.

Interface

A needle guidance system was built, incorporating real-time ultrasound images and the tracking information of the surgical tools, shown in Figure 4.2a. The user interface for the needle intervention guidance system was a 3D AR environment (Figure 4.2b). Ultrasound images were streamed in real-time, via the Ulterius software development kit (Ultrasonix, Analogic Corp., USA), and displayed in the AR environment. The image quality and visibility were kept intact for optimal visualization. In addition, a virtual representation of the needle (in red), its trajectory (in blue), and one centimeter markings along the trajectory (in yellow) were

(a)   (b)
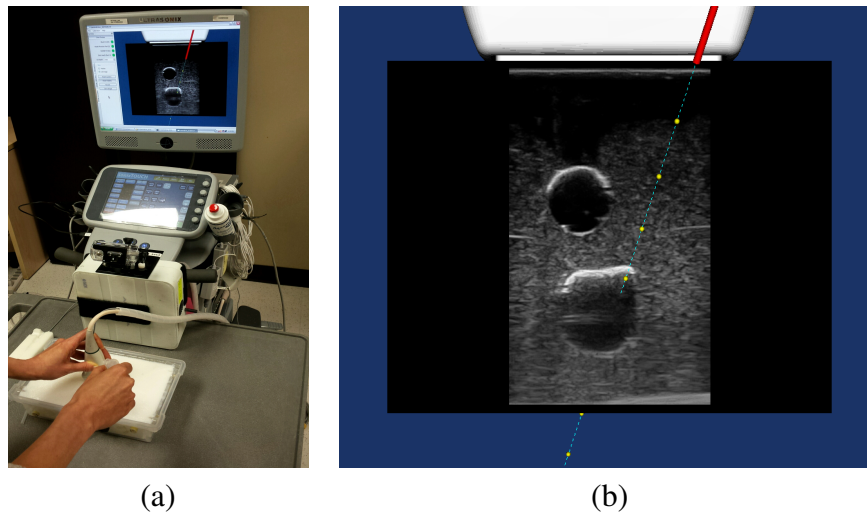
Figure 4.2: Example of the AR-UIG system in use (a) with a virtual surgical scene (b).

displayed, providing the user with a rapid understanding of the needle position with respect to the image plane. The choice of different colours ensured an easy differentiation of these components and an intuitive identification of the needle tip. All the surgical instruments were accurately calibrated and spatially registered, so that the reflection of the needle in ultrasound coincided with the cross-section of the needle's widget with the ultrasound image in the AR environment.

4.2.2 Motivation of the Design Based on Guidelines

In collaboration with an expert clinical user, several prominent design decisions were made in the development process, prior to evaluation. These decisions can all be motivated through the general guidelines for AR-UIG systems, specifically:

1. ***All the software was installed directly on the ultrasound scanner, and all hardware is physically attached to the scanner.*** Primarily, this was motivated by *minimizing the OR footprint*, but also encourages the system to be more *plug-and-play* in that all the equipment required to perform the intervention is localized to a single physical object. Additionally, this acted as a natural fail-safe mechanism in that all the materials required to perform the cannulation under standard ultrasound-only guidance are immediately

accessible.

2. ***The system includes a pre-calibrated probe and needle calibration widget.*** The work-flow for the system was designed to be as simple as possible, minimizing the number of calibration steps. As ultrasound calibration can be complicated and require special-ized phantoms and a water bath, the probe was pre-calibrated and would require only infrequent re-calibration. Because a new and sterilized needle is required for each pro-cedure in the clinic, the needle calibration was kept as part of the procedure. The needle calibration was designed to be performed in a simple (i.e. single action) manner, us-ing a calibration widget. Both of these features were motivated by the *plug-and-play* guideline.

3. ***The interface is minimal with only a virtual screen, start button and tracking error indicators.*** The design of the interface was minimized to limit the cognitive load and complexity of the user interface, motivated by *minimalism*. Only the components that are important to using the system were included in the interface. Since it is the most im-portant component of the interface, the virtual screen covered the majority of the display. The start-stop button would start and end the tracking information recording, restricting unnecessary data collection. Tracking error indicators were included in the side panel of the interface to notify the user if any of the surgical tools got out of the magnetic field. This particular design was motivated by *transparency*.

4. ***The needle widget has trajectory indication, depth markings, and colour-code.*** A large part of the design of the needle widget, specifically the colour code was to allow it to be easily identifiable while ensuring a level of *minimalism*. The addition of trajectory indication was to *minimize mental transformation* by not requiring the clinical user to estimate where the needle would intersect with the image plane, but to explicitly show it.

5. ***Ultrasound image is shown face-on.*** One facet of the system design explicitly stated by the clinician was to display the ultrasound image face-on, that is, with the highest

possible visibility. This made the image displayed by the AR system visually similar to that portrayed by the ultrasound scanner without AR, taking advantage of *similarity to existing workflow*, while emphasizing *high ultrasound visibility*.

6. ***A visible model of the probe is included.*** Motivated by the guideline on *minimizing mental transformation*, a model of the probe was displayed to reduce the mental transformation regarding the position of the probe and needle with respect to each other. In addition, displaying the probe model made the AR visualization more representative of the actual surgical scene, complying with the *representativeness* guideline.

7. ***No automatic target identification is employed.*** The IJV and carotid artery (CA) are easily identifiable in ultrasound. As a result, target identification was not categorized as a necessary component for the guidance system. Therefore, any form of target identification other than the ultrasound image itself, such as target segmentation or a virtual model of the target, was not incorporated in the AR-UIG system design. This design decision kept the interface simple and image visibility high, while eliminating image occlusion and other sources of error, including inattentional blindness, segmentation or registration error. This was done in accordance to the *minimalism*, *transparency*, and *high ultrasound visibility* guidelines.

As stated in Section 2.3, using guidelines during the design process often leads to improved systems with positive feedback and evaluation. It is worth emphasizing that this system, prior to user evaluation, received Health Canada clearance (Class III) for human trials. This is in part due to its similarity to existing AR-UIG systems, being motivated, and having its design explicitly justified, by the described guidelines.

4.3 Novice-User Study

4.3.1 Objective

The objective of this study was to evaluate the AR-UIG system against traditional ultrasound-only guidance in a phantom experiment with novice users. The hypothesis was that by displaying the needle trajectory and an improved visualization of the needle tip, the AR-UIG system would improve needle navigation and positioning in a phantom IJV.

4.3.2 Methods

Experimental Setup

In this experiment, a precalibrated 18 G Aurora needle (NDI, Canada) was used, which has a 5-DoF magnetic sensor integrated into its tip. Therefore, no needle calibration was required.

A phantom was designed and developed to represent an average IJV/CA anatomy, simulating a simple needle placement task. The mean diameters of the left IJV and CA in adults are 14 ± 5 mm and 6.5 ± 1.0 mm, respectively [118, 199], and the IJV is usually positioned laterally and anteriorly to the CA at a depth of 1 to 1.5 cm below the skin [52]. The phantom IJV and CA were designed to have a diameter of 12.3 mm and 8 mm, respectively, and the phantom IJV was positioned laterally and anteriorly to the phantom CA at a shallow depth from the surface of the phantom. To construct the phantom, plastic straws and metal tubes of different sizes were used as molds for the IJV and CA. Three supporting blocks, Figure 4.3a, were placed at three different angles along the length of the container on each side in order to account for anatomical variations and reduce training effects. Straws and metal tubes were placed inside the holes of the support block, Figure 4.3b. The plastic container was then filled with liquid polyvinyl alcohol (PVA) and subjected to two freezing-thaw cycles, forming solid PVA-Cryogel (PVA-C), which is a tissue mimicking material under ultrasound [197]. Next, the straws were removed from the PVA-C block, and penrose tubes filled with water were passed
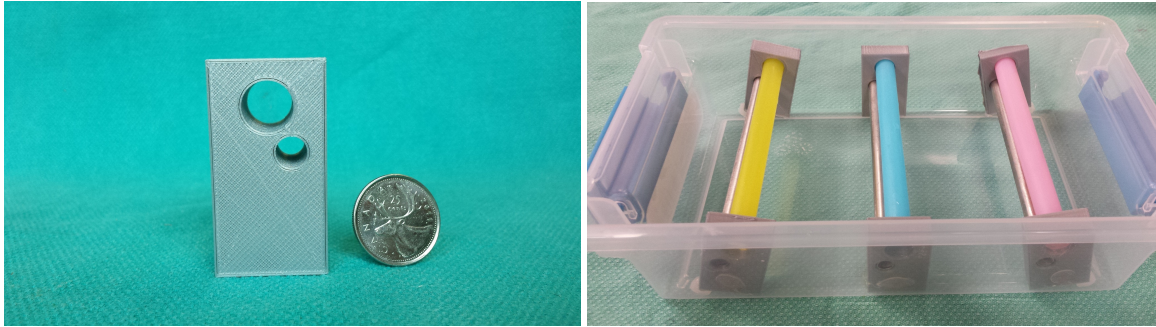
(a) A rapid prototyped support block to keep the straws and tubes in place.

(b) Phantom prior to introduction of PVA-C, showing three CA/IJV combinations.
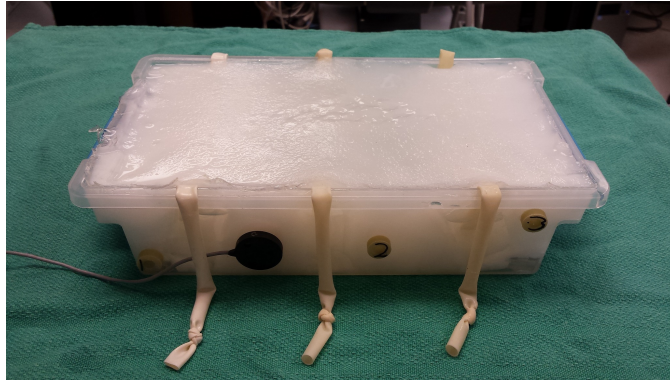
(c) The phantom used for the novice user study, consisting of a PVA-C block with water-filled tubes simulating the CA and IJV.

Figure 4.3: Phantom employed in the novice user study.

through the phantom CA vessels (Figure 4.3c) so that they could be pulsed, by squeezing one end periodically, to create a more realistic representation of the CA as visualized in ultrasound. The phantom IJV vessels were also filled with water, as a surrogate for blood. An Aurora 6-DoF magnetic sensor, 25 mm disc, (NDI, Canada) was placed on the phantom box as a tracking reference to accommodate for any overall shift of the phantom relative to the ultrasound probe. An ultrasound image of a healthy volunteer and the phantom are shown in Figure 4.4.

Study Design

Eighteen novice participants were recruited. After a brief training phase (approximately 20 min), in which the participants could familiarize themselves with both the ultrasound and AR guidance systems, the participants performed a set of two central line procedures, one using
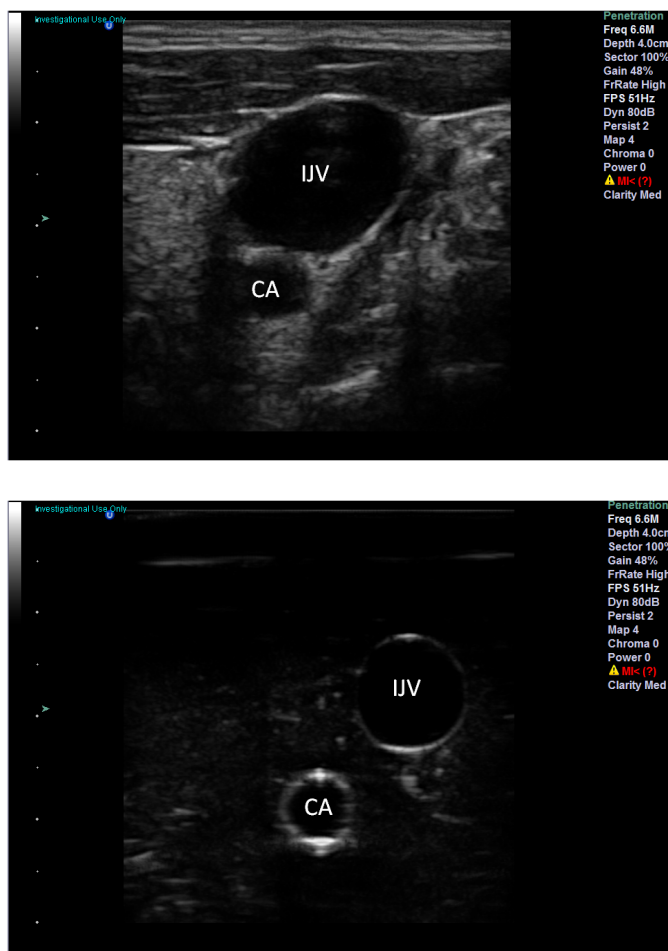
Figure 4.4: Ultrasound images of (top) a healthy volunteer and (bottom) the phantom. Each image is labeled with the CA and IJV for reference and employed in the user study.

the AR-UIG system and one only employing ultrasound. The order in which these tasks were performed was randomized to control for training effect. The task was defined as complete when the participant reported the needle to be in the IJV in the phantom. After a period of one week, each participant performed an additional set of central line procedures and the opposite order was used. In this study, the desired target for needle placement is any location within the phantom IJV. This is similar to the clinical CVC procedures, in which any location along the IJV inferior to the carotid bifurcation is considered adequate for central line insertion.

Evaluation Metrics and Statistical Analysis

Evaluation Metrics

For each procedure, two performance metrics were collected: procedure time and normalized needle path-length, i.e. tortuosity. The time taken to deliver the procedure was measured directly by our tracking software. Lower procedure times are desirable to minimize patient discomfort and to improve clinical workflow. The normalized tortuosity is a measure of how much the needle path deviates from a straight line during the procedure. Needle retraction, for example, would result in a longer needle path length. This metric is defined as the ratio of the actual traveled path divided by the length of a straight line connecting the start and end locations, Figure 4.5. This metric was calculated using the needle tracking measurement.
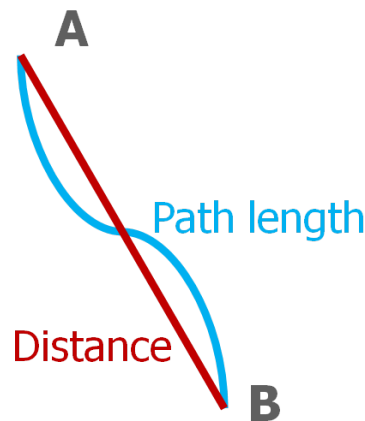
Figure 4.5: The normalized needle path-length is defined as the ratio of the traveled path, blue, to the shortest distance between the initial needle insertion point (A) and the final position (B), red.

Statistical Analysis

The results were processed using two-way analysis of variance (ANOVA) with the guidance system type (AR-UIG vs. ultrasound-only) and the trial number (1 to 4) as factors. To correct for multiple comparisons, the Holm-Bonferroni correction was used with a combined significance of $p \leq 0.05$.

4.3.3   Results

Box-plots organizing the data by the guidance system type are shown in Figure 4.6, with the AR-UIG system labeled as AR and ultrasound-only as US. The bottom and top edges of the box indicate the 25th and 75th percentiles, respectively. The whiskers extend to the most extreme data points not considered outliers, and the outliers are shown with the plus symbol. The central mark indicates the median. The 95% confidence interval (CI) on the average improvement in terms of time for AR compared to ultrasound-only guidance was 3.5 ± 1.4 s. The 95% CI on the average improvement in terms of normalized needle path-length for AR compared to ultrasound-only guidance was 150 ± 40%. The results demonstrated that both the system type and trial number had a significant effect on both metrics with no significant interaction effect. The AR-UIG system showed a significant improvement in terms of procedure time and needle path tortuosity. In addition, compared to ultrasound-only guidance, AR showed a lower interquartile range, implying more consistent performance across participants.
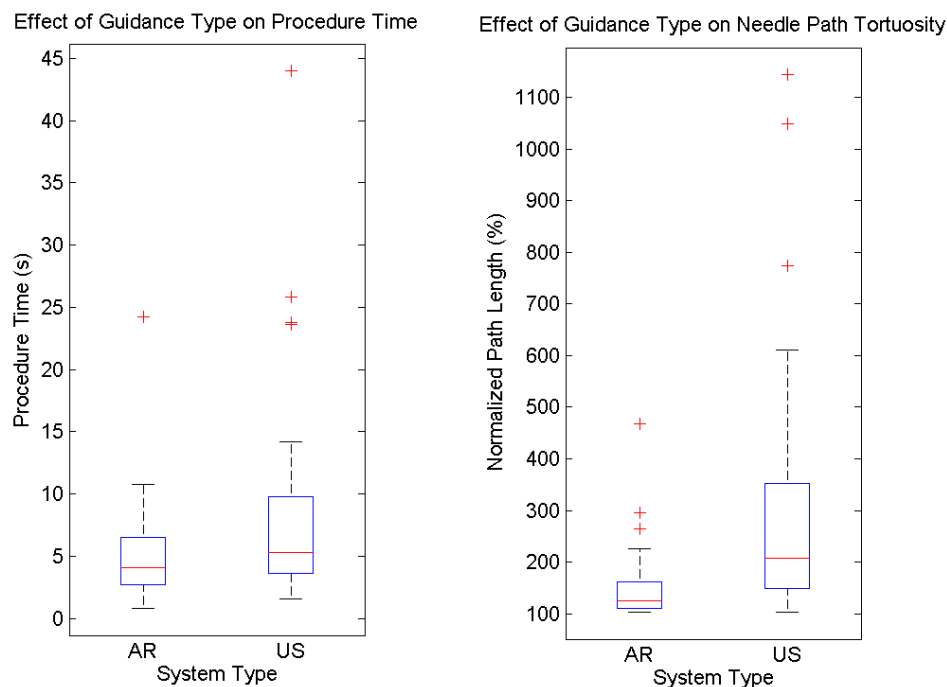
Figure 4.6: Results organized by guidance system type, with the AR-UIG system labeled as AR and ultrasound-only as US. The AR-UIG system significantly outperformed ultrasound-only in terms of both time and normalized needle path-length (tortuosity).

A significant training effect was detected in the ANOVA test. To examine this effect, the time and tortuosity results re-organized by trial are plotted in Figure 4.7. Because there was no significant interaction between system type and trial number, Figure 4.7 shows the results for ultrasound-only and AR guidance combined. For both metrics, there was a clear improvement over the first three trials which qualitatively confirmed the existence of a strong training effect for novice users for the procedure as a whole. For both time and tortuosity, the interquartile range decreased over the first three trials while keeping a consistent lower bound indicating that not only was performance better on average, it was also more consistent amongst participants.

In terms of safety, there was only one incident in which the phantom CA was punctured, and this trial occurred under ultrasound-only guidance. A larger study is required to determine if there is a significant difference in terms of the number of CA punctures given their infrequency under both guidance modalities.
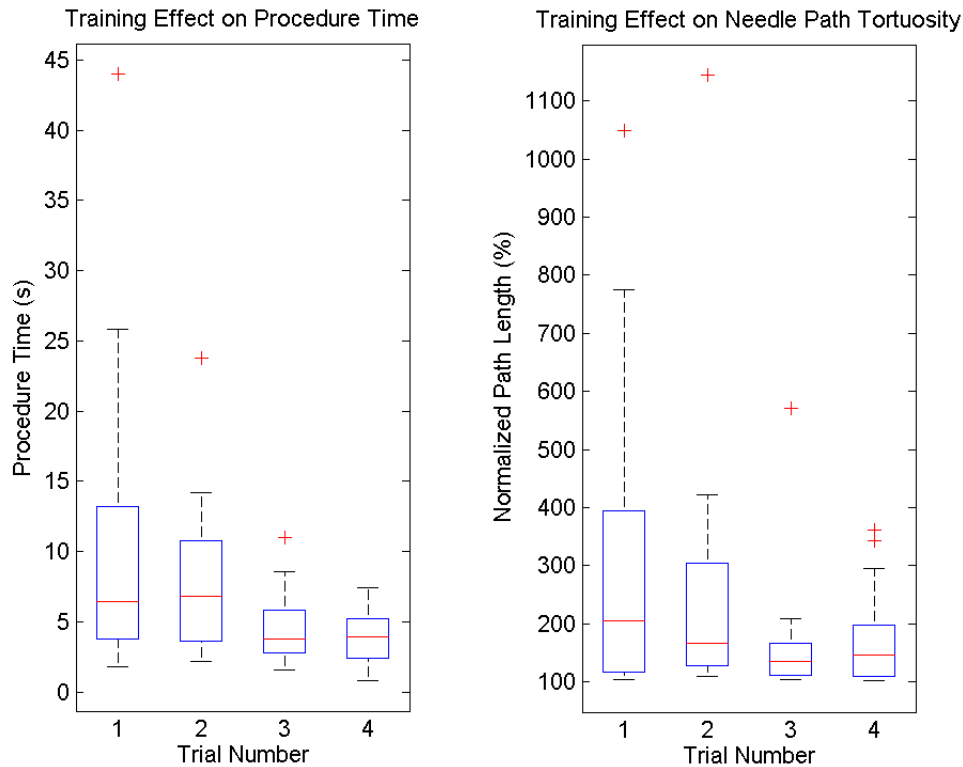
Figure 4.7: Combined results organized by trial number. A significant training effect was observed for both metrics which is evident from the first three trials.

4.3.4 Discussion

In this study, a preliminary evaluation of an AR-UIG system, tailored to central line insertions, was performed. This AR-UIG system combined a magnetically tracked needle and ultrasound probe into a lightweight framework that is run directly from the ultrasound scanner itself. This study is a precursor to evaluating this system using physicians who routinely perform central line procedures to better gauge clinical applicability, discussed in Section 4.4. For evaluation purposes, we investigated the performance of novice users guiding needle in a simulated central line procedure using an in-house designed phantom. The results indicated that the AR-UIG system significantly outperformed traditional ultrasound-only guidance in terms of both time and normalized needle path-length, implying that the AR can make the central line procedure easier while minimizing patient discomfort with novice operators. Additionally, the AR-UIG showed more consistent performance than ultrasound-only guidance with fewer outliers and a tighter interquartile range, suggesting that the AR-UIG system can accommodate for variations amongst interventionalists, such as in the interpretation of the ultrasound images. Although these results are preliminary and use a novice participant group, they are promising as the AR-UIG system enters trials with expert interventionalists.

4.4 Expert-User Study

4.4.1 Objectives

The objectives of this study were twofold. The first was to quantify the distance between the needle tip and ultrasound image plane in a simulated CVC procedure performed by experienced operators. This distance serves as a quantitative measure of how effectively ultrasound is employed for IJV needle placement. Our hypothesis was that not all experienced physicians closely follow the needle tip in the image and that the tip-to-image plane distance is greater in procedures with adverse outcomes, compared to successful trials. The second objective was to

assess the performance of the AR-UIG system against conventional B-mode ultrasound guidance with expert operators. This evaluation is a necessary step prior to embarking on clinical trials.

4.4.2 Methods

Experimental Setup

The human IJV is usually positioned lateral and anterior to the CA, with a wide degree of variation in size and position, as shown in the ultrasound images of two healthy volunteers in Figure 4.8. For the expert user study, a neck phantom was developed to simulate a challenging needle placement task by placing the CA over the IJV. This ensured that the participants would only use ultrasound, and not anatomical landmarks, for guidance, allowing isolation of operator factors and standardization of the level of procedure difficulty.

To construct the phantom, three sets of IJV and CA molds were 3D printed (Figure 4.9a) based on models obtained from a patient CT. The CA/IJV pairs were fixed in a rigid box at slightly different orientations to account for patient anatomical variations (Figure 4.9b). Next,

(a)   (b)
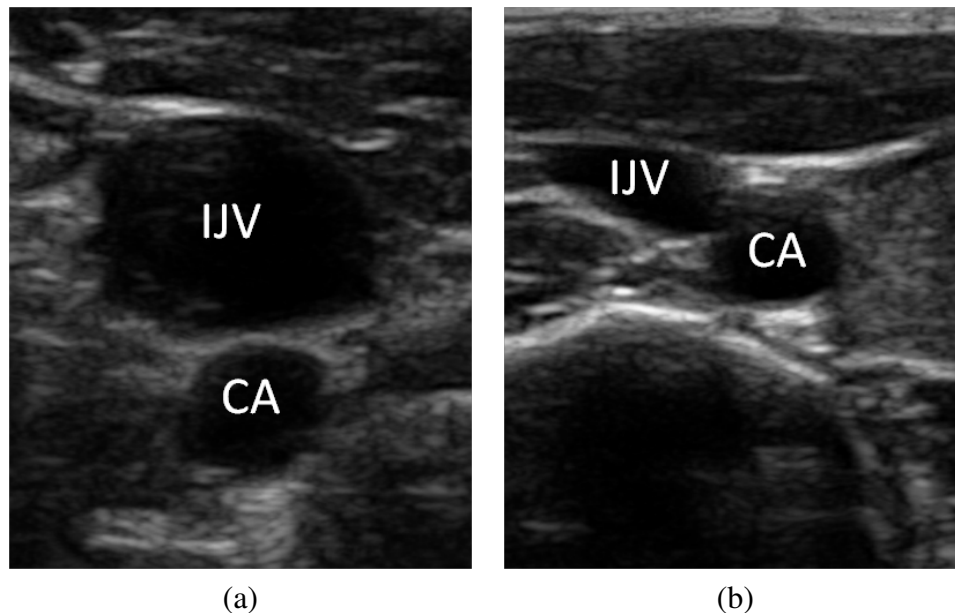
Figure 4.8: Ultrasound images of two healthy volunteers, displaying anatomical variations.
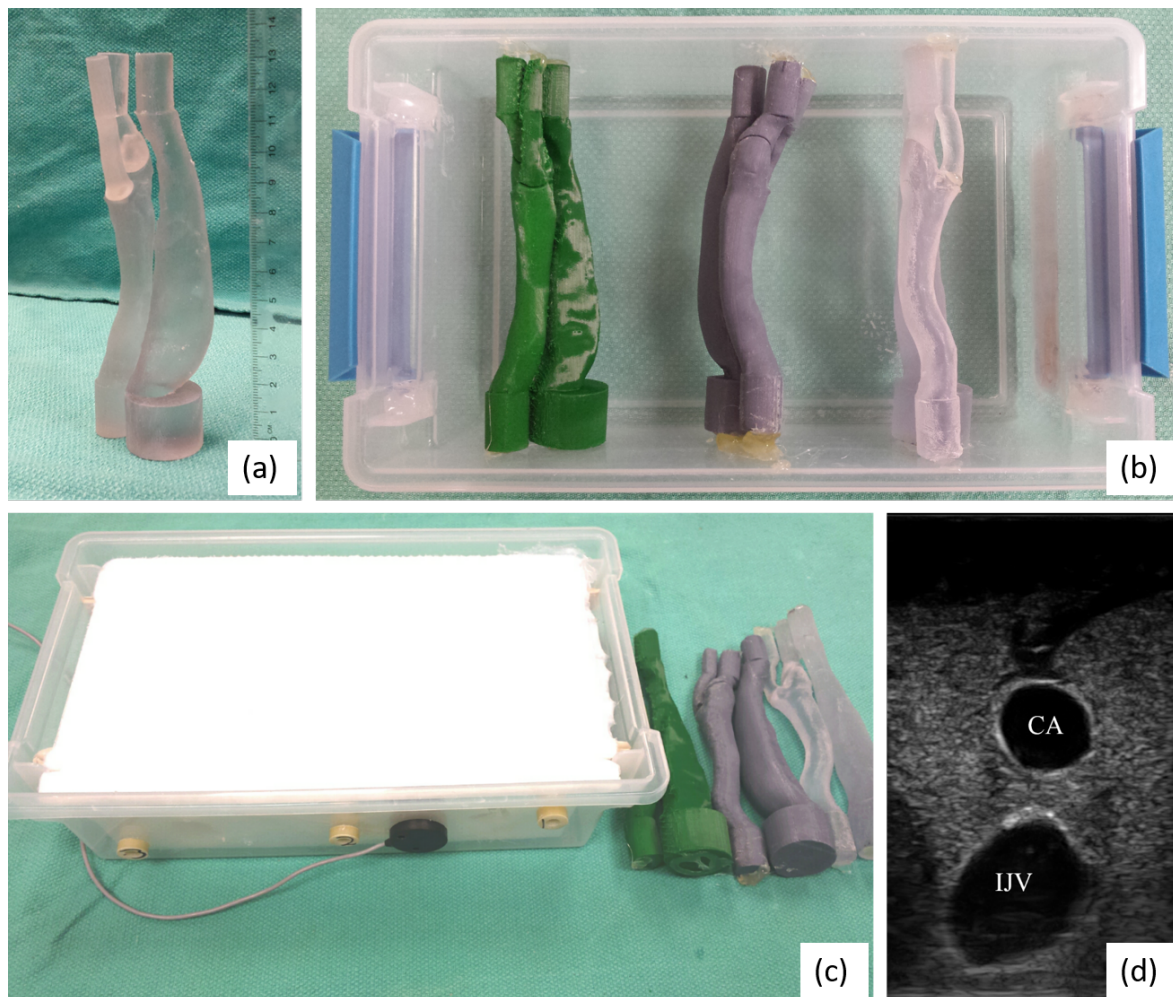
Figure 4.9: (a) A 3D printed IJV-CA pair in anatomic position. (b) Three sets of IJV-CA pairs used as molds for phantom construction. The molds were fixed in a container at different orientations to account for anatomical variation. Note the CA mold was placed over the IJV to represent a challenging case for needle placement. (c) The phantom after the PVA-C solidified and molds were removed, leaving hollow vessel-like structures inside the PVA-C. The hollow vessels were filled with water to simulate blood and serve as an ultrasound coupling medium. (d) An ultrasound image of one of the IJV-CA pairs in the phantom.

the box was filled with liquid PVA, which was subjected to a single freeze-thaw cycle [197]. Finally, the models were removed once the PVA-C had set (Figure 4.9c). The vessels were filled with water, which simulates blood and serves as an ultrasound coupling medium. Figure 4.9d shows an ultrasound image of the phantom. The phantom was tracked using a 6-DoF magnetic sensor attached to the box (Figure 4.9c). For evaluation purposes, a surface model of the vessels inside the phantom was created by segmenting a computed tomography (CT) scan of

the phantom. The surface model was registered to the phantom using a set of hemispherical divots rigidly attached to the phantom container (Figure 4.9c) and segmented in the CT volume.

The experiments were performed using a standard surgical needle commonly used for IJV cannulations (Figure 4.1a). The needle was calibrated prior to each experiment using the technique described in Section 4.2.1.

Study Design

Expert operators, including physicians, residents, and fellows in the anesthesiology departments at our institution (University Hospital, London Health Sciences Centre, London, Canada), were invited to participate in this study. This study was conducted under Research Ethics Board (REB) protocol #107254. The participants were first asked to read the *Letter of Information and Consent*, in which the study objectives and procedures were explained. Upon providing informed consent, participants were asked the following questions: (1) Approximately, how long have you been performing the IJV cannulation procedure? (2) Approximately, how many times a month do you perform the IJV cannulation procedure?

Next, participants underwent a brief training phase in which the task and and visualization used in the AR-UIG was explained to them, and they could familiarize themselves with the AR-UIG system, the phantom, and its ultrasound images. Prior to the start of the study, participants were asked to perform the phantom IJV cannulation using the AR-UIG at least once. After they felt comfortable with the AR-UIG system, the participants were asked to perform an IJV needle placement in a phantom under both ultrasound-only guidance and AR-UIG. The order in which the guidance system was assigned was randomized. It was emphasized that they should perform the task as they would on a patient. It was the participants' choice to use the transverse or long-axis view [206] and insert the needle out-of-plane or in-plane, as illustrated in Figure 4.10. As this study focused on a targeting task only, rather than the interpretation of ultrasound images, the phantom IJV in the image was identified and pointed out to the participant prior to needle insertion to clarify any confusion about its position. The participants were
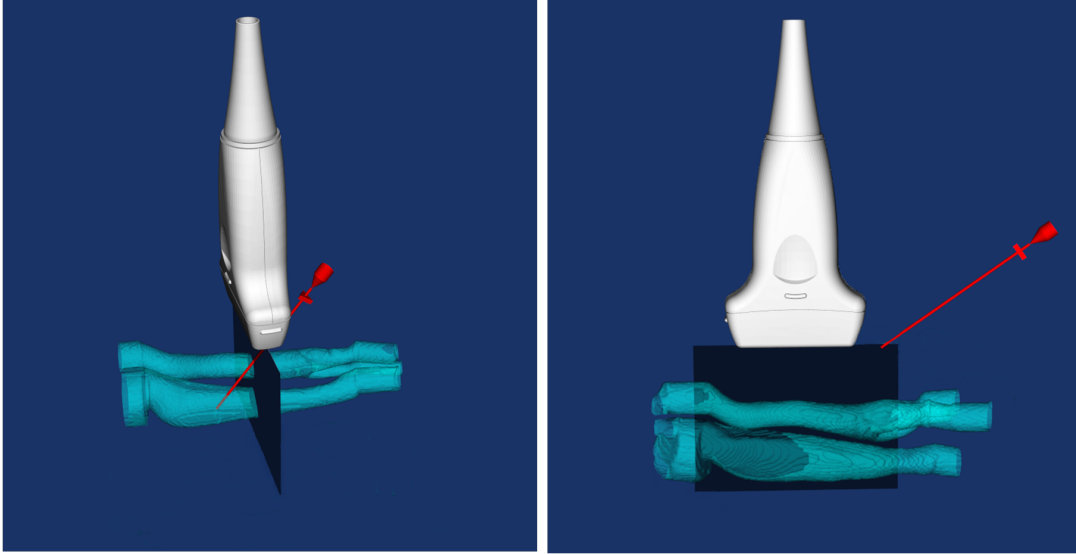
Figure 4.10: (Left) In the most common ultrasound guidance technique, the transverse visualization is used, and the needle is inserted out-of-plane, proceeding through the image plane. (Right) In the in-plane approach, the needle is inserted in the ultrasound image plane, displaying the entire length of the needle in the image. Commonly, the long-axis view is used with the in-plane technique. However, in a modified approach, the probe could be placed in the long-axis, and the needle inserted out-of-plane; this is known as the oblique approach.

asked to report the completion of the task when they felt confident that the needle was inside the phantom IJV. The needle, ultrasound probe, and phantom were tracked at all times, for both guidance systems, and the tracking information for all surgical instruments were recorded at 30 Hz.

4.4.3   Quantitative analysis of expert operator factors

This section addresses the first objective of the expert user study, that is quantifying the distance between the needle tip and the image plane during needle navigation and placement in a phantom IJV. This work presents the first quantitative analysis of the needle tip localization error in ultrasound and evaluates the efficacy of ultrasound guidance implementation by experienced operators.

Evaluation Metrics and Statistical Analysis

Evaluation Metrics

Quantitative analysis and evaluations were performed after completion of all experiments. The primary performance evaluation metrics were the success of the procedure and the distance between the needle tip and image plane. We compared the needle tip to image plane distance between the successful and unsuccessful groups to evaluate our hypothesis that keeping the needle tip closer to the image plane is predictive of successful outcomes. The secondary evaluation metrics included procedure time and normalized needle path-length, which were compared between successful and unsuccessful groups. The evaluation metrics are further explained in the following paragraphs.

Success of the procedure was defined as needle placement inside the phantom IJV without puncturing the CA. To determine success, a virtual environment was constructed comprising a model of the vessels, ultrasound image plane, and needle. Using the tracking information, the procedure was duplicated in the virtual environment. Figure 4.11 illustrates one time-point of the replay, i.e. the duplicated procedure, from which an independent observer determined whether the procedure had been successful. The ultrasound guidance mode used during the procedure was also identified from the replay.

Distance analysis was performed using the position measurements with a focus on the out-of-plane approach, because of its common use in CVC procedures [201]. To account for the possible lack of ultrasound guidance immediately after needle insertion, the first intersection of the needle tip with the image plane was marked as the start of the procedure for distance and time analysis. In the out-of-plane cases, the distance between the needle tip and image plane along the needle shaft was calculated for the entire procedure. A negative distance indicated that the needle tip was behind the image plane and had not penetrated it. Conversely, a positive distance indicated the needle tip had passed through the image plane (Figure 4.12). The average absolute distance was calculated for each participant.

For the in-plane cases, since the needle trajectory is entirely within, or is parallel to the
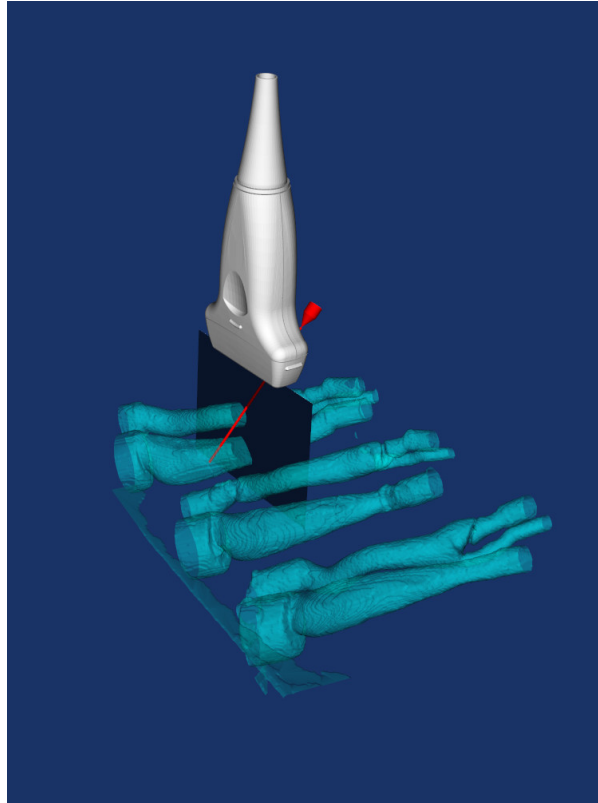
Figure 4.11: Using the tracking information, a virtual representation of the needle (red), ultrasound image plane (black), and three CA-IJV pairs in the phantom (light blue) were displayed in a virtual reality environment. This allowed replaying the procedure for validating the needle tip position with respect to the ultrasound image plane and target throughout the entire procedure.

image plane, the shortest (i.e. perpendicular) distance between the needle tip and image plane, was calculated. While the perpendicular distance is a suitable metric for the in-plane approach, it could be misleading for the out-of-plane procedures and was not used in such cases. For example, at steep insertion angles, while the perpendicular distance between the needle tip and image plane may be relatively small, the actual intersection of the needle tip and image would occur much further along the needle trajectory.

The procedure duration and normalized needle path-length for each trial were calculated using the timestamps and position measurements recorded by the tracking software, respectively.
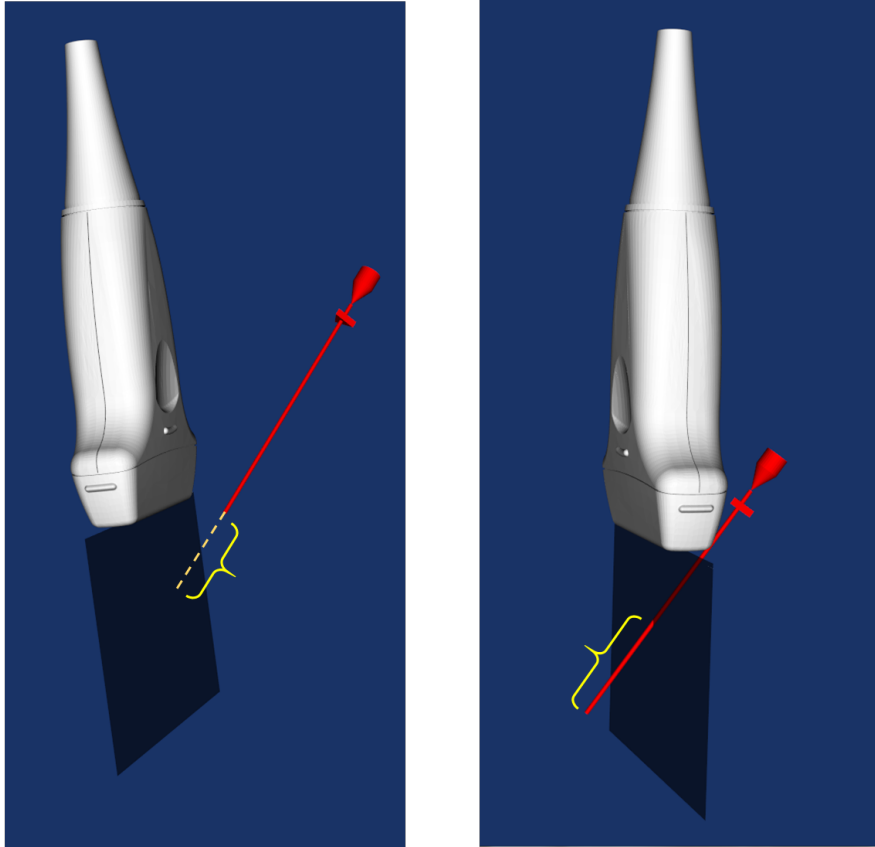
Figure 4.12: The distance between the needle tip and the ultrasound image plane was calculated along the needle shaft. (Left) a negative distance indicated that the needle tip had not intersected the image plane. (Right) a positive distance indicated the needle tip was through the image plane.

Statistical Analysis

The metrics used to compare the successful and unsuccessful procedures (in terms of distance, time, and normalized path-length) include: mean, median, standard deviation (STD), and 95% CI on the difference between means. Statistical significance was determined via unpaired two-tailed t-tests.

Results

Twenty-five physicians were recruited, and one dataset was omitted from analysis due to tracking failure. The results obtained from the remaining 24 datasets are presented here.

All participants were experienced in using real-time ultrasound guidance for CVC proce-

dures, and on average had 10 years of experience in IJV cannulations, with a median of 8.5 years. The minimum and maximum years of experience were 2 and 30, respectively. The mean and median of the number of procedures performed per month by all participants were 8.7 and 5.5, respectively.

Different ultrasound guidance techniques were used by the participants for needle placement. In the 24 successfully recorded procedures, three participants used the in-plane technique, 18 employed the out-of-plane technique, two switched to the in-plane technique after failing to achieve a successful needle placement with the out-of-plane approach (with one using the transverse view and the other using the long-axis view), and one inserted the needle at a steep angle approximately parallel to the image plane, without intersecting the image plane. The techniques used in the last three cases are referred to in the following discussion as mixed approaches.

Overall, 14 procedures were performed successfully and 10 unsuccessfully. In the out-of-plane cases, two participants failed to place the needle in the IJV, four punctured the CA, and three punctured the CA and also failed to cannulate the IJV. All three in-plane procedures were performed successfully. In one of the mixed approaches, the CA was punctured. The incident rate of phantom CA puncture was 8/24 (33%). In the 10 unsuccessful cases, the participants had, on average, 10.4 years of experience and performed the procedure 9.2 times per month.

In the out-of-plane cases, the distance from the needle tip to the image plane was calculated along the needle shaft after the first image plane crossing mark. Examples of the calculated distances are shown in Figure 4.13. If the needle tip had been followed in the image, its distance to image plane would consistently be close to zero. The average needle tip to image plane distance for each procedure was calculated using the absolute value of the distances. The statistical analyses of the evaluation metrics for the out-of-plane procedures are summarized in Table 4.1. The needle tip to image plane distances for unsuccessful procedures, 17.6 mm, was significantly greater than for successful trials, 11.5 mm, ($p = 0.04$). The results from other metrics strongly suggested that compared to successful trials, unsuccessful cases took
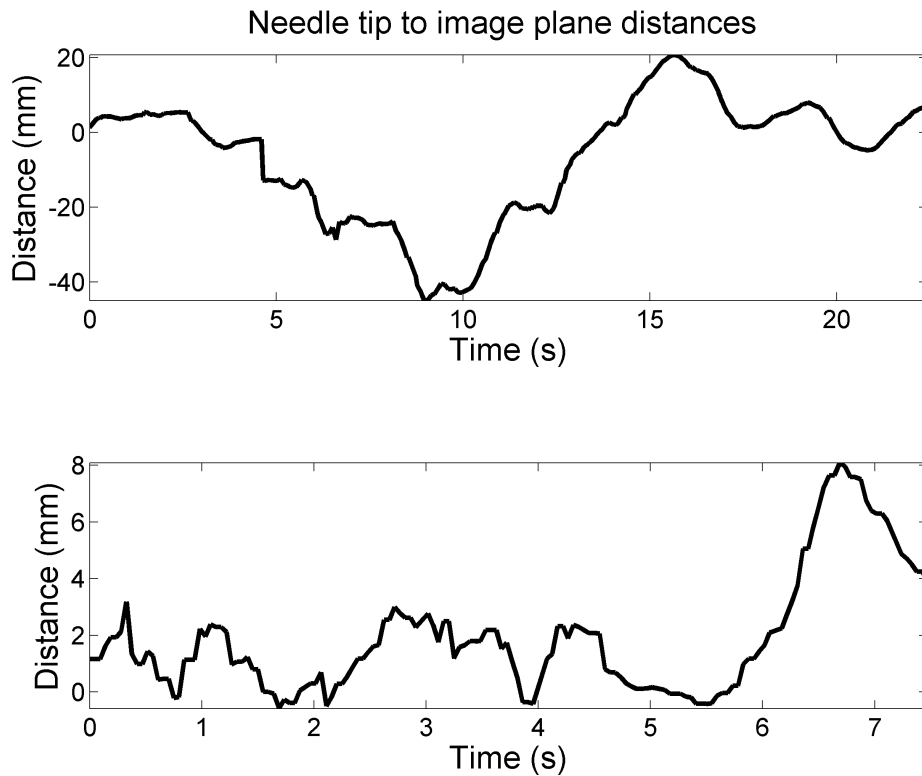
Figure 4.13: Examples of needle tip to image plane distances for two participants during needle placement in the phantom IJV. Negative distances indicate that the needle tip had not crossed the image plane, while positive distances indicate the needle tip was through and past the image plane. If the needle tip was kept in the image, the distances between the image plane and needle tip throughout the procedure would be close to zero.

longer ($p = 0.07$) and had a greater normalized path-length ($p = 0.13$). We observed that most participants, particularly in the unsuccessful cases, did not move the probe to continuously keep the needle tip in the image plane. Instead, after the initial scanning to localize the insertion site and part of the IJV to cannulate, the probe was kept fixed over the selected region of interest

In the in-plane cases, the probe was positioned in two different ways while keeping the needle length in the image plane. In two cases, the probe was positioned along the long-axis and in one case along the short axis (the oblique approach) [215]. All these three procedures were performed successfully. The analyses of the evaluation metrics for the in-plane cases are provided in Table 4.2.

Table 4.1: The average distance between the needle tip and image plane, the procedure time, and the needle path-length ratio for the out-of-plane procedures (N = 18). The difference between the means for a given metric was calculated by subtracting the mean of unsuccessful trials (N = 10) from the mean of successful procedures (N = 14). Therefore, the negative sign indicates a lower value of the metric for the successful procedures, which is a desirable effect. The asterisk indicates statistical significance ($p < 0.05$).

	Average Distance (mm)*		Time (s)		Normalized Path-length	
	Successful	Unsuccessful	Successful	Unsuccessful	Successful	Unsuccessful
Mean ± STD	12±5	18±6	14±7	23±12	5±4	10±10
Median	12	17	13	22	3	6
Mean Difference (95% CI)	-6.1 (-11.9,-0.03)		-9.0 (-19.1,1.0)		-5.8 (-13.5,1.9)	

Table 4.2: The average perpendicular distance between the needle tip and image plane, procedure time, and needle path-length ratio for the in-plane procedures (N = 3; all successful).

	Average Distance (mm)	Time (s)	Normalized Path-length
Mean ± STD	3±1	16±11	3±3
Median	4	16	2

In two of the mixed approach cases, the needle was completely retracted from the phantom to transition from the out-of-plane to in-plane technique, leading to large variations in the position measurements. In the third case, using the transverse view and an out-of-plane needle insertion technique, the needle was kept outside of and parallel to the image plane during most of the procedure. To avoid introducing error or bias, we refrained from manually segmenting these datasets into in-plane and out-of-plane cases. These three datasets were excluded from analysis.

Discussion

The importance of real-time assessment of needle position in ultrasound during IJV cannulation cannot be overstated [33]. In an effort to better identify the limitations and opportunities for further improvement of real-time ultrasound guidance, we quantitatively analyzed its implementation by experienced operators in a simulated IJV cannulation experiment, with the needle tip-to-image plane distance as the primary metric. Quantitative assessment of needle tip insertion under real-time ultrasound guidance for IJV cannulations and application of tracking technology for post procedural analysis was not investigated prior to this work to the best of our knowledge.

Compared to its commercial counterparts, the customized phantom was cost effective and allowed simulation of a challenging IJV access scenario to reinforce the use of real-time ultrasound for needle guidance. The main advantage of the phantom study was that it allowed isolation of operator factors, removing complications caused by environmental and patient factors. The rate of phantom CA puncture incidence in this study (33%) was higher than the reported incident rate in clinic (1.5%) [124, 132], likely due to performing a rare and challenging needle placement task.

At our institution, real-time ultrasound guidance is taught with a focus on the out-of-plane technique with transverse visualization and is routinely used for central line insertions. However, the participants included staff and fellows trained at other Canadian institutions or abroad. We observed a relatively large degree of variability in how ultrasound guidance was employed. In one scenario, while employing transverse visualization, the needle was inserted almost perpendicular to the phantom surface and parallel to the image plane. In this approach, the needle tip cannot be easily visualized in the image and the movement of the phantom, caused by needle insertion, was likely used for guidance rather than the needle tip location. Due to compressibility of the IJV, in practice, steep insertion of the needle may increase the risk of penetrating the posterior vessel wall and possibly the CA. Another uncommon technique used by two participants was the oblique approach, which is not recommended due to the increased risk of arterial

punctures when the CA is positioned medially to the IJV [215]. Apart from these cases, the participants chose the out-of-plane technique with the transverse view or the in-plane approach with the longitudinal visualization. Advantages and disadvantages of both in-plane and out-of-plane techniques have been comprehensively discussed in the literature [72, 203].

We observed that, in most cases, ultrasound guidance was not fully employed to localize and visualize the needle tip during needle insertion and placement, but rather used as an augmented landmark technique to identify the target and insertion site. The suggested technique to achieve direct visualization of the needle tip is to tilt or scan the transducer back and forth, especially when deflected out of the image [33, 149]. Failure to adjust the probe to locate the needle tip during the procedure led to the relatively large distances between the needle tip and image plane in the unsuccessful cases. In the successful out-of-plane cases, most participants followed the needle tip closely by scanning the ultrasound probe or moving it side to side during needle insertion and positioning in the phantom. We observed a significant difference between the average needle tip to image plane distance for the successful and unsuccessful procedures, suggesting that closely following the needle tip in the image positively affects procedure outcomes. The average distance in the unsuccessful trials, 18 ± 6 mm, was relatively large, considering the average diameter of the right IJV in adults (17 ± 5 mm) [199].

In the in-plane cases, the needle was kept close to the image plane (3 mm on average) and due to ultrasound beam thickness, the needle was likely visualized during the procedures, even if it was not placed exactly within the image plane. The disadvantage of this approach however is that the ultrasound probe may slide over the CA without the operator being aware, especially in cases where the CA and IJV lie parallel to one another, which may result in inadvertent CA puncture. Comparing the safety of different ultrasound guidance techniques requires further investigation in a larger study and is outside the scope of this work. Analysis of the secondary metrics suggested that unsuccessful procedures may take longer and feature more tortuous paths compared to successful trials. This may suggest a difference in expertise between those who continuously followed the needle in ultrasound versus those who did not.

While keeping the needle in the image plane is challenging, some participants did in fact maintain the tip in the ultrasound beam during the entire procedure, indicating that correctly identifying and following the needle tip is possible. However, performing a large number of rather simple procedures does not help develop the cognitive and associated skills that lead to superior performance [201]. Achieving expert level performance requires deliberate practice and is not necessarily correlated with greater professional experience [61]. Closely following the needle tip in ultrasound may just be a matter of deliberate practice. Despite current limitations of B-mode ultrasound guidance, such as 2D visualization of a 3D environment, CVC procedure outcomes could be improved by rigorously following the needle tip in ultrasound. In addition to deliberate practice, greater emphasis on the importance of needle tip tracking in real-time ultrasound during training and skill assessment may accelerate acquisition of advanced skills.

Currently, while there is no standardized training for real-time ultrasound guidance in CVC procedures, and skill is assessed purely by observation [191], tracking technologies open new avenues for training and quantitative skill assessment. Moreover, such technologies enable the integration of an AR environment in training simulators and image guidance systems [169]. The goal of AR is to complement the clinicians conventional visualization with necessary information, and AR environments have proven to be reliable and effective in minimally invasive neurosurgical interventions [139]. Despite the wide use of tracking technologies and AR environments in image-guided surgery and therapy [170], their applications in anesthesiology have not been thoroughly explored. Most recently, a study on the feasibility of AR simulators for training in central line showed promising results [176]. However, application of tracking technology for post-procedural analysis and quantitative skill assessment in CVC procedures was not investigated prior to this work. Integrating tracking technology into ultrasound guidance systems could enhance ultrasound training by providing the means to record the trainees performance for a retrospective quantitative analysis and assessment.

Recently, several ultrasound scanners have integrated AR environments to overlay a virtual

representation of the needle position and trajectory on real-time ultrasound images to improve needle visualization for multiple applications [223], similar to the AR-UIG presented in this chapter. Tracking technology and AR guidance systems may address challenges in training and retaining of real-time ultrasound guidance skills.

In summary, this study provided the first quantitative analysis of the needle tip to image plane distance as a measure of efficacy in implementing real-time ultrasound guidance. The needle tip was not always followed in the image, resulting in a relatively large distance between the needle tip and image, which was significantly greater in unsuccessful procedures compared to the successful ones. While further investigation in a clinical setting is required, we expect similar findings in the clinic.

4.4.4   AR-UIG system evaluation

This section addresses the second objective of the expert user study, that is to evaluate the performance of the AR-UIG system against conventional B-mode ultrasound guidance with expert operators.

Evaluation Metrics and Statistical Analysis

Evaluation Metrics

The evaluation metrics used were as follows: (1) occurrence of phantom IJV puncture, (2) occurrence of phantom CA puncture, (3) whether or not the procedure was successful (i.e. IJV puncture without CA puncture), (4) procedure time, and (5) normalized needle path length, i.e. tortuosity. To evaluate the first three metrics, using the tracking information, the procedure was replayed after completion of the experiments. In the replay of each procedure, the position of the needle, ultrasound image plane, and a model of the phantom were displayed from two different angles. From the replay, an observer carefully identified the success of the procedure and occurrence of adverse outcomes, such as CA puncture and failure in placing the needle in the IJV. The time taken to complete the procedure was measured directly by our tracking

software. Lower procedure times imply minimized patient discomfort and improved clinical workflow. The position measurements from the tracking information were used to calculate the normalized needle path-length.

Statistical Analysis

Statistical significance for the first three metrics was determined via a chi-square test, and the latter two via a two-tailed t-test, applied to results from the successful procedures, i.e. procedures in which the needle was placed in the phantom IJV without puncturing the CA.

Results

Twenty five experienced physicians were recruited for the study. One dataset was excluded from analysis due to tracking failure. The average experience of the participants in IJV cannulations under ultrasound guidance was 10 years. We observed that the phantom CA was punctured inadvertently and also that the final position of the needle was not always inside the IJV under both guidance scenarios. Results are shown in Table 4.3 with time and tortuosity results summarized for successful procedures. After statistical correction, no metric displayed a significant difference between the two guidance systems.

Table 4.3: Quantitative results for both guidance systems.

	ultrasound-only ($N = 24$)	AR-UIG system ($N = 25$)
Number of IJV cannulations	19	24
Number of CA puncture	8	9
Number of successful procedures	14	16
Procedure time ± STD (s)	26±31	37±35
Normalized needle path length ± STD	4±4	6±5

Discussion

Unlike the novice user study, the performance of the AR-UIG system was not statistically different from ultrasound-only guidance with expert operators. The participating clinicians had a high level of experience with ultrasound guidance. However, their practice with the AR-UIG was very limited in comparison. While these factors may have affected the results, the unexpected user variability and certain aspects of the guidance system could have contributed to the lackluster outcomes. A discussion on the user variability and a critique of the design decisions are provided in the following.

User Variability

Despite a close collaboration with an expert anesthesiologist, we faced an unexpected and large degree of variability in how the participants employed both the ultrasound-only and AR-UIG systems. While positioning the ultrasound image plane axially and taking an out-of-plane approach with respect to the needle trajectory (Figure 4.14a) is the technique taught in our institution, some participants performed the procedure using two different in-plane techniques. One approach positions the ultrasound probe coronally (Figure 4.14b), and the other has the ultrasound probe axially positioned, similar to the out-of-plane approach (Figure 4.14c), but both use an in-plane needle trajectory.

This variability in use was not anticipated during the development process. Thus, the system was optimized towards a particular approach determined by the collaborating clinician and supported in the literature [20]. However, there is no standard method of teaching and practising ultrasound guidance for central venous cannulation, and some of the participants in our study were trained in different institutes, where ultrasound guidance may be taught differently. From our experience, after years of using ultrasound guidance, clinicians tend to find techniques that work best for them, which may be different from the technique being taught or even best clinical practices.

Critique of Design Decisions

While compliant with and justified by the guidelines, the design decisions on the ultrasound

(a)   (b)   (c)
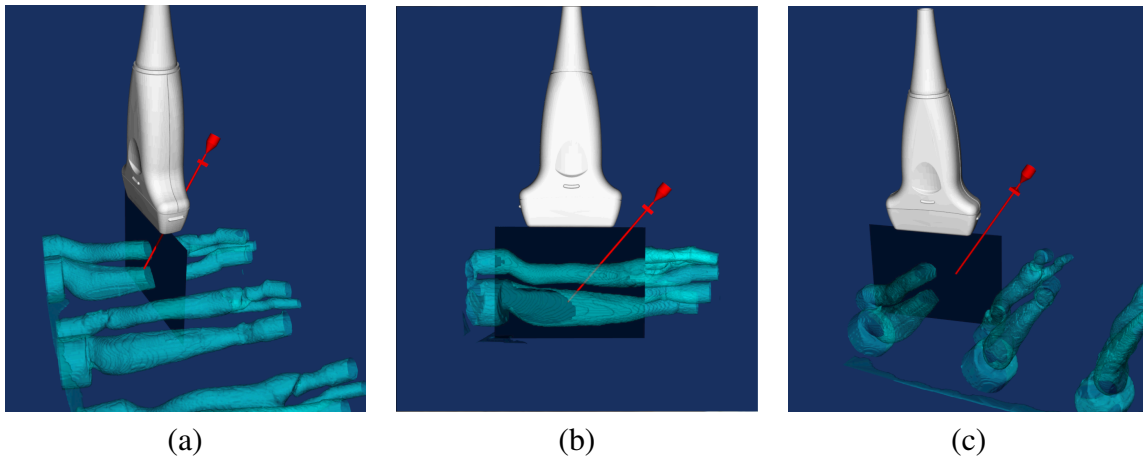
Figure 4.14:   Different needle placement techniques for central line insertion are presented. These illustrations do not represent the visualization used in the guidance system during the procedure. Commonly, the needle is inserted out-of-plane (a), proceeding through the image plane, with ultrasound providing a transverse view of the vessels. The needle can also be placed in-plane, with ultrasound displaying the vessels longitudinally (b) or cross-sectionally (c).

image display, interface, and needle model visualization (items 3, 4 and 5 on our list of design decisions, Section 4.2.2) resulted in suboptimal evaluation outcomes.

Displaying the ultrasound image face-on resulted in partial occlusion of the image by the needle's virtual representation. By showing the ultrasound image on a 2D plane, we did not take advantage of the 3D nature of the AR environment, which became a limitation especially in the in-plane cases, or in the out-of-plane cases in which the needle was inserted at a steep angle. While the data could have been presented to the operator using stereoscopic 3D, this approach, requiring wearing of additional eyewear and display on a monitor separate from that of the ultrasound scanner, was deemed to be too intrusive.

In the in-plane approach, the ultrasound image and the needle were often parallel. Due to the visualization in a 2D plane, the needle model would have a similar visualization regardless of its distance to the image plane, resulting in uncertainties about the needle position. Also, our system was not designed to provide a measure of distance between the needle and the image plane for such situations. The needle model would also occlude the ultrasound image, preventing the operator from using ultrasound to identify the needle's true position. As a result, the guidance provided was not optimal for the in-plane approach.

In the out-of-plane approach, at steep insertion angles, the needle model occluded the view of the trajectory, resulting in suboptimal use of the guidance system for needle navigation and placement. In such cases, displaying the image at an oblique angle would perhaps result in a more effective use of the navigation system. The occlusion likely had a counter effect on mental transformation and cognitive load.

Ultimately, trading ultrasound visibility with minimizing needle trajectory occlusion is a result of conflicting interface design criteria. By having a single view of the virtual scene, (i.e. an emphasis on minimalism) the system was not capable of simultaneously providing the clinician with a view of the ultrasound image and of the surgical scene as a whole, hampering its ability to handle the variability of approaches in the procedure.

Keeping the needle tip in the image plane is a key safety measure in practice. The needle and trajectory models were designed to simplify needle tip localization and insertion trajectory. However, some participants inserted the needle upon finding an optimal trajectory without scanning the phantom along the trajectory to ensure a clear path prior to needle insertion or without following the needle tip in ultrasound during needle navigation, resulting in inadvertent CA punctures. While this issue may have been resolved with more training, the AR-UIG system did not encourage best clinical practices.

4.5 Discussion and Future Directions

This chapter evaluated the performance of an AR-UIG system tailored to central line procedures against conventional ultrasound-only guidance in iterative user studies; explored the application of the system for quality assurance and quantitative skill assessment; and presented a critique on the design decisions made for the development of the AR-UIG system.

Performing user studies under laboratory study conditions is an important aspect of image guidance system evaluation, which aims to determine whether the system is accepted by the end-user and fulfills its specific purpose [98]. Conducting a novice user study, prior to evaluat-

ing an AR-UIG system with experienced clinicians, provides a baseline for the comparison and assessment of the system, eliminating bias towards any of the image guidance systems under study. It is also expected that if the AR-UIG's performance does not surpass that of the conventional guidance system in a novice user study, it is unlikely to achieve different results with an expert cohort. However, achieving performance improvement with an AR-UIG system in a novice cohort does not assure similar findings with expert operators. Therefore, it is necessary to perform iterative user studies with novice and expert operators prior to clinical evaluations.

Despite the favourable findings in the novice user study, we did not observe any significant performance improvement with the AR-UIG system compared to conventional ultrasound guidance in the expert user study. To address the issues caused by the visualization used in the AR-UIG system, currently, this system is going through a process of re-development. We have consulted with another clinician trained at a separate institution, specifically chosen for her diverse training background. Our consulting clinicians will also be involved in small-scale evaluations throughout the re-development of the AR-UIG. In the next iteration of the system, the screen will be split in two windows; one showing the ultrasound image face-on and the other showing the image at an oblique angle along with the virtual objects. This visualization may address issues concerning depth perception and image occlusion without reducing the visibility of the ultrasound image.

One of the major concerns in ultrasound-guided central line insertions, deserving of greater attention, is the lack of standardized and adequate training [20]. In this context, in addition to their use in an interventional setting, AR guidance systems could be used for enhanced teaching and training purposes. Advantages of AR training has been demonstrated for ultrasound-guided facet joint injections where it improved the safety and success rate compared with traditional ultrasound-only training [224]. One way to enhance ultrasound guidance training using AR systems is to display a model of the anatomy in a 3D AR environment along with the ultrasound image and virtual representations of surgical tools in use, such as a needle. This visualization could be used to teach the trainees how to interpret the ultrasound image with

respect to the underlying anatomy and needle position so that they would be better able to perform the procedure using conventional ultrasound guidance. Such systems could be used with physical or simulated phantoms, incorporating patient specific models. Tracking technology and AR-based training systems provide interesting opportunities for quantitative assessments of training quality and retainment of skills.

This work had several limitations. While the phantom used in the expert user study was more realistic than that employed in the novice user study, by incorporating a realistic IJV and CA model, the phantom IJV was not compressible and there was no pulsation in the phantom CA. Moreover, the water pressure in the IJV and CA pairs, in both phantoms, was not physiological. As a result, the CA punctures could not be easily identified by the participants during the procedure. The next iteration of the phantom is currently being developed to simulate more realistic functionalities by incorporating a vessel wall and pulsation, generated by a heart-lung machine, to the phantom CA. It is important to note that the constraints of the phantom did not affect the study of needle tip identification and positioning under real-time ultrasound guidance. Another limitation of this study was that we did not account for needle bending in the calculation of the needle tip position. However, we believe that bending in our experiment was minimal due to the soft texture of the phantoms.

Chapter 5

Augmented Reality Ultrasound Guidance System for Epidural Injections

This chapter is adapted from the following manuscripts:

- Ameri, Golafsoun, Jungik Son, Jingwei Liang, F. Stuart Foster, Sugantha Ganapathy, and Terry M. Peters. "Development of a high frequency single-element ultrasound needle transducer for anesthesia delivery." In SPIE Medical Imaging, pp. 101390S-101390S. International Society for Optics and Photonics, 2017.

- Ameri, Golafsoun, Adam Rankin, John S. H. Baxter, Sugantha Ganapathy, Terry M. Peters, and Elvis C. S. Chen. "Development and evaluation of an augmented reality A-mode ultrasound guidance system for spinal anesthesia: preliminary results." (In preparation for submission to IEEE Transactions on Biomedical Engineering)

5.1 Introduction

The general structure of the epidural injection procedure includes four main steps: targeting, navigation, positioning, and validation. The goal of the targeting step is to localize the interspinous level of interest and the puncture site. In the navigation step, the goal is to advance the

needle in tissue towards the epidural space along the most optimal path while avoiding vertebral contact and minimizing retraction and redirection of the needle. The final steps involve positioning the needle in the epidural space and validating its successful placement. Traditionally, anatomical landmark guided techniques are used to perform these steps [46]. During the targeting step, correct identification of a given lumbar interspace via palpation is as low as 29-30% [26, 46, 74]. Identification of an optimal insertion site and needle trajectory, during the navigation step, cannot be predicted by the landmark-based guidance techniques, which can result in multiple needle passes and vertebral contact [107]. While the loss-of-resistance (LOR) is the gold-standard approach for needle positioning in the epidural space and for validation, it is not infallible and could lead to accidental dural puncture with an incidence of up to 5% [74].

The use of pre-operative ultrasound scanning improves the correct identification of the target spinal level (a success rate of 70%) [74]. However, needle navigation and positioning in the epidural space remain challenging even under ultrasound guidance. Due to challenges in identifying the relatively deep spinal anatomical structures and the needle in ultrasound, real-time ultrasound guidance has not been widely adopted for epidural injections [24, 41].

Most recently, the potential benefits of several state-of-the-art technologies have been investigated to overcome challenges in ultrasound-guided epidural injections, either during the navigation or positioning steps. Several augmented reality (AR) guidance systems have been developed to address the challenges with needle tip visualization in ultrasound during the navigation step [73, 177, 184]. Examples of such technologies include SonixGPS (BK Ultrasound, Analogic, MA, USA), Clear Guide One (Clear Guide Medical, MD, USA), and eZGuide (eZono, AG, Germany). In these techniques, both the needle and the ultrasound image are tracked. The tracking information is then used to overlay the needle trajectory and calculated needle tip position on the 2D ultrasound image. While these guidance systems have shown promising results in preliminary studies, large clinical studies are needed to determine the value of these technologies [137, 138, 187]. In addition, due to the 2D nature of the display, such visual-

izations may lead to ambiguity regarding the angle between the image plane and the needle. Despite the potential advantage of these systems for needle navigation, they do not address challenges in needle positioning in the epidural space under ultrasound guidance.

In order to improve localization of the epidural space for needle positioning, Chiang *et al.* [39] proposed placing an ultrasound transducer, with a centre frequency of 40 MHz, at the needle tip and displaying the raw radio frequency (RF) signal, known as A-mode ultrasound, on an oscilloscope [39] or an LCD monitor [123]. Despite the promising preliminary results in detecting the LF and dura in a pig model, the low acoustic penetration rate at 40 MHz may not be sufficient for manipulating the needle as it is advanced in tissue in practice. Moreover, displaying the RF data on a separate display than the ultrasound image may result in split attention and increase the complexity of the task.

In summary, the current state-of-the art techniques do not address challenges in both needle navigation and positioning in the epidural injections under image guidance. Integration of AR, B-mode ultrasound, and A-mode ultrasound may address these challenges.

5.1.1   Objectives

The overall objective of this chapter is to develop an AR ultrasound image guidance (AR-UIG) system, integrating AR, B-mode ultrasound, and A-mode ultrasound, to address the challenges in both needle navigation and positioning in epidural injections. The specific objectives include:

1. Design and develop a tracked high-frequency single-element ultrasound transducer housed at the tip of a hypodermic tube, which can be inserted in an epidural introducer needle.

2. Verify the electrical and acoustic performance of the developed transducer and evaluate its sensitivity to detecting the ligamentum flavum (LF) and dura in a porcine model.

3. Design and develop an AR-UIG system tailored to epidural injections to overcome challenges in both needle navigation and positioning.

4. Perform the initial small-scale evaluation of the performance of the AR-UIG system in a laboratory setting.

5.1.2   Contributions

1. In this work, a high-frequency single-element ultrasound transducer was designed and developed. The transducer and a magnetic sensor were successfully integrated in a 19 gauge hypodermic tube that fits inside a 16 gauge surgical needle.

2. The performance of the tracked needle transducer was successfully evaluated in a water tank and euthanized porcine model. The designed transducer is sensitive to detecting the LF and dura of a porcine model.

3. An AR-UIG system, tailored to epidural injections, was designed based on the development guidelines, described in section 2.3.

4. The AR-UIG was implemented and developed in 3D Slicer, an open source platform. This implementation is released on 3D Slicer and is available to developers interested in implementing similar guidance systems.

5. The technical feasibility of the AR-UIG system was evaluated in a preliminary user study under laboratory conditions using a custom-made lumbar spine phantom model.

5.2   Tracked Needle Transducer Design, Development, and Evaluation

To overcome challenges in the epidural space identification and needle positioning within it, a single-element ultrasound transducer, housed at the tip of a hypodermic tube was developed. The needle transducer can be placed inside a surgical introducer needle, containing a sharp tip that cuts through tissue, replacing the needle stylet. The received A-mode ultrasound signal
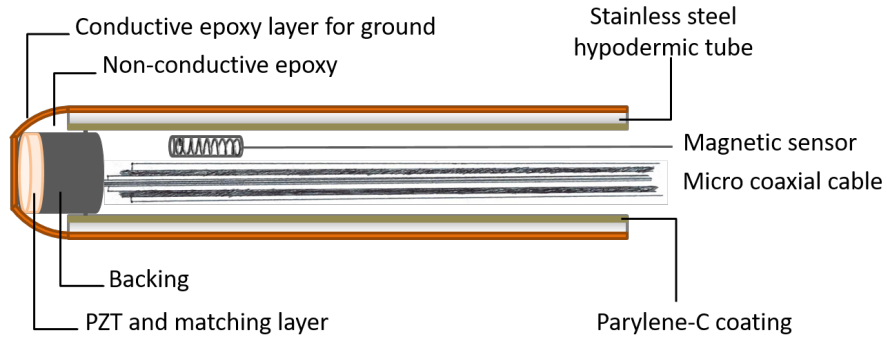
Figure 5.1: A schematic of the tracked needle transducer (not to scale).

provides information about tissue layers, such as the LF and dura, that are immediately in front of the needle tip. To integrate the needle position in an AR-UIG system, the needle transducer was tracked using a magnetic sensor. Details of the tracked single-element needle transducer design criteria, fabrication methodology, and evaluation results are presented in this section.

5.2.1   Ultrasound Needle Transducer Design and Development

The design criteria for the needle transducer were determined after discussions with a collaborating expert anesthesiologist and included the use of an introducer needle with a maximum diameter of 16 gauge and an acoustic penetration depth of 1.5-2 cm. Therefore, a 19 gauge hypodermic tube with an inner diameter of 0.89 mm was used to house the transducer, which is the largest stylet diameter that fits inside a 16 gauge surgical needle, often used for epidural injections. To provide an acoustic penetration depth of 2 cm in tissue and the highest axial resolution possible, a centre frequency of 20 MHz was chosen for the single-element ultrasound transducer. In collaboration with the Device Development Lab at Sunnybrook Health Sciences Centre (Toronto, ON, Canada), the needle transducer was fabricated and the sensor integrated inside the housing hypodermic tube. A schematic of the designed transducer is shown in Figure 5.1. Several milestones for the development of the needle transducer were set to achieve an optimal fabrication process and allow intermediate testing. Details of the prototyping process are provided below.
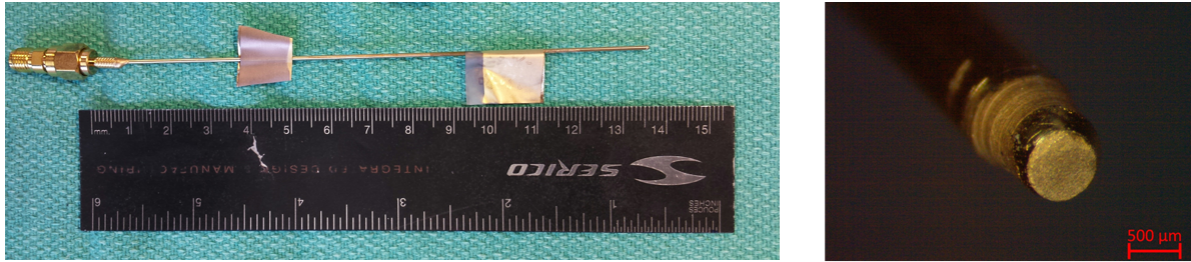
Figure 5.2: A 20 MHz forward looking ultrasound needle transducer and its cross-section. The transducer is housed at the tip of a 19 gauge hypodermic tube.

The First Transducer Fabrication Iteration

In the first iteration of the needle transducer fabrication process, a composite material, consisting of PZT-5H, EPO-TEK® 301 (Epoxy Technology Inc., MA) and TRS 610HD (TRS Technologies, PA), was used. First, it was cut into an octagonal shape with an average diameter of 0.8 mm. The transducer elements went through an extra hand-lapping step to improve circularity. The thickness of the ceramic (95 μm) was tailored to allow for a hight frequency signal with a center frequency of 20 MHz. A lossy conductive epoxy (EPO-TEK® H20E, Epoxy Technology Inc., MA) was then used as the backing material. This material was also used to secure a lead wire to the backing layer. The inside of a 19 gauge stainless steel hypodermic tube was coated with Parylene-C to provide electrical insulation. Next, the transducer was mounted slightly in front of the hypodermic tube's tip. Finally, a layer of gold was sputtered on the surface of the transducer as well as the tip of the hypodermic tube, to create an electrode on the front of the transducer, which was electrically connected to the hypodermic tube and used as the ground for the transducer circuitry. Note that the hypodermic tube and the micro coaxial cable connected to the backing share the same ground. One of the fabricated needle transducers and its cross-sectional view are shown in Figure 5.2.

The Second Transducer Fabrication Iteration

In the second iteration of the needle transducer fabrication, the transducer element was coated with a matching layer. In this prototype, the same transducer composite element as in the first prototype was fabricated with a conductive matching layer (EPO-TEK® H20E). The final thicknesses of the composite element and the matching layer were 98 μm and 24 μm, respec-

(a)	(b)
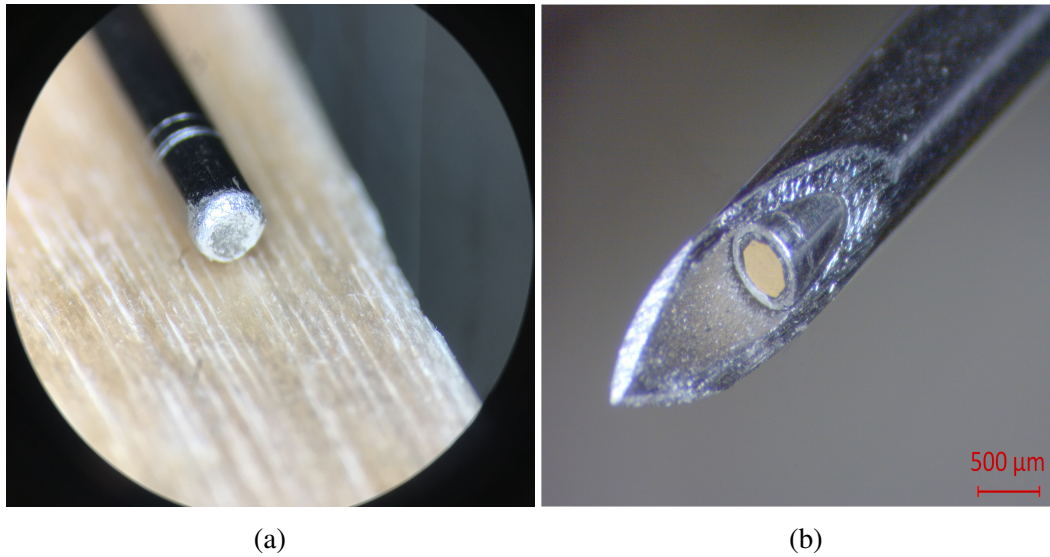
Figure 5.3: (a) Cross-section of the needle transducer with a matching layer. (b) Needle transducer placed inside the introducer needle.

tively. After the transducer was cut into an octagonal shape and was manually formed into a more circular shape, it was inserted into the hypodermic tube and mounted in such a manner that its front tip was slightly exposed (0.5 mm). Then, non-conductive epoxy was used to insulate all sides of the transducer element, leaving the matching layer untouched. After the non-conductive epoxy cured, the conductive epoxy (H20E) was applied on top of the non-conductive epoxy base to bridge the matching layer and the hypodermic tube. The cross-sectional view of this transducer is shown in Figure 5.3a. An example of the full embodiment of the needle transducer inside an introducer needle is shown in Figure 5.3b.

The Third Transducer Fabrication Iteration

In the third transducer development iteration, a similar transducer as the second prototype was developed. In this round, once the transducer was mounted slightly in front of the hypodermic tube's tip, a 5-degrees-of-freedom (DoF) magnetic sensor, 0.3 mmx13 mm, (Aurora, NDI, Canada) was placed inside the cannula, just behind the transducer, close to the tip, as shown in Figure 5.1.

In order to provide a stable connection between the needle transducer and an SMA connector, prevent contact between the bare end of the transducer and magnetic sensor wires, and
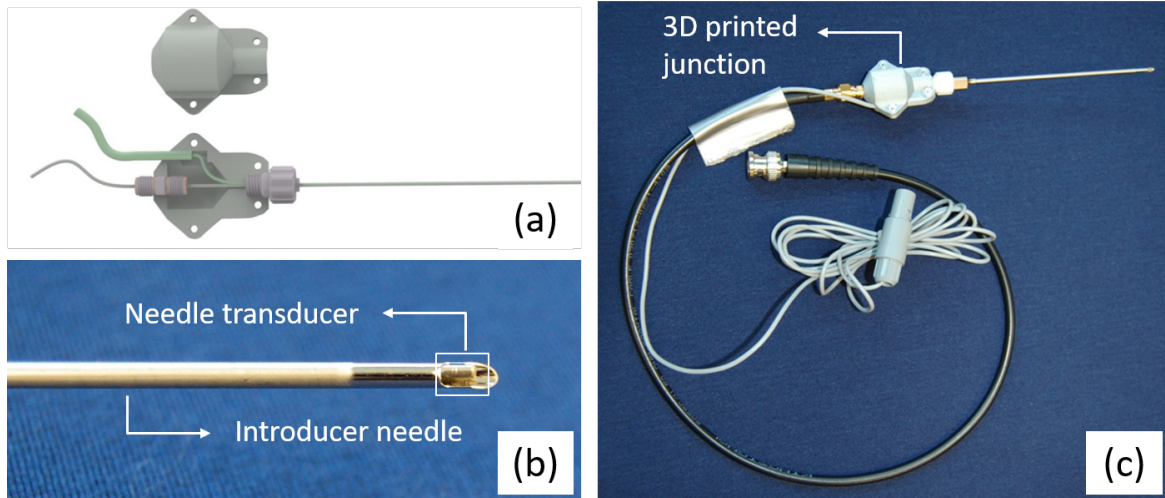
Figure 5.4: (a) A schematic of the needle transducer assembly inside the wye junction. The transducer and the magnetic sensor wires were placed inside the wye junction and soldered to appropriate cables. (b) After the tracked needle transducer was secured inside the wye junction, it was inserted in a 16 gauge introducer needle. (c) The introducer needle is connected to the wye junction via a luer lock connector.

facilitate soldering the wires to appropriate cables, a connecting wye junction was designed and 3D printed (Ultimaker, The Netherlands), shown in Figure 5.4a. The introducer needle can slide over the needle transducer and connect to the 3D printed junction via a luer lock connector.

A-mode Signal Generation and Acquisition

An Olympus pulser-receiver (5072PR, Olympus Corporation, MA, USA) was used to drive the transducer. This unit provides a variable pulse repetition frequency and gain setting, which were set to 100 Hz and 40 dB, respectively.

Real-time data acquisition was performed via a peripheral component interconnect (PCI) digitizer (U1070A Acqiris, Agilent, CA, USA). The analog output of the pulser-receiver can directly connect to the PCI board via a BNC cable. This interface allows direct data acquisition on a PC for further processing and connection to other software components. RF data acquisition parameters were set using the C++ interface of the digitizer. The sampling frequency and acquisition depth were set to 420 MHz (the maximum available rate) and 2 cm, respectively.

5.2.2   Ultrasound Needle Transducer Evaluation

The electrical and acoustic characteristics of the first and second transducer prototypes were validated. The metrics used for the validation include electrical impedance, return loss, and pulse-echo response measurements. Moreover, the sensitivity and performance of the second prototype, i.e. the transducer with a matching layer, was evaluated in a porcine model. Details of the experiments are described below.

Experimental Setup

Electrical Impedance and Return Loss Measurements

The electrical impedance of the transducers was measured using an E5071C network analyzer (Agilent Technologies, CA, USA). The return loss, i.e. the reflection coefficient, of the transducers was also measured with the network analyzer, and was used to evaluate the power transmission efficiency of the transducers.

Pulse Echo Measurements

For the pulse-echo measurements, a 1-mm thick glass plate, used as a reflector, was placed in a water container. The glass plate was supported on two aluminum bars to elevate it above the bottom of the container. The needle transducer was then normally oriented to the glass plate.

Ex-vivo Experiment

In an *ex-vivo* experiment, the pulse-echo measurements were performed on a freshly euthanized pig using the second transducer prototype. In this experiment, the RF data from the ligamentum flavum (LF) and dura mater in the porcine lumbar spine were collected. The echoes from the dura mater were obtained once the LF was punctured. To verify the location of the needle tip, B-mode ultrasound guidance was used for needle navigation and placement. Once the needle transducer was placed at the target, pulse-echo measurements were performed and recorded directly in a PC using the described setup. A 14 gauge Tuohy needle was used for this experiment as we did not have access to a smaller gauge introducer needle at the time of the experiments.

5.2.3 Results

Electrical Impedance and Return Loss Measurements

The electrical impedance of the first and second transducer prototypes, measured by the RF network analyzer, were 105 and 63 Ω, respectively, at 20 MHz. The return loss measurements for both transducers are shown in Figure 5.5. The lowest return loss for the first and second transducers are -3.5 and -4 dB at 20 MHz, respectively, corresponding to approximately 60% power transmission at 20 MHz for each transducer.
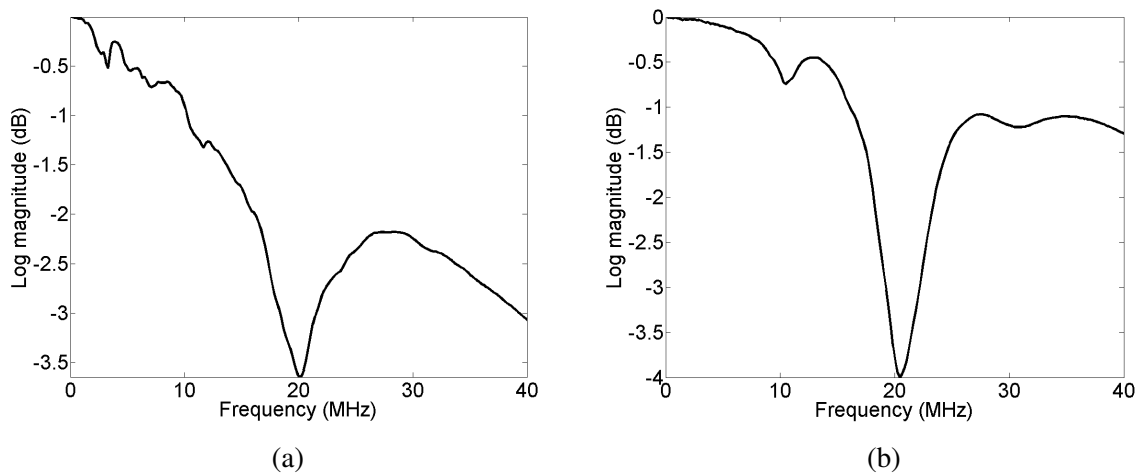
Figure 5.5: The return loss measurement of (a) the first needle transducer, without a matching layer, and (b) the second needle transducer, with a matching layer.

Pulse Echo Measurements

The RF signal from the glass plate received by each transducer along with their spectra are shown in Figure 5.6. In this experiment, the RF data were not amplified as the received echoes were easily detectable. The axial resolution of the transducers were characterized by the full width at half maximum (FWHM), i.e. the pulse length at half of the maximum signal peak. The FWHM of the first and second transducer were 80 μm and 60 μm, respectively, measured from the plots shown in Figure 5.6. Note the time measurement was converted to distance using the speed of sound in water at room temperature. The -6 dB bandwidth of the first and second transducer was 5.7 MHz and 12.2 MHz, respectively.
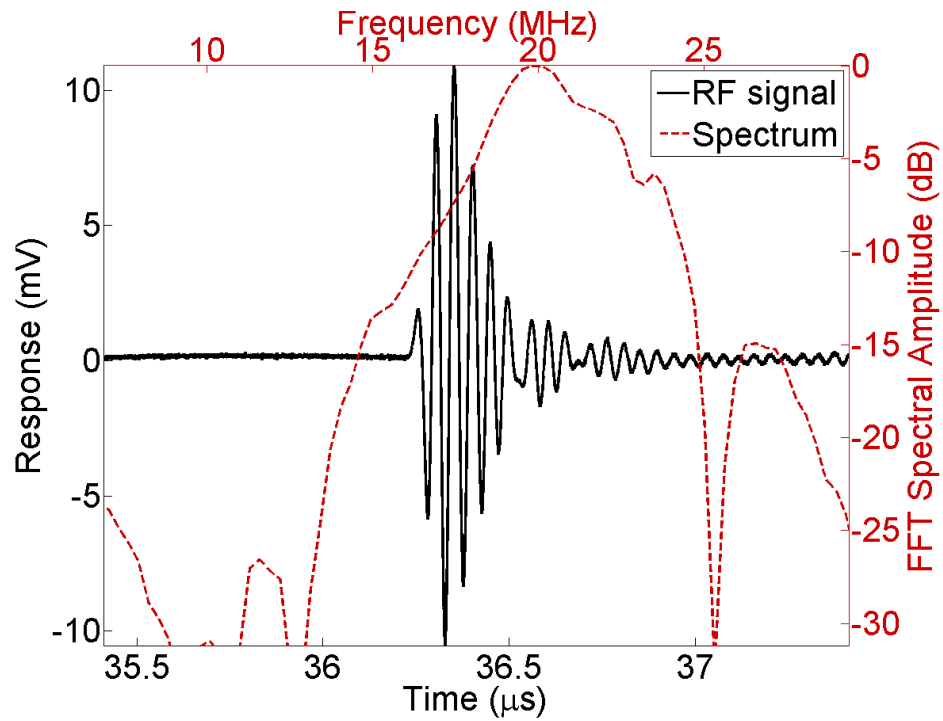
(a)
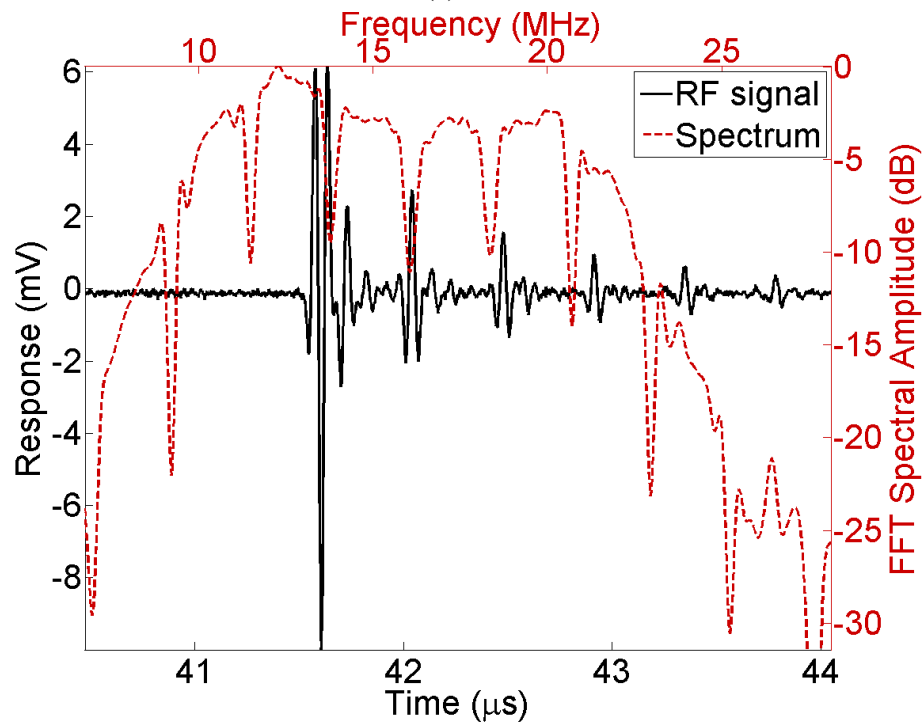
(b)

Figure 5.6: Pulse-echo response and normalized frequency spectrum of the (a) first and (b) second needle transducer. A 1-mm thick glass plate was used as the reflector.

Ex-vivo Experiment

Figure 5.7 shows the amplified RF signals received from the LF and dura mater of a euthanized porcine model using the second needle prototype.

(a)

(b)
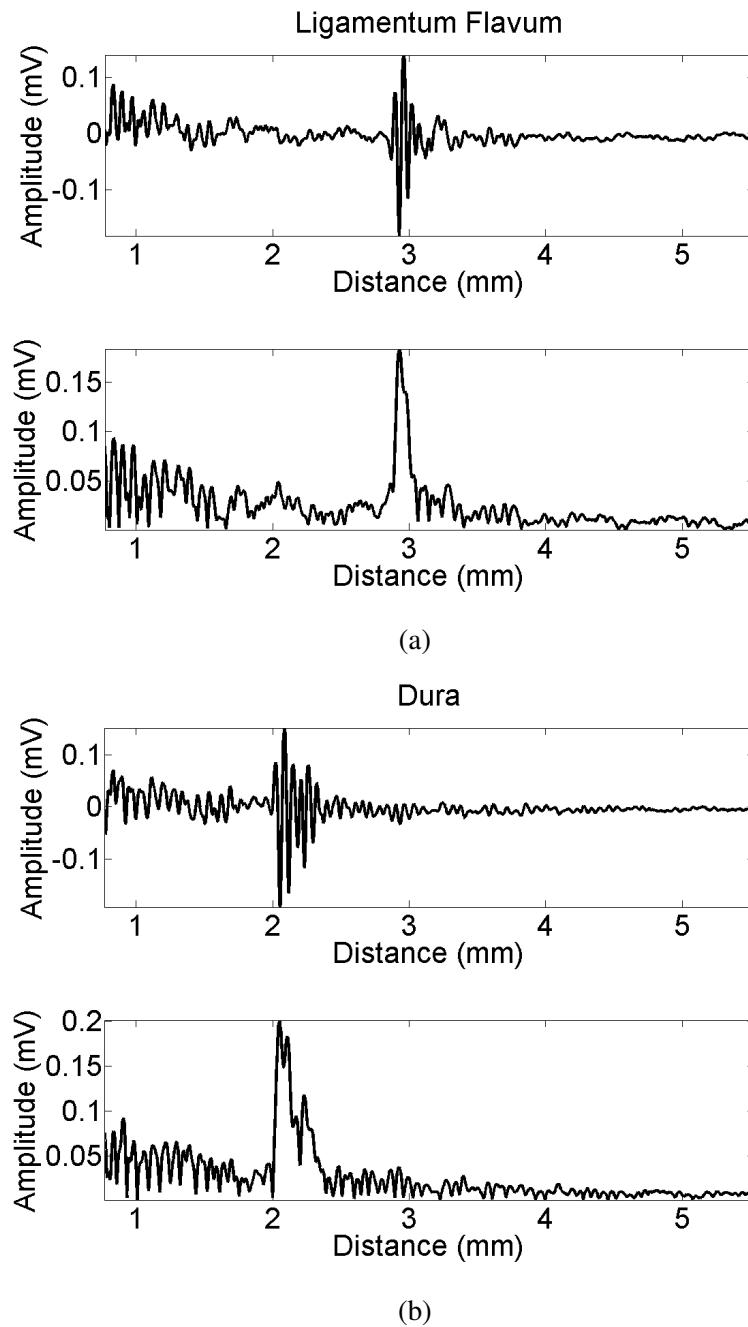
Figure 5.7: The raw RF signal (top row) and its envelope (bottom row) from the euthanized porcine model's (a) LF and (b) dura mater.

5.2.4 Discussion

In this work, the design and development of forward looking single-element needle transducers was presented and the performance of the transducers was evaluated in pulse-echo measurements and an *ex-vivo* porcine model study. While the first iteration of the needle transducers did not include a matching layer, it played an important role as a proof-of-concept in pulse-echo measurements. The performance and sensitivity of the transducer in tissue was improved by including a matching layer in the second generation of needle transducers.

The results from the return loss measurements showed that both transducers had their optimal transmission at 20 MHz. Both transducer prototypes had good sensitivity in the pulse-echo measurements with a glass reflector. A frequency downshift in the spectrum of the second transducer was observed, which is likely due to the deviation of the matching layer's thickness from the ideal thickness, i.e. one quarter of the wavelength. Also, compared to the first prototype, the second transducer had a broader bandwidth, indicating that it was highly damped.

With respect to electrical impedance matching, it is desirable that the electrical impedance of the transducer matches that of electrical devices connected to it, which is often 50 Ω, to maximize power transmission and minimize signal reflection. However, while the electrical impedance of both transducers were higher than 50 Ω, the power transmission was sufficient for the preliminary experiments.

The results from the *ex-vivo* experiment indicated that the developed needle transducer could detect different tissue layers. However, we were not able to identify the LF and dura in the same echo. It is important to note that the angle of incidence in each experiment may have been different, affecting the signal strength and tissue boundary detectability. The needle was unlikely to be placed at an exactly perpendicular angle with respect to the surface of the LF or dura, which would reduce the back-scattered signal strength.

5.3 Design and Development of the AR-UIG System

This section describes the integration of the pulse-echo system described above into an AR-based image-guidance system. An AR guidance system was designed in line with the development guidelines discusses in section 2.3. The constituting components of the system are described below.

5.3.1 System Design

Hardware

The AR guidance system comprised an ultrasound scanner (SonixTouch, BK Ultrasound, Analogic Corp., USA), the custom-made needle transducer described above, and a magnetic tracking system (Aurora, NDI, Canada). For tracking purposes, a 6-DoF magnetic sensor was attached to the ultrasound probe and a 5-DoF sensor integrated within the stylet of the needle transducer. Computation and visualization were performed on an Intel® Core™ i7 CPU and NVIDIA GeForce GTX 1070 GPU. A standard 24-inch desktop monitor was used to display the AR visualization.

Software

Two open source software applications were employed in our system:

1. the PLUS server application (www.plustoolkit.org) [122],

2. 3D Slicer with the SlicerIGT extension (www.slicerigt.org) [63].

The PLUS server enables real-time synchronized data acquisition, via the Ethernet network, from the magnetic tracking system, B-mode ultrasound images from the scanner, and A-mode ultrasound from the needle transducer. 3D Slicer provides a platform for not only medical image processing, but also application prototyping and distribution to the community via an online extension manager for academic and commercial use. The SlicerIGT extension provides an integrated OpenIGTLink interface, which allows the exchange of various data types,
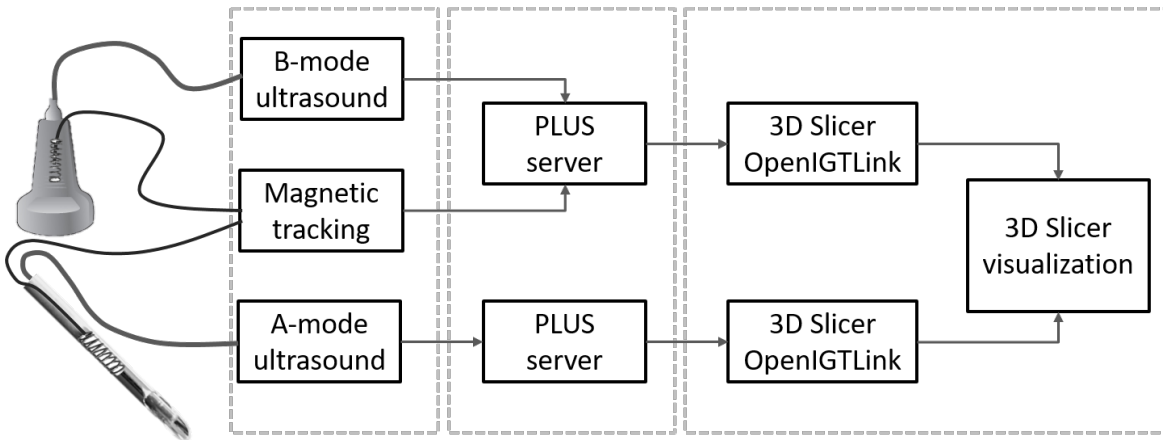
Figure 5.8: Overview of the hardware and software components in the AR-UIG system.

including real-time ultrasound images and tracking data, with external tools. In our guidance system, two PLUS server applications and two OpenIGTLink connections were used to communicate between the imaging systems and the visualization platform. A schematic of the connection between different components of the guidance system is shown in Figure 5.8.

Interface

The visualization screen is split into two windows, one showing the B-mode ultrasound image face on, referred to as the 2D window, and the other, a 3D environment, displaying B-mode ultrasound as well as a virtual representation of the needle, its trajectory, and depth markings along the trajectory.

In the 2D window, the intersection of the needle with the image is shown as a contour on the B-mode ultrasound image. Therefore, for out-of-plane needle insertions, the contour would have a circular shape and for in-plane needle insertions, it would be elliptical. When the needle is completely co-planar with the ultrasound slice, the needle tip is delineated by a triangular shape. This visualization helps differentiate the in-plane and slightly off-angled insertion angles, which often occur during navigation.

In the 3D environment, to visualize the insertion angle between the image plane and the needle, the B-mode image is shown at an oblique angle. This visualization helps redirect the needle and keep it in the image plane during navigation. Showing the 2D and 3D windows side-
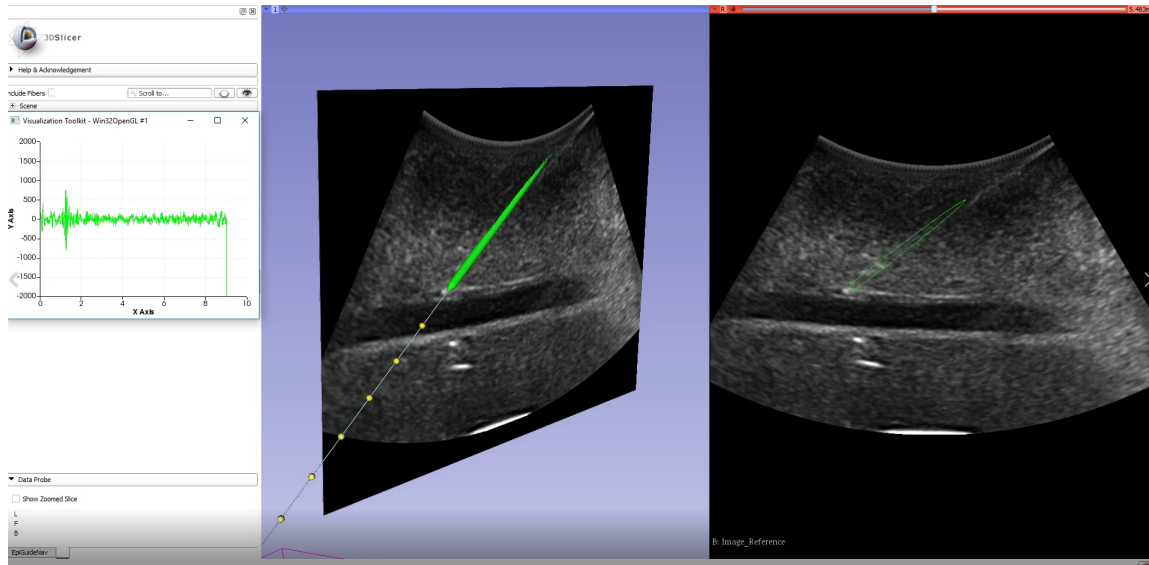
Figure 5.9: The interface of the AR-UIG system developed for epidural injection. The 3D AR scene displays the B-mode ultrasound image at an oblique angle, providing a simple visualization of the position of the needle and the ultrasound image plane. The B-mode image is shown in the 2D window on the right, along with a faint contour of the intersection of the needle with the image plane. A-mode ultrasound is shown in a separate window on the left.

by-side has the advantage of maintaining high image quality and transparency while providing an intuitive visualization of the needle trajectory in 3D space. To improve needle navigation, the virtual needle is equipped with a model of its trajectory with a sequence of uniformly spaced 1 cm markings, giving the user a rapid understanding of the depth of penetration beyond, or remaining depth to, the ultrasound plane. The virtual trajectory may also help to identify an optimal trajectory path prior to needle insertion, reducing bone contact and needle retraction.

A-mode ultrasound is also integrated in this platform and shown in a separate window next to the 3D environment. The interface of the AR guidance system is shown in Figure 5.9.

Ultrasound and needle calibration

Ultrasound calibration is a fundamental criterion for the integration of ultrasound images in AR environments. Ultrasound calibration was performed using the point-to-line registration technique, described in [37], a technique that results in highly accurate calibration with a low number of measurements. In this work, the ultrasound calibration was performed using 12 images of an 18 gauge Aurora needle, which has a 5-DOF magnetic sensor integrated into its

cannula close to the tip.

The tracked needle was also calibrated, via a pivot calibration using the PLUS library [122], providing the transformation between the needle tip and the coordinates of the tracking sensor embedded in the hypodermic tube. To perform the calibration, the tracked needle transducer was placed inside the introducer needle first, and then the needle assembly was pivoted at its tip.

5.3.2   Motivation of the Design Based on Guidelines

1. ***The interface is minimal with a drop-down button for choosing the guidance modality and a start-stop button for saving the tracking data.*** The interface includes (1) two side-by-side windows for AR guidance and ultrasound image visualization, (2) a resizable window to display A-mode ultrasound, (3) a button with a drop-down list of available guidance systems, including ultrasound-only, ultrasound and AR (i.e. the 2D and 3D windows without A-mode ultrasound), as well as the complete AR-UIG system, with A-mode ultrasound.

2. ***Ultrasound image is shown face-on in one of the visualization windows.*** To ensure that the ultrasound image is highly visible, it was shown face-on in the 2D window of the AR-UIG. This design decision was motivated by the guidelines for *similarity to existing workflow* and *high ultrasound visibility*.

3. ***The intersection of the needle with the image plane is delineated with a virtual contour on the ultrasound image.*** A computer-generated virtual contour was used to delineate the intersection of the needle with the image plane on the ultrasound image to improve needle visualization and identification in ultrasound, lowering the cognitive load. The contour was narrow, with low colour saturation to prevent image occlusion, especially for the in-plane needle insertions. This design decision was motivated by the *minimizing mental transformation, minimalism*, and *high ultrasound visibility* guidelines.

4. ***The needle model has trajectory indication, depth markings, and colour-code.*** The colour, shape, and size of the needle model were chosen in such a way to simplify needle tip visualization in the 3D scene. The needle trajectory provided a simple and intuitive representation of the needle trajectory with respect to the image plane in a 3D environment. This visualization helps identify an optimal needle path to the target during navigation. The depth markings improve depth perception and provide a rapid understanding of the distance between the needle tip and the image plane, lowering the cognitive load. This design decision was motivated by the *minimalism* and *minimizing mental transformation* guidelines.

5. ***In the 3D AR scene, the ultrasound image is displayed at a fixed oblique angle.*** The virtual camera was set to display the ultrasound image at a fixed angle regardless of the movement of the probe. This ensured that the ultrasound image would always be in the field of view and provided a standardized visualization of the image for all users. By displaying the image at an oblique angle, the orientation of the needle with respect to the image plane could be easily identified during navigation, addressing problems with depth perception, encountered in the AR-UIG developed for central line procedures, described in Section 4.4.4. This design decision was motivated by the *minimalism*, and *minimizing mental transformation* guidelines.

6. ***No automatic target identification is employed.*** To minimize the complexity of the system, maintain high image visibility, and eliminate sources of error due to segmentation or registration, the bone or the epidural space was not automatically identified in either B-mode images or A-mode ultrasound. This design decision was motivated by *transparency to the clinician, minimalism*, and *high ultrasound visibility* guidelines.

7. ***All the information and visualization is shown on one display.*** The B-mode ultrasound image, the 3D scene, and A-mode ultrasound were all displayed on one monitor. Therefore, the user would not need to switch between monitors or oscilloscope to visualize the

data. This is directly motivated by the *minimalism, minimize mental transformation*, and *minimal operating room footprint* guideline.

5.3.3   Best Practice Considerations for the AR-UIG Development

1. ***The clinical problem was outlined by an expert anesthesiologist and continual consultation was maintained during the development process.*** Clinical input from an expert anesthesiologist, i.e. an end-user of the system, was used to design the AR-UIG. During the consultation, the clinical problems with the current techniques used for epidural injections were thoroughly discussed and possible solutions to address some of the problems specific to image guidance were conceptualized. Multiple methods for the visualization of the data were developed and discussed with expert clinicians and their feedback incorporated to refine the guidance system.

2. ***Small scale evaluation of the AR-UIG was performed.*** Different components of the AR-UIG were evaluated with the collaborating expert anesthesiologist during the development process. One of the early stage experiments involved a performance evaluation of the needle transducer. For the evaluation of the AR-UIG system, a small-scale study was performed with novice users and two collaborating anesthesiologists, discussed in Section 5.4, as a precursor to a larger evaluation study involving expert operators.

3. ***The AR-UIG was designed to provide sufficient image guidance for different needle insertion techniques.*** To increase the practicality of the AR-UIG system for epidural injections, it was made versatile to variations in needle insertion techniques and angles. Displaying the ultrasound image at an oblique angle in the 3D scene was a design decision that enabled this versatility.

4. ***The AR-UIG system has multiple functionalities.*** The AR-UIG system was developed as a multi-use tool. Functionalities such as recording and replay were integrated in the

AR-UIG system, enabling the system to be used not only as a guidance system, but also a platform for training and quality assurance.

5.4   AR-UIG System Evaluation

5.4.1   Objectives

One of the objectives of this study was to conduct the first small-scale evaluation of the AR-UIG system with an expert operator other than our collaborating anesthesiologist. The other objective was to perform a preliminary evaluation of the performance of the AR-UIG system in a laboratory setting with novice operators. The following comparisons were made for the evaluation of different components of the AR-UIG system:

- B-mode ultrasound and AR guidance against ultrasound-only guidance,

- B-mode ultrasound, AR, and A-mode ultrasound against ultrasound-only guidance,

- B-mode ultrasound, AR, and A-mode ultrasound against B-mode ultrasound and AR guidance.

5.4.2   Methods

Experimental Setup

The phantom design requirements for this study included developing a phantom that would (1) simulate the lumbar spinal vertebrae, soft tissue, LF, and dura, (2) be both ultrasound and computed tomography (CT) compatible, and (3) not provide any haptic feedback when the phantom LF is traversed, to ensure that operators use image guidance for needle navigation and positioning and not anatomical landmarks or haptic feedback. Materials and techniques used to model different parts of the spine anatomy are described below.

Figure 5.10: 3D printed lumbar spine model.

Lumbar spine model

A 3D printed lumbar spine model (L2-L5), obtained from a human CT scan, was used to simulate the vertebrae. To preserve the anatomical distance between the vertebrae, they were printed on a solid plate, Figure 5.10. The 3D printed spine model was further fixated inside a Lexan box to eliminate any movement during and after the addition of a soft tissue model.

Soft tissue model

A gelatin-based medium, comprising a mixture of 66% (v/v) water, 27% (v/v) gelatin, 2.5% (v/v) metamucil fibre (Psyllium Hydrophilic Mucilloid) as a scattering agent, and 4% (v/v) citric acid powder as preservative was used to mimic the ultrasound properties of soft tissue.

LF and dura models

To facilitate phantom construction, models of the LF and dura were simplified by assuming a flat surface for each layer, rather than their natural tubular structures. As the LF and dura model should appear hyperechoic and the epidural space hypoechoic compared to the surrounding medium, similar to ultrasound images of the human spine, as well as be readily visible in CT for validation purpose, the LF, dura, and epidural space had to consist of a different combination of soft tissue mimicking materials. It was also important that these materials would spread easily over the gelatin layer and around the vertebral body of the spine model to form a realistic thickness for the LF and dura, i.e. around 1 mm. Multiple phantom materials were tested for modeling the LF and dura, which include:

1. PVA-C doped with a CT contrast agent, 5% (w/w) iodixanol (Visipaque^{TM}, GE Health-
   care). This material would appear hypoechoic in ultrasound with hyperechoic boundaries
   against the tissue mimicking material. Therefore, a thicker layer of PVA-C placed in be-
   tween two layers of the tissue mimicking material would model the LF and dura bound-
   aries as well as the epidural space. However, while the contrast between the gelatin mix
   and PVA-C in both CT and ultrasound was sufficient, these materials would not adhere to
   one another properly, resulting in air gaps between the two surfaces, producing artifacts
   in ultrasound. In addition, there was a sensible haptic feedback while inserting a needle
   from gelatin to the PVA-C layer, which was not ideal for this study.

2. A mixture of gelatin and graphite to model the LF and dura and clear gelatin, without
   any scattering particles, to model the epidural space. While the boundaries in ultrasound
   were identifiable, the graphite mixture did not produce sufficient contrast in CT.

3. Silicone doped with Barium (5% (w/w)), as a CT contrast agent, to model the LF and
   dura and clear gelatin to model the epidural space. The boundaries between the soft tissue
   mimicking material, silicone, and clear gelatin were clearly visible in both ultrasound
   and CT. However, the high acoustic attenuation of the silicone mixture resulted in poor
   visualization of the phantom layers placed below it.

4. Clear gelatin doped with Barium (3% (w/w)) to model the LF and dura and clear gelatin
   to model the epidural space. The clear gelatin appears hypoechoic in ultrasound result-
   ing in clear boundaries against the soft tissue mimicking material. This combination of
   phantom materials resulted in the best results under ultrasound and CT without resulting
   in a sensible haptic feedback. Therefore, it was used to construct the phantom.

To construct the phantom, the 3D printed spine model was rigidly fixed in the phantom box,
into which soft tissue mimicking material was poured up to the depth at which the epidural
model was to be constructed. A thin layer of the clear gelatin and Barium mix (around 1 mm
in thickness) was poured on the surface of this layer to model the dura. A layer of clear gelatin,
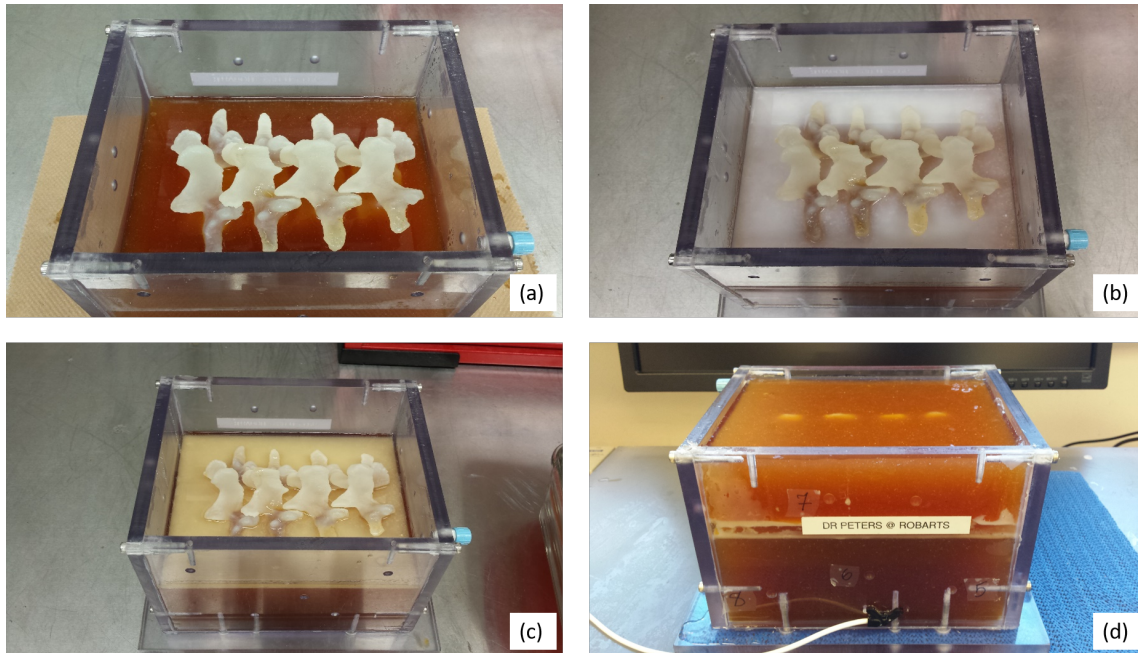
Figure 5.11: (a) The 3D printed spine model was fixed in the phantom box and soft tissue mimicking material was poured in the box, covering the spinal canal up to the depth of the epidural space. (b) A thin layer of the clear gelatin and Barium mix was poured on the surface of the layer constructed in the previous step after it had solidified. (c) A layer of clear gelatin was poured on top of the phantom surface, and after it hardened, another layer of the Barium mixture was poured on top of it. (d) The phantom box was filled with the tissue mimicking gelatin mixture, and a magnetic tracking sensor was rigidly attached to the phantom box.

without any scattering agent was poured on top of the dural surface as a model of the epidural space. The thickness of this layer was around 7 mm, similar to that in human adults [156]. Another thin layer of the Barium mixture was applied as a model of the LF. Finally, the rest of the phantom box was filled with the tissue mimicking gelatin mix. The thickness of this layer was 3.5 cm. Note that after applying each layer, the phantom was placed in a fridge or left at room temperature to let the phantom material solidify. Figure 5.11 illustrates different stages of phantom construction. An ultrasound image of the phantom and a healthy volunteer are shown in Figure 5.12 for visual comparison.

The phantom was tracked using a 6-DoF Aurora magnetic sensor (NDI, Canada) rigidly attached to the phantom container. For evaluation purposes, a surface model of the phantom LF and dura was created by segmenting those layers in a CT scan of the phantom. The surface
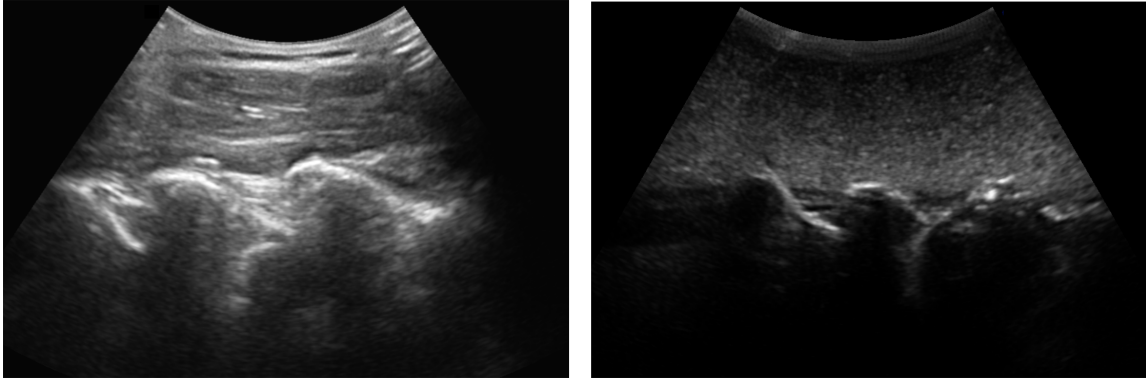
Figure 5.12: An ultrasound image of a healthy volunteer's lumbar spine (left) and the spine phantom (right).

model was registered to the physical phantom using a set of divots grooved on the sides of the phantom container and segmented in the CT volume. During the experiments, a thin layer of water was added on the surface of the phantom to improve acoustic coupling.

Study Design

A novice user study was performed with four participants, who were familiar with ultrasound imaging but had no training in a clinical setting. In addition, one expert anesthesiologist was invited to participate in the study and provide qualitative feedback on the AR-UIG system.

Prior to the experiments, during a brief training phase, participants could familiarize themselves with the phantom, ultrasound images of the phantom and needle, A-mode ultrasound, and the AR-UIG system. Once ready, the participants were asked to place the needle in the phantom epidural space under three different image guidance systems, including: (1) ultrasound-only, (2) ultrasound and AR, and (3) ultrasound and AR and A-mode guidance. The order in which a given guidance modality was used was randomized.

For timing purposes, participants were asked to inform the researcher conducting the study when they were ready to puncture the phantom and when they were confident that the needle tip was at the target to mark the beginning and end of the procedure, respectively. The guidance system's software recorded the position of the ultrasound probe, needle, and phantom during the entire procedure. To assess the perceived workload, participants were asked to complete

the NASA Task Load Index (NASA-TLX) assessment at the end of each trial. For the expert operator, this step was replaced with providing a thorough feedback on the guidance system. The NASA-TLX questionnaire includes the following questions regarding different aspects of the workload:

1. Mental demand: How mentally demanding was the task?

2. Physical demand: How physically demanding was the task?

3. Temporal demand: How hurried or rushed was the pace of the task?

4. Performance: How successful were you in accomplishing what you were asked to do, with a score of zero being perfect?

5. Effort: How hard did you have to work to accomplish your level of performance?

6. Frustration: How insecure, discouraged, irritated, stressed, and annoyed were you?

Evaluation Metrics and Statistical Analysis

The quantitative evaluation metrics used in this study were success, procedure time, and normalized needle path-length. Success of the procedure was defined as placing the needle in the phantom epidural space without puncturing the dura. The time taken to complete the procedure was measured using the timestamps of the pose measurements recorded by the software. The normalized needle path-length was calculated using the pose measurements. The NASA-TLX was used as the qualitative evaluation metric.

Statistical significance for time and normalized needle path-length were determined via Wilcoxon rank-sum tests to account for the low number of trials [167]. A chi-square test was used to determine significance for the rate of success with each modality. To correct for multiple comparisons, the Holm-Bonferroni correction was used with a combined significance of $p \leq 0.05$.

5.4.3 Results

Novice User Study

Overall, four novice operators participated in the study and seven trials were performed. (Due to a hardware failure, discussed in section 5.5, the experiments had to be terminated.) All the participants had experience with ultrasound imaging and needle appearance in ultrasound. However, they had no prior training on ultrasound-guided needle placement in ultrasound for spinal procedures. Each participant went through a training phase to become familiar with the procedure and the phantom.

An independent observer determined the success of the procedures from the replay of each procedure in 3D Slicer. In the replay, the 3D model of the dural and LF layers, obtained from a CT scan of the phantom, were displayed along with the ultrasound image and virtual models of the needle and its trajectory. The space between the dural and LF layers defined the phantom epidural space. An instance of a replay of one of the procedures is shown in Figure 5.13, which illustrates an instance of the replay of a successful trial in which the needle was placed in the phantom epidural space without perforating the dura.
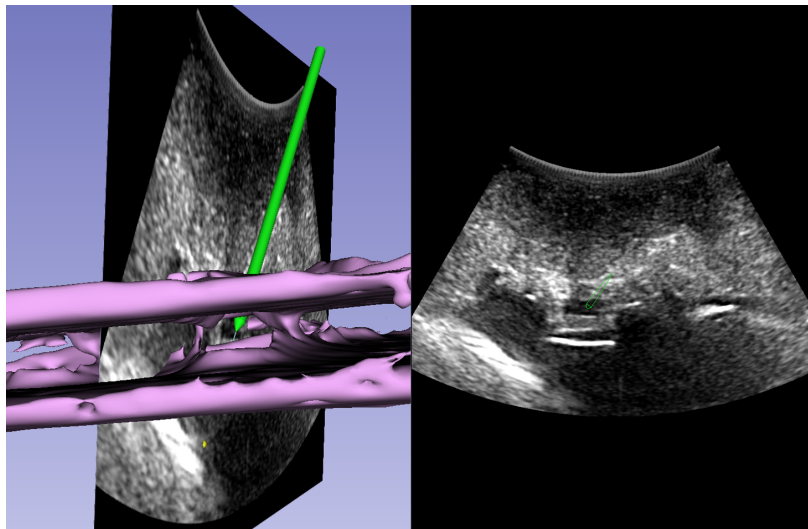
Figure 5.13: The tracking information from the phantom, ultrasound probe, and needle allowed replaying the procedure for identifying the final position of the needle tip to determine success of the procedure. In the replay, a model of the LF and dura is shown (in violet) in addition to the entire AR visualization used during the procedure.
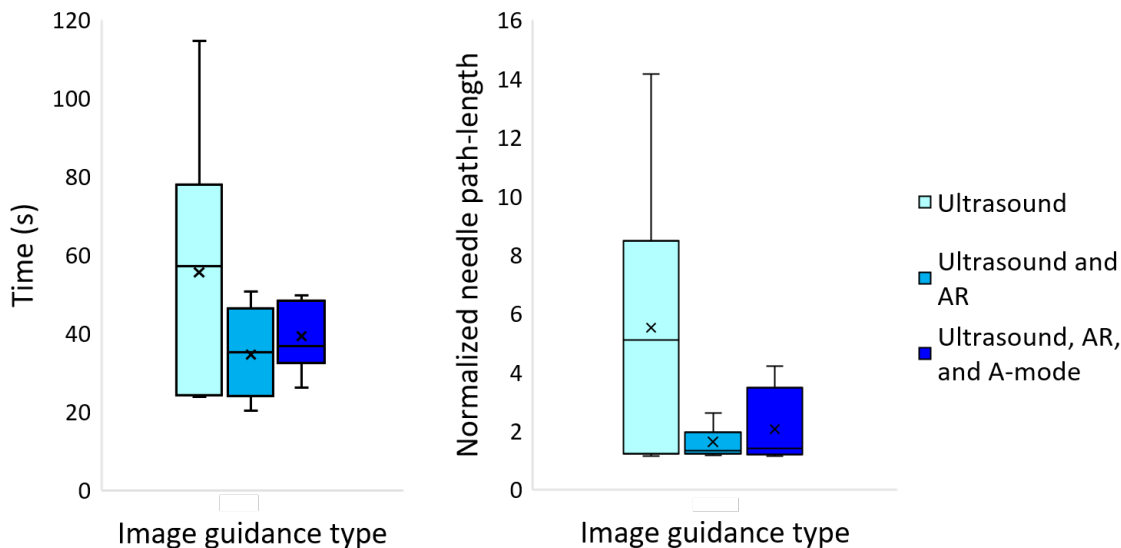
Figure 5.14: The time and normalized needle path-length measurements for all three modes of image guidance.

All the procedures performed under AR guidance, with or without A-mode ultrasound, were completed successfully without puncturing the phantom dura. However, in three trials performed under ultrasound-only guidance, the dura was punctured (an incidence of 43%). This observation suggested that the AR-UIG system may improve needle tip placement in the target epidural space.

The data distribution for procedure duration and normalized needle path-length are shown in Figure 5.14, and the results are summarized in Table 5.1. The results suggested that the procedure may take longer and feature more tortuous paths under ultrasound-only guidance compared to the AR-UIG system. However, due to the small sample size, no significant difference was found between the guidance systems.

Analysis of the NASA TLX showed that the "frustration" levels were lower with the AR-UIG system, with and without A-mode ultrasound, compared to ultrasound-only guidance ($p \leq 0.006$ before correction). The results also showed a decrease in the required effort to perform the task with ultrasound and AR, compared to ultrasound-only guidance ($p \leq 0.04$ before correction). After applying Holm-Bonferroni correction, no statistical significance was achieved. The results from the NASA TLX are shown in Figure 5.15.

Table 5.1: Procedure time and normalized needle path-length results for each image guidance mode (N = 7). Ultrasound-only guidance is labeled as US.

	Time (s)			Normalized Path-length		
	US	US+AR	US+AR+A-mode	US	US+AR	US+AR+A-mode
Mean ± STD	56±34	35±11	40±9	6±5	2±1	2±1
Median	57	35	37	5	1	1

Feedback from an Experienced Anesthesiologist

An expert anesthesiologist, with prior experience with AR guidance systems and ultrasound-guided needle interventions, was asked to use the guidance system for placing a needle in the phantom and provide his feedback on the AR-UIG system interface and the setup. The clinician's comments are summarized below.

AR-UIG interface

While the 3D view added value to the guidance system and improved needle navigation, displaying a 3D scene on a 2D monitor was not ideal as it lacked a sense of depth, weakening its effectiveness. On the other hand, the virtual overlay of the needle intersection with the image plane on the 2D ultrasound image strongly improved needle visualization and provided a rapid understanding of whether the shaft or the needle tip was intersecting the image plane.

As clinicians do not get training for and are not used to employing A-mode ultrasound, our expert clinician expresses concern over how effective its visualization was. Interpreting the A-mode signal to determine the corresponding tissue boundary for each peak was challenging. When there were no clear peaks in the signal, there was no motivation for using A-mode ultrasound for guidance, especially that the target was visible in B-mode ultrasound in this experiment. The addition of A-mode ultrasound did not seem to add much value to the guidance system.

Overall, the AR-UIG system improved needle visualization, navigation, and positioning at
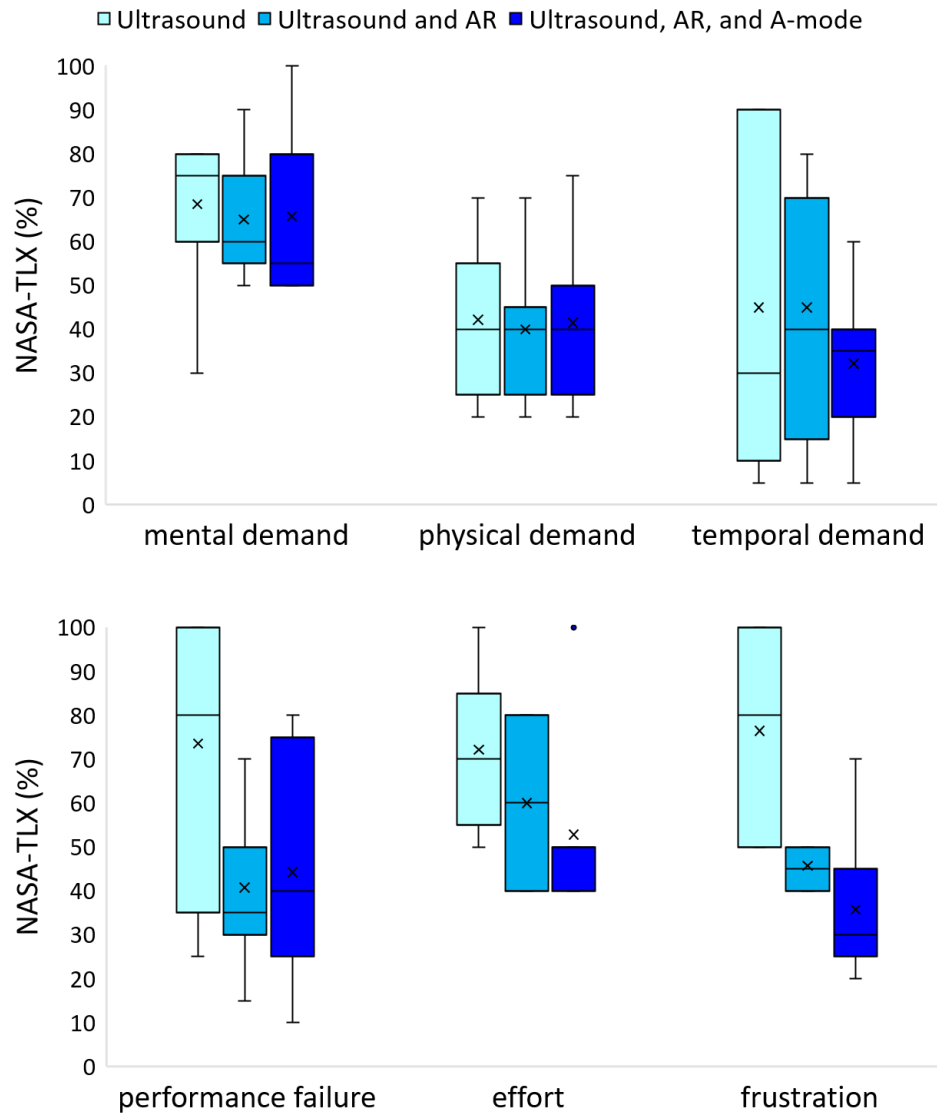
Figure 5.15: The results from the NASA TLX for all three modes of image guidance. The cross symbol and the dot indicate the mean and outliers, respectively.

the target. The performance of the AR-UIG system may be improved if A-mode ultrasound could be displayed in an intuitive manner.

Phantom

The phantom simulated a straightforward case as it did not incorporate factors such as obesity or spinal disorders. Due to the relatively thin layer of the soft tissue model in the phantom, compared to what is expected in obese patients, there was not much resistance on the needle, making needle advancement in the phantom easy. Unlike in the challenging cases faced in

the clinic, ultrasound images of the phantom provided sufficient image guidance for needle placement at the target. Increasing the thickness of the soft tissue model would increase the difficulty of the task and represent a more realistic scenario.

5.4.4 Discussion

In this preliminary user study, the technical feasibility of the AR-UIG system interface, tailored to epidural injections, was validated. This study served as the initial small-scale evaluation of the design decisions under laboratory conditions. In this evaluation, the performance of two different modes of guidance provided by the AR-UIG system, i.e. (i) B-mode and AR guidance and (ii) B-mode, AR, and A-mode guidance, were compared to ultrasound-only guidance and against each other.

The results from the novice user study and feedback from an expert anesthesiologist illustrated that while the two modes of guidance in the AR-UIG system performed similarly, employing them may outperform ultrasound-only guidance. In addition, the phantom dura was punctured multiple times under ultrasound-only guidance, whereas all the procedures performed under AR guidance were completed successfully. The feedback from the participants on the task load and perceived outcome strongly suggested that performance effort and frustration were reduced with the AR-UIG system.

Even though the use of A-mode US was strongly motivated by an unmet need perceived by an expert anesthesiologist, in this very preliminary study, displaying A-mode ultrasound for needle positioning was not perceived as an effective adjunct to the guidance system due to difficulties in interpreting the signal. Currently, training and interpreting A-mode is not routine in clinical education, exacerbating issues with interpretibility. To overcome this challenge, more training should be included and different ways of integrating the A-mode signal in the guidance system need to be developed. The effects of different levels of training on using A-mode ultrasound as well as the learnability of different representations of A-mode ultrasound need to be investigated.

One of the main advantages of this phantom was that it possessed the property that, if left at room temperature for several hours, needle tracks in the phantom would disappear, making the phantom reusable. In this study, a single phantom was used over the entire course of the experiments. While the phantom met all the design criteria and its B-mode ultrasound images met the requirements for the study, it had several limitations. For example, the LF and dura layers were not easily identifiable in A-mode ultrasound, especially at oblique needle insertion angles. Although this, in part, is a result of the narrow beamwidth of the single-element transducer, the relatively smooth surface of the phantom LF and dura boundaries may have resulted in specular reflections, redirecting the beam away from the transducer surface, reducing their detectability by the needle transducer. Another limitation of the phantom was that the epidural space was at a relatively shallow depth from the surface of the phantom, simulating a simple clinical case. In addition to increasing this depth, the phantom can be further improved to simulate a more realistic epidural space model by incorporating tubular structures for the LF and dura, instead of flat surfaces.

Overall, the results elucidated that the interface design decisions for the AR-UIG system were appropriate and compared to ultrasound-only guidance, the AR-UIG system may improve needle navigation and placement in the phantom epidural space. The novice user study will be extended to further evaluate the performance of the AR-UIG system with a larger sample size. In addition, a similar evaluation will be performed with expert operators to investigate the clinical utility of the AR-UIG system.

5.5   Discussion and Future Directions

This chapter presented the design, development, and validation stages, for both hardware and software components, of an AR-UIG system tailored to epidural injections. This work explored the feasibility of integration of B-mode and A-mode ultrasound into a functional AR guidance system to address both navigation and positioning challenges faced in cannulation of

the epidural space. An ultrasound needle transducer was successfully designed and developed to provide relatively subtle, fine-grained, and continuous guidance for needle tip positioning in the epidural space. The AR-UIG system interface was designed using the guidelines introduced in Section 2.3, considering development best practices and lessons learned from our earlier studies with the guidance system developed for central line procedures. The initial, small-scale evaluation of the the AR-UIG demonstrated the validity of the guidance system design. Nonetheless, this AR-UIG system presented a set of unique challenges and yet opportunities for further improvement of the system and extending its applications, as discussed below.

The needle transducer was relatively fragile due to its small size and fabrication process. As a result, one major set back was its susceptibility to wear and tear. In spite of the extensive care taken during manual handling of the needle transducer, after preforming multiple experiments, the coating of the transducer was damaged, most likely a result of physical contact between the side of the transducer and the introducer needle. As a result, when placed in a conducting medium, the transducer would short-circuit. As it stands, the needle transducer design lacks the robustness required for longitudinal studies. Modifying the needle transducer design to integrate the single-element transducer inside the hypodermic tube, rather than positioning it slightly in front of the opening of the cannula, may increase its robustness and durability. One should keep in mind that, for clinical use, the needle transducer will be designed as a disposable medical device, and for active electrical devices directly inserted in the human body, additional regulatory requirements must be fulfilled.

In addition to providing improved ergonomics, placing the magnetic sensor inside and close to the tip of the hypodermic tube (around 2 cm from the tip), as opposed to its proximal end, improves the needle calibration accuracy by reducing the lever effect, which relates to the dependency of rotational error on the distance between the sensor and the point of interest along the needle. This design also improves the reliability of needle tip pose measurements from tracking, due to minimal needle bending close to the distal end of the needle. However,

it does not mitigate errors in needle shaft pose estimation caused by needle bending in tissue.

While the AR-UIG was designed to address challenges in both positioning and navigation for needle placement in the epidural space, in the evaluation study, navigation was the dominant task, and it overwhelmed any difference that could have been seen in positioning. An experimental design where the navigation and positioning tasks are decoupled may separate the effects of the AR-UIG on each specific task and provide a better structure for studying the capabilities of the guidance system for navigation and positioning. Such a design could involve using separate phantoms that target only navigation or positioning. Nonetheless, the challenges with interpreting the current presentation of A-mode ultrasound in the AR-UIG system need to be addressed and this could be achieved by showing the signal as a 1D color image or displaying the prominent peaks in the signal as virtual objects in front of the needle. Further investigation is required to determine efficacy of such visualizations.

The AR-UIG was designed and developed as a multi-use system, including functionalities such as recording and playback that facilitate utilizing the system for training and quantitative skill assessment. One of the future directions of this project involves evaluating the system as a training platform for teaching ultrasound-guided epidural injections, using simulated or physical spine phantoms.

While the current iteration of the AR-UIG system did not include any anatomical models, incorporating such models may facilitate identification of the interspinous opening in ultrasound at the expense of increasing the complexity of the visualization interface. Investigating the effectiveness of including spinal models in the AR-UIG system constitute another future direction of this research project.

The simple design of the instrumented needle and the AR guidance system allows providing a relatively low cost and accessible guidance system, whose applications can be extended to a large number of clinical procedures, where a needle or a surgical tool is employed. These applications include spinal taps, biopsy, brachytherapy, minimally invasive cardiac procedures, and external ventricular drain.

Chapter 6

Conclusions

While more and more interventional procedures in anesthesiology leverage the benefits of image guidance, particularly ultrasound imaging, many challenges remain in the application of such technologies. The motivation for this thesis was to address some of the specific limitations of ultrasound-guided needle interventions, including needle tip visualization in ultrasound, via advanced visualization techniques, namely augmented reality (AR). In an effort to explore the feasibility and utility of such visualization systems in anesthesiology, this thesis examined the general structure of functional AR guidance systems suitable for ultrasound-guided needle interventions. Multiple components of a functional AR system, including ultrasound calibration, interface design, and data visualization, were examined in this thesis, a summary of which is provided in the following section.

6.1 Contributions of the Thesis

Despite the extensive use of AR ultrasound image guidance (AR-UIG) systems in image-guided surgery and therapy, the goals, guidelines, and best practices for the development of such tools were not clearly reported prior to this work. In Chapter 2, the first steps towards defining a framework for developing such systems were taken. This chapter brought together the goals of AR-UIG systems as well as a list of guidelines and best practices for their de-

135

velopment, taking into account the nuances for medical software development. The goals of an AR-UIG system, unambiguous and desirable for a given clinical application, help justify and elucidate system requirements and evaluation approaches. Development guidelines, essentially, promote these goals and are used by the designer of such tools to identify best design decisions, the implementation of which is directed by best development practices. With the applications of AR guidance systems increasing more than ever, this work aimed to open the dialogue in the AR image guidance community about fundamentals of functional AR guidance systems to facilitate the development of such systems.

Ultrasound calibration, a fundamental criterion for the inclusion of ultrasound images in a functional AR-UIG system, often relies on localizing a number of fiducials in B-mode ultrasound images. The accuracy of fiducial localization affects the total accuracy of ultrasound calibration. In Chapter 3, the effects of image construction type as well as phantom materials on fiducial localization and total ultrasound calibration accuracy were studied. For Z-bar calibration, it was shown that synthetic aperture imaging (SAI) improved ultrasound calibration by reducing fiducial localization error, fiducial registration error, and target registration error. The study of phantom physical properties, such as material and geometrical size, concluded that the image reconstruction and beamforming technique should be considered when designing ultrasound calibration phantoms. This work resulted in a series of recommendations for improving ultrasound calibration, including using (1) small PVA-C tubes (around 3 mm in diameter) with SAI and (2) plastic straws (7 mm in diameter) when only conventional B-mode ultrasound is available.

Chapter 4 provided an evaluation and a critique of the design decisions made for an AR-UIG system tailored to central line procedures to improve needle tip visualization in ultrasound. Evaluation of the system was performed against conventional ultrasound-only guidance in a novice and an expert user study on custom-made phantoms. Performance of the novice operators significantly improved with the AR-UIG system in terms of time and normalized needle path-length. However, the AR-UIG system did not significantly affect the performance

of expert operators. The interface design decisions that resulted in the lackluster outcomes were critiqued within the context of the AR-UIG system development guidelines. This work highlighted the importance of forming design decisions based on the described development guidelines and yet bearing in mind that the success of an AR-UIG system ultimately relies on the successful balancing of competing guidelines in each design decision, directed by clinical use.

Moreover, in this chapter, the concept of quantitative skill assessment for teaching and deliberate practice of ultrasound guidance for central line procedures was proposed and the role of tracking technologies in providing platforms for standardized teaching and quality assurance discussed. The study with experienced operators showed not only the variability in, but also the inadequacy of the implementation of ultrasound image guidance for needle navigation and placement in a simulated central line procedure performed by experienced physicians. The findings restated that great professional experience does not necessarily result in expert level performance, a concept well established in expert performance studies.

Chapter 5 discussed the design, development, and preliminary evaluation of an AR-UIG system tailored to epidural injections. The software was developed on an open source platform, i.e. 3D Slicer, and made available to developers interested in implementing similar guidance systems. This guidance system was designed to address challenges in both navigation and positioning of a needle in the epidural space by integrating AR visualization, B-mode, and A-mode ultrasound. A-mode ultrasound was provided using a high-frequency single-element ultrasound transducer housed at the tip of a 19 gauge hypodermic tube, which would fit inside the introducer needle. The design, development, and evaluation of this transducer were discussed in this chapter.

The visualization interface included B-mode ultrasound integrated within a 3D AR scene, in which a virtual representation of the needle and its trajectory were displayed. In an adjacent 2D scene, the B-mode image was displayed face-on, similar to the visualization on the scanner. The 2D image was augmented with a virtual contour of the needle intersection with the image

plane. The 3D and 2D visualizations were provided to guide needle navigation to the vicinity of the epidural space. A-mode ultrasound was displayed to provide fine grained guidance for needle positioning. Results from the preliminary evaluation study, performed by novice operators, suggested that this AR-UIG system has potential to improve needle navigation and positioning in the phantom epidural space compared to ultrasound-only guidance.

6.2   Areas not Discussed and Concurrent Developments

This thesis focused on the role of AR-UIG systems for needle interventions in anesthesiology, integrating external magnetic sensors for tracking purposes required for navigation and A-mode ultrasound, obtained from a miniaturized needle ultrasound transducer, for positioning. Tangential to this work, there has been major developments by other researchers to overcome challenges with the use of external tracking and miniaturized imaging systems for applications in image-guided interventions. As these techniques could be integrated in AR-UIG systems with applications in anesthesiology, they are briefly discussed in this section.

Currently, external tracking technologies, such as optical or magnetic tracking systems, are used for tracking purposes in image guided interventions. However, the cost and OR footprint of these technologies may prohibit them from wide adoption beyond the major hospitals. While it is expected that these technologies will become more prevalent and accessible over time, efforts for developing ultrasound-based tracking have been underway, aiming to eliminate the need for external tracking systems for ultrasound-guided procedures. One of the ultrasound-based tracking techniques that has been proposed by Mung *et al.* involves integrating one or more ultrasound transducer elements on a surgical tool [150, 151]. In this technique, the acoustic pulses from these active ultrasound elements are picked up by an ultrasound receiver, such as a conventional ultrasound probe, and the time-of-flight is calculated to localize the active element accurately. Although this technique is still in its infancy, it is promising and the needle transducer, developed in this thesis, is a perfect candidate for it. Pulses sent by the

needle transducer or the subtle vibrations of the needle during ultrasound transmission could be picked up by a commercially available ultrasound probe and used to localize the needle tip.

Another approach investigated for ultrasound-based tracking involves automatic segmentation of the needle in ultrasound images by extracting signatures from the needle in the image [11, 12, 13, 54, 158, 210, 222]. Multiple techniques have been investigated for identifying the needle tip in 3D ultrasound, including, but not limited to, Hough transform, time-series analysis, and machine learning.

With regards to augmenting surgical tools with miniaturized imaging systems, optical coherence tomography has also been integrated within a needle bore for extracting information from the tissue structures in front of the needle tip for applications in anesthesiology [55, 198]. Moreover, Finlay *et al.* [66] have invented and validated an all-optical ultrasound probe for *in vivo* medical imaging in a porcine heart model. This system uses two optical fibers, one with a coating that enables generation of ultrasound photoacousticly, and the other with an interferometer detecting reflected ultrasound from tissue. One of the main advantages of this technology over electronic ultrasound transducers is the small size of the fiber optics, making them suitable for miniaturization and integration in small bore catheters and needles. In addition, this technique eliminates the direct insertion of active electronics components into the surgical tool and therefore into the body, facilitating obtaining regulatory clearance.

6.3   A Look to the Future

While many technologies are currently being developed in parallel to address different challenges in ultrasound-guided procedures in anesthesiology, it is envisaged that in the future, the most successful of these technologies will come together to provide a comprehensive solution to the extant clinical challenges in such procedures. The path toward a commercially viable and accessible guidance system for anesthesiology will be similar to that in other fields, such as neurosurgery that have had a longer history of image guidance. While several systems

with seemingly different functionalities have been developed in purely research settings, to-day, only a handful of functional neuronavigation systems are commercially available, which integrate many aspects of early developments, from image processing to advanced visualiza-tion techniques. The features of an all encompassing, multiuse guidance system for needle interventions in anesthesiology will include advanced 3D visualization displays, provided by, for example, HMDs or stereoscopic systems, image-based tracking, and needles augmented with sensing capabilities. Such advanced displays will overcome challenges with the physical disconnect between the display and the surgical site, lowering the cognitive load. Image-based tracking will reduce not only the cost, but also improve the ergonomics, making the system more accessible and easy to use. "Smart" surgical tools, providing sensing capabilities directly from the needle tip, combined with advanced data processing techniques will enable the needle itself to "see" where it is going. Such functionality will detect the anatomical structures in front of the needle tip and monitor its position with respect to the target.

In addition to enhancing all aspects of ultrasound-guided needled interventions, from tar-geting to navigation to positioning, such a system will impact teaching and training, skill as-sessment, standardization of practice, and adoption in the clinic. As discussed in this thesis, currently, there is no standardized method for teaching ultrasound guidance. However, in the future, multiuse guidance systems will open doors for enhanced training, skill assessment, and deliberate practice, where the trainees or experienced operators can review and assess their performance post-procedurally, using the same guidance system that they would employ for image guidance in the clinic. Such a guidance system will facilitate standardization of teach-ing, training, and even practice of needle interventions.

As the visualization techniques become increasingly mature and imaging systems more miniaturized and accessible, the ease of use, multi-functionality, and added clinical value of ul-trasound guidance systems will lower the adoption barrier and the training required for achiev-ing expert level performance. In turn, this will lead to accurate needle placements, reduced healthcare costs, and improved patient care.

Bibliography

[1] www.schlespain.com/wpblog/?page_id=1881.

[2] Kamyar Abhari, John SH Baxter, Elvis C. S. Chen, Ali R Khan, Terry M Peters, Sandrine de Ribaupierre, and Roy Eagleson. Training for planning tumour resection: augmented reality and human factors. *IEEE Transactions on Biomedical Engineering*, 62(6):1466–1477, 2015.

[3] Hadim Akoglu, Serhan Piskinpasa, Ezgi C Yenigun, Ramazan Ozturk, Fatih Dede, and Ali R Odabas. Real-time ultrasound guided placement of temporary internal jugular vein catheters: Assessment of technical success and complication rates in nephrology practice. *Nephrology*, 17(7):603–606, 2012.

[4] Golafsoun Ameri, John SH Baxter, A Jonathan McLeod, Uditha L Jayaranthe, Elvis CS Chen, and Terry M Peters. Synthetic aperture imaging in ultrasound calibration. In *SPIE Medical Imaging*, pages 90361I–90361I. International Society for Optics and Photonics, 2014.

[5] Golafsoun Ameri, A Jonathan McLeod, John SH Baxter, Elvis CS Chen, and Terry M Peters. Line fiducial material and thickness considerations for ultrasound calibration. In *SPIE Medical Imaging*, pages 941529–941529. International Society for Optics and Photonics, 2015.

[6] David Armstrong. Epidurals linked to paralysis seen with $300 billion pain market.

[7] Christian Ayoub, Catherine Lavallée, and André Denault. Ultrasound guidance for internal jugular vein cannulation: Continuing professional development. *Canadian Journal of Anesthesia/Journal Canadien d'anesthésie*, 57(5):500–514, 2010.

[8] Michael P Bannon, Stephanie F Heller, and Mariela Rivera. Anatomic considerations for central venous cannulation. *Risk Manag Healthc Policy*, 4:27–39, 2011.

[9] Michael Baumann, Pierre Mozer, Vincent Daanen, and Jocelyne Troccaz. Prostate biopsy assistance system with gland deformation estimation for enhanced precision. In *International Conference on Medical Image Computing and Computer-Assisted Intervention*, pages 67–74. Springer, 2009.

[10] Jeffrey Bax, Derek Cool, Lori Gardi, Kerry Knight, David Smith, Jacques Montreuil, Shi Sherebrin, Cesare Romagnoli, and Aaron Fenster. Mechanically assisted 3D ultrasound guided prostate biopsy system. *Medical Physics*, 35(12):5397–5410, 2008.

[11] Parmida Beigi, Robert Rohling, Septimiu E Salcudean, and Gary C Ng. Spectral analysis of the tremor motion for needle detection in curvilinear ultrasound via spatiotemporal linear sampling. *International Journal of Computer Assisted Radiology and Surgery*, 11(6):1183–1192, 2016.

[12] Parmida Beigi, Robert Rohling, Tim Salcudean, Victoria A Lessoway, and Gary C Ng. Needle trajectory and tip localization in real-time 3-D ultrasound using a moving stylus. *Ultrasound in Medicine & biology*, 41(7):2057–2070, 2015.

[13] Parmida Beigi, Robert Rohling, Tim Salcudean, Victoria A Lessoway, and Gary C Ng. Detection of an invisible needle in ultrasound using a probabilistic svm and time-domain features. *Ultrasonics*, 78:18–22, 2017.

[14] David Belavy, MJ Ruitenberg, and RB Brijball. Feasibility study of real-time three-/four-dimensional ultrasound for epidural catheter insertion. *British Journal of Anaesthesia*, 107(3):438–445, 2011.

[15] Leila Besharati Tabrizi and Mehran Mahvash. Augmented reality–guided neurosurgery: accuracy and intraoperative application of an image projection technique. *Journal of Neurosurgery*, 123(1):206–211, 2015.

[16] Paul J Besl and Neil D McKay. Method for registration of 3-D shapes. In *Robotics-DL tentative*, pages 586–606. International Society for Optics and Photonics, 1992.

[17] Christoph Bichlmeier, Felix Wimmer, Sandro Michael Heining, and Nassir Navab. Contextual anatomic mimesis hybrid in-situ visualization method for improving multi-sensory depth perception in medical augmented reality. In *Mixed and Augmented Reality, 2007. ISMAR 2007. 6th IEEE and ACM International Symposium on*, pages 129–138. IEEE, 2007.

[18] Nykolai Bilaniuk and George SK Wong. Speed of sound in pure water as a function of temperature. *The Journal of the Acoustical Society of America*, 93(3):1609–1612, 1993.

[19] Mark Billinghurst, Raphael Grasset, and Julian Looser. Designing augmented reality interfaces. *ACM Siggraph Computer Graphics*, 39(1):17–22, 2005.

[20] Michael Blaivas and Srikar Adhikari. An unseen danger: Frequency of posterior vessel wall penetration by needles during attempts to place internal jugular vein central catheters using ultrasound guidance. *Critical Care Medicine*, 37(8):2345–2349, 2009.

[21] Andrew Bowdle. Vascular complications of central venous catheter placement: Evidence-based methods for prevention and treatment. *Journal of Cardiothoracic and Vascular Anesthesia*, 28(2):358–368, 2014.

[22] Chuck Bradley. Retrospective transmit beamformation. ACUSON SC2000 volume imaging ultrasound system (white paper). *Available online, URL* : *www.siemens.com.tr/i/Assets/saglik/Whitepaper_Bradley.pdf*, 2008.

[23] Andreas Hjelm Brandt, Martin Christian Hemmsen, Peter Møller Hansen, Signe Sloth Madsen, Paul Suno Krohn, Theis Lange, Kristoffer Lindskov Hansen, Jørgen Arendt Jensen, and Michael Bachmann Nielsen. Clinical evaluation of synthetic aperture harmonic imaging for scanning focal malignant liver lesions. *Ultrasound in Medicine & biology*, 41(9):2368–2375, 2015.

[24] Silke Brinkmann, Geneviève Germain, Andrew Sawka, Raymond Tang, and Himat Vaghadia. Is there a place for ultrasound in neuraxial anesthesia? *Imaging in Medicine*, 5(2):177–186, 2013.

[25] Silke Brinkmann, Raymond Tang, Andrew Sawka, and Himat Vaghadia. Single-operator real-time ultrasound-guided spinal injection using SonixGPS® a case series. *Canadian Journal of Anesthesia/Journal canadien d'anesthésie*, 60(9):896–901, 2013.

[26] CR Broadbent, WB Maxwell, R Ferrie, DJ Wilson, M Gawne-Cain, and R Russell. Ability of anaesthetists to identify a marked lumbar interspace. *Anaesthesia*, 55(11):1122–1126, 2000.

[27] Mikael Brudfors, Alexander Seitel, Abtin Rasoulian, Andras Lasso, Victoria A Lessoway, Jill Osborn, Atsuto Maki, Robert N Rohling, and Purang Abolmaesumi. Towards real-time, tracker-less 3D ultrasound guidance for spine anaesthesia. *International Journal of Computer Assisted Radiology and Surgery*, 10(6):855–865, 2015.

[28] John Canny. A computational approach to edge detection. *IEEE Transactions on Pattern Analysis and Machine Intelligence*, (6):679–698, 1986.

[29] L Cavanna, G Civardi, P Mordenti, D Vallisa, R Bertè, and C Di Nunzio. Central venous catheter care for the patients with cancer: ultrasound-guided insertion should be strongly recommended for internal jugular vein catheterization. *Annals of oncology*, page mdt387, 2013.

[30] William F Chandler, James E Knake, John E McGillicuddy, Kevin O Lillehei, and Terry M Silver. Intraoperative use of real-time ultrasonography in neurosurgery. *Journal of Neurosurgery*, 57(2):157–163, 1982.

[31] Wilson M Chang, Nikhil B Amesur, Roberta L Klatzky, Albert B Zajko, and George D Stetten. Vascular access: Comparison of us guidance with the sonic flashlight and conventional us in phantoms. *Radiology*, 241(3):771–779, 2006.

[32] Wilson M Chang, Michael B Horowitz, and George D Stetten. Intuitive intraoperative ultrasound guidance using the sonic flashlight: a novel ultrasound display system. *Operative Neurosurgery*, 56(suppl_4):ONS–434, 2005.

[33] G. A. Chapman, D. Johnson, and A. R. Bodenham. Visualisation of needle position using ultrasonography. *Anaesthesia*, 61(2):148–158, 2006.

[34] Elvis CS Chen, A Jonathan McLeod, John S. H. Baxter, and Terry M Peters. Registration of 3D shapes under anisotropic scaling: Anisotropic-scaled iterative closest point algorithm. *International Journal of Computer Assisted Radiology and Surgery*, 10(6):867–878, 2015.

[35] Elvis CS Chen, A Jonathan McLeod, John SH Baxter, and Terry M Peters. An iterative closest point framework for ultrasound calibration. In *Augmented Environments for Computer-Assisted Interventions*, pages 69–79. Springer, 2015.

[36] Elvis CS Chen, A Jonathan McLeod, Uditha L Jayarathne, and Terry M Peters. Solving for free-hand and real-time 3D ultrasound calibration with anisotropic orthogonal procrustes analysis. In *SPIE Medical Imaging*, pages 90361Z–90361Z. International Society for Optics and Photonics, 2014.

[37] Elvis CS Chen, Terry M Peters, and Burton Ma. Guided ultrasound calibration: where, how, and how many calibration fiducials. *International Journal of Computer Assisted Radiology and Surgery*, 11(6):889–898, 2016.

[38] Thomas Kuiran Chen, Adrian D Thurston, Randy E Ellis, and Purang Abolmaesumi. A real-time freehand ultrasound calibration system with automatic accuracy feedback and control. *Ultrasound in Medicine & Biology*, 35(1):79–93, January 2009.

[39] Huihua K Chiang, Qifa Zhou, M Susan Mandell, Mei-Yung Tsou, Shih-Pin Lin, K Kirk Shung, and Chien-Kun Ting. Novel epidural needle with embedded high-frequency ultrasound transducer- epidural access in porcine model. *Anesthesiology*, 114(6):1320, 2011.

[40] Richard Y Chiao and Lewis J Thomas. Synthetic transmit aperture imaging using orthogonal golay coded excitation. In *Ultrasonics Symposium, 2000 IEEE*, volume 2, pages 1677–1680. IEEE, 2000.

[41] Ki Jinn Chin, Manoj Kumar Karmakar, and Philip Peng. Ultrasonography of the adult thoracic and lumbar spine for central neuraxial blockade. *The Journal of the American Society of Anesthesiologists*, 114(6):1459–1485, 2011.

[42] Olivier Choquet and Xavier Capdevila. Three-dimensional high-resolution ultrasound-guided nerve blocks: a new panoramic vision of local anesthetic spread and perineural catheter tip location. *Anesthesia & Analgesia*, 116(5):1176–1181, 2013.

[43] K Cleary and T M Peters. Image-guided interventions: technology review and clinical applications. *Annu Rev Biomed Eng*, 12:119–142, 2010.

[44] Roch M Comeau, Abbas F Sadikot, Aaron Fenster, and Terry M Peters. Intraoperative ultrasound for guidance and tissue shift correction in image-guided neurosurgery. *Medical Physics*, 27(4):787–800, 2000.

[45] International Electrotechnical Commission. *Medical device software- software life cycle processes*. IEC Standard 62304, 2006.

[46] Patrick H Conroy, Cédric Luyet, Colin J McCartney, and Paul G McHardy. Real-time ultrasound-guided spinal anaesthesia: a prospective observational study of a new approach. *Anesthesiology Research and Practice*, 2013, 2013.

[47] Randall C Cork, Joseph J Kryc, and Robert W Vaughan. Ultrasonic localization of the lumbar epidural space. *Anesthesiology*, 52(6):513–515, 1980.

[48] JM Currie. Measurement of the depth to the extradural space using ultrasound. *BJA: British Journal of Anaesthesia*, 56(4):345–347, 1984.

[49] Maria E Currie, A Jonathan McLeod, Rajni Patel, Terry M Peters, and Bob Kiaii. Augmented reality system for ultrasound guidance of transcatheter aortic valve replacement. *Canadian Journal of Cardiology*, 31(10):S182, 2015.

[50] Andrei Danilchenko and J Michael Fitzpatrick. General approach to first-order error prediction in rigid point registration. *Medical Imaging, IEEE Transactions on*, 30(3):679–693, 2011.

[51] Getulio R de Oliveira Filho, HP Gomes, MHZ Da Fonseca, JC Hoffman, SG Pederneiras, and JHS Garcia. Predictors of successful neuraxial block: a prospective study. *European Journal of Anaesthesiology*, 19(6):447–451, 2002.

[52] Bart G Denys and Barry F Uretsky. Anatomical variations of internal jugular vein location: Impact on central venous access. *Critical Care Medicine*, 19(12):1516–1519, 1991.

[53] Bart G Denys, Barry F Uretsky, and P Sudhakar Reddy. Ultrasound-assisted cannulation of the internal jugular vein. A prospective comparison to the external landmark-guided technique. *Circulation*, 87(5):1557–1562, 1993.

[54] Mingyue Ding and Aaron Fenster. A real-time biopsy needle segmentation technique using hough transform. *Medical Physics*, 30(8):2222–2233, 2003.

[55] Zhenyang Ding, Qinggong Tang, Chia-Pin Liang, Kyle Wu, Anthony Sandlerc, Hui Li, and Yu Chen. Imaging spinal structures with polarization-sensitive optical coherence tomography. *IEEE Photonics Journal*, 8(5):1–8, 2016.

[56] Sarah R Drewett. Central venous catheter removal: procedures and rationale. *British journal of nursing*, 9(22):2304–2315, 2000.

[57] Matt Dunleavy. Design principles for augmented reality learning. *TechTrends*, 58(1):28–34, 2014.

[58] PJ Edwards, DJ Hawkes, DLG Hill, D Jewell, R Spink, A Strong, and M Gleeson. Augmentation of reality using an operating microscope for otolaryngology and neurosurgical guidance. *Journal of Image Guided Surgery*, 1(3):172–178, 1995.

[59] Joerg Ender, Jasmina Končar-Zeh, Chirojit Mukherjee, Stephan Jacobs, Michael A Borger, Christoph Viola, Michael Gessat, Jens Fassl, Friedrich W Mohr, and Volkmar Falk. Value of augmented reality-enhanced transesophageal echocardiography (TEE) for determining optimal annuloplasty ring size during mitral valve repair. *The Annals of Thoracic Surgery*, 86(5):1473–1478, 2008.

[60] Nancy Epstein. The risks of epidural and transforaminal steroid injections in the spine: Commentary and a comprehensive review of the literature. *Surgical Neurology International*, 4:74, 2013.

[61] K. Anders Ericsson. Deliberate practice and acquisition of expert performance: A general overview. *Academic Emergency Medicine*, 15(11):988–994, 2008.

[62] Azharhosein Faraz, Terry M Peters, and Elvis CS Chen. Automatic real-time intraoperative 2D bi-plane ultrasound calibration during *in situ* minimally invasive heart surgery. *International Journal of Computer Assisted Radiology and Surgery, Suppl 1*, page S112, 2015.

[63] Andriy Fedorov, Reinhard Beichel, Jayashree Kalpathy-Cramer, Julien Finet, Jean-Christophe Fillion-Robin, Sonia Pujol, Christian Bauer, Dominique Jennings, Fiona Fennessy, Milan Sonka, and J. Buatti. 3D slicer as an image computing platform for the quantitative imaging network. *Magnetic Resonance Imaging*, 30(9):1323–1341, 2012.

[64] Neil G Feinglass, Steven R Clendenen, Klaus D Torp, R Doris Wang, Ramon Castello, and Roy A Greengrass. Real-time three-dimensional ultrasound for continuous popliteal blockade: a case report and image description. *Anesthesia & Analgesia*, 105(1):272–274, 2007.

[65] Robinson M Ferre and Mark Mercier. Novel ultrasound guidance system for real-time central venous cannulation: safety and efficacy. *Western Journal of Emergency Medicine*, 15(4):536, 2014.

[66] Malcolm C Finlay, Charles A Mosse, Richard J Colchester, Sacha Noimark, Edward Z Zhang, Sebastien Ourselin, Paul C Beard, Richard J Schilling, Ivan P Parkin, Ioannis Papakonstantinou, and Adrien E Desjardins. Through-needle all-optical ultrasound imaging in vivo: a preclinical swine study. *Light: Science & Applications*, 6(12):e17103, 2017.

[67] J Michael Fitzpatrick. Fiducial registration error and target registration error are uncorrelated. In *SPIE Medical Imaging*, pages 726102–726102. International Society for Optics and Photonics, 2009.

[68] J Michael Fitzpatrick and Jay B West. The distribution of target registration error in rigid-body point-based registration. *Medical Imaging, IEEE Transactions on*, 20(9):917–927, 2001.

[69] J Michael Fitzpatrick, Jay B West, and Calvin R Maurer Jr. Predicting error in rigid-body point-based registration. *Medical Imaging, IEEE Transactions on*, 17(5):694–702, 1998.

[70] Gillian L Foxall, Jonathan G Hardman, and Nigel M Bedforth. Three-dimensional, mul-tiplanar, ultrasound-guided, radial nerve block. *Regional Anesthesia and Pain Medicine*, 32(6):516–521, 2007.

[71] Catherine H Frazier and William D O'Brien. Synthetic aperture techniques with a vir-tual source element. *IEEE Transactions on Ultrasonics, Ferroelectrics, and Frequency Control*, 45(1):196–207, 1998.

[72] James LH French, Nick J Raine-Fenning, Jonathan G Hardman, and Nigel M Bedforth. Pitfalls of ultrasound guided vascular access: The use of three/four-dimensional ultra-sound. *Anaesthesia*, 63(8):806–813, 2008.

[73] Henry Fuchs, Etta D Pisano, William F Garrett, Gentaro Hirota, Mark Livingston, Mary C Whitton, and Stephen M Pizer. Towards performing ultrasound-guided needle biopsies from within a head-mounted display. In *Visualization in Biomedical Comput-ing*, pages 591–600. Springer, 1996.

[74] G Furness, MP Reilly, and S Kuchi. An evaluation of ultrasound imaging for identifica-tion of lumbar intervertebral level. *Anaesthesia*, 57(3):277–280, 2002.

[75] K Lokke Gammelmark and J Arendt Jensen. Duplex synthetic aperture imaging with tissue motion compensation. In *Ultrasonics, 2003 IEEE Symposium on*, volume 2, pages 1569–1573. IEEE, 2003.

[76] K Løkke Gammelmark and J Arendt Jensen. Multielement synthetic transmit aperture imaging using temporal encoding. *IEEE Transactions on Medical Imaging*, 22(4):552–563, 2003.

[77] Darrell J Gaskin and Patrick Richard. The economic costs of pain in the united states. *The Journal of Pain*, 13(8):715–724, 2012.

[78] Ralf E Gebhard, Treniece N Eubanks, and Rachel Meeks. Three-dimensional ultrasound imaging. *Current Opinion in Anesthesiology*, 28(5):583–587, 2015.

[79] Sean Gill, Purang Abolmaesumi, Gabor Fichtinger, Jonathan Boisvert, David Pichora, Dan Borshneck, and Parvin Mousavi. Biomechanically constrained groupwise ultrasound to CT registration of the lumbar spine. *Medical Image Analysis*, 16(3):662–674, 2012.

[80] PL Gleason, Ron Kikinis, David Altobelli, William Wells, Eben Alexander III, Peter McL Black, and Ferenc Jolesz. Video registration virtual reality for nonlinkage stereotactic surgery. *Stereotactic and Functional Neurosurgery*, 63(1-4):139–143, 1994.

[81] Clifford S Goodman. *TA101: Introduction to health care technology assessment*. National Library of Medicine, 1998.

[82] Alan S Graham, Caroline Ozment, Ken Tegtmeyer, Susanna Lai, and Dana AV Braner. Central venous catheterization. *New England Journal of Medicine*, 356(21):e21, 2007.

[83] Thomas Grau, Rudiger W Leipold, Renate Conradi, and Eike Martin. Ultrasound control for presumed difficult epidural puncture. *Acta Anaesthesiologica Scandinavica*, 45(6):766–771, 2001.

[84] Thomas Grau, Rudiger W Leipold, Renate Conradi, Eike Martin, and Johann Motsch. Ultrasound imaging facilitates localization of the epidural space during combined spinal and epidural anesthesia. *Regional Anesthesia and Pain Medicine*, 26(1):64–67, 2001.

[85] Thomas Grau, Rudiger W Leipold, Renate Conradi, Eike Martin, and Johann Motsch. Efficacy of ultrasound imaging in obstetric epidural anesthesia. *Journal of Clinical Anesthesia*, 14(3):169–175, 2002.

[86] Daipayan Guha, Naif M Alotaibi, Nhu Nguyen, Shaurya Gupta, Christopher McFaul, and Victor XD Yang. Augmented reality in neurosurgery: A review of current concepts

and emerging applications. *Canadian Journal of Neurological Sciences*, 44(3):235–245, 2017.

[87] Jens Munk Hansen and Jorgen Arendt Jensen. Compounding in synthetic aperture imaging. *IEEE Transactions on Ultrasonics, Ferroelectrics, and Frequency Control*, 59(9), 2012.

[88] M Christian Hemmsen, P Møller Hansen, Theis Lange, J Munk Hansen, K Lindskov Hansen, M Bachmann Nielsen, and J Arendt Jensen. In vivo evaluation of synthetic aperture sequential beamforming. *Ultrasound in Medicine and Biology*, 38(4):708 – 716, 2012.

[89] M Christian Hemmsen, J Hee Rasmussen, and J Arendt Jensen. Tissue harmonic synthetic aperture ultrasound imaging. *The Journal of the Acoustical Society of America*, 136(4):2050–2056, 2014.

[90] Antony Hodgson. Computer-assisted orthopedic surgery. In Terry Peters and Kevin Cleary, editors, *Image-Guided Interventions: technology and applications*, pages 333–386. Springer Science & Business Media, 2008.

[91] Berthold KP Horn. Closed-form solution of absolute orientation using unit quaternions. *JOSA A*, 4(4):629–642, 1987.

[92] Po-Wei Hsu, Richard W Prager, Andrew H Gee, and Graham M Treece. Freehand 3D ultrasound calibration: A review. In *Advanced Imaging in Biology and Medicine*, pages 47–84. Springer Berlin Heidelberg, 2009.

[93] Po-Wei Hsu, Richard W Prager, Andrew H Gee, and Graham M Treece. *Freehand 3D ultrasound calibration: A review*. Springer, 2009.

[94] Judy Hung, Roberto Lang, Frank Flachskampf, Stanton K Shernan, Marti L McCulloch, David B Adams, James Thomas, Mani Vannan, and Thomas Ryan. 3D echocardiogra-

phy: a review of the current status and future directions. *Journal of the American Society of Echocardiography*, 20(3):213–233, 2007.

[95] Kaku Irisawa, Dai Murakoshi, Atsushi Hashimoto, Katsuya Yamamoto, and Toshiro Hayakawa. Needle tip visualization by bevel-point ultrasound generator and prototype photoacoustic imaging system. In *Photons Plus Ultrasound: Imaging and Sensing 2017*, volume 10064, page 1006448. International Society for Optics and Photonics, 2017.

[96] Asgeir S Jakola, Ingerid Reinertsen, Tormod Selbekk, Ole Solheim, Frank Lindseth, Sasha Gulati, and Geirmund Unsgård. Three-dimensional ultrasound–guided placement of ventricular catheters. *World Neurosurgery*, 82(3):536–e5, 2014.

[97] Pierre Jannin, J Michael Fitzpatrick, David Hawkes, Xavier Pennec, Ramin Shahidi, and Michael Vannier. Validation of medical image processing in image-guided therapy. *IEEE Transactions on Medical Imaging*, 21(12):1445–9, 2002.

[98] Pierre Jannin and Werner Korb. Assessment of image-guided interventions. In Terry Peters and Kevin Cleary, editors, *Image-Guided Interventions: technology and applications*, pages 531–549. Springer Science & Business Media, 2008.

[99] J Arendt Jensen, S Ivanov Nikolov, K Løkke Gammelmark, and M Høgholm Pedersen. Synthetic aperture ultrasound imaging. *Ultrasonics*, 44:e5–e15, 2006.

[100] Christian Jenssen, Boris Brkljacic, Michael Hocke, A. Ignee, Fabio Piscaglia, Maija Radzina, Paul S Sidhu, and Christoph F Dietrich. EFSUMB Guidelines on Interventional Ultrasound (INVUS), Part VI - Ultrasound-guided vascular interventions. *Ultraschall in der Medizin*, 37(5):473–476, 2016.

[101] Angela N Johnson, Jeffery S Peiffer, Nahi Halmann, Luke Delaney, Cindy A Owen, and Jeff Hersh. Ultrasound-guided needle technique accuracy: Prospective comparison of passive magnetic tracking versus unassisted echogenic needle localization. *Regional Anesthesia and Pain Medicine*, 42(2):223, 2017.

[102] Peter Jordan. Standard IEC 62304-medical device software-software lifecycle processes. 2006.

[103] Dimitrios Karakitsos, Nicolaos Labropoulos, Eric De Groot, Alexandros P Patrianakos, Gregorios Kouraklis, John Poularas, George Samonis, Dimosthenis A Tsoutsos, Manousos M Konstadoulakis, and Andreas Karabinis. Real-time ultrasound-guided catheterisation of the internal jugular vein: a prospective comparison with the landmark technique in critical care patients. *Critical Care*, 10(6):R162, 2006.

[104] Mustafa Karaman, Hasan S Bilge, and Matthew O'Donnell. Adaptive multi-element synthetic aperture imaging with motion and phase aberration correction. *IEEE Transactions on Ultrasonics, Ferroelectrics, and Frequency Control*, 45(4):1077–1087, 1998.

[105] Mustafa Karaman, Pai-Chi Li, and Matthew O'Donnell. Synthetic aperture imaging for small scale systems. *IEEE Transactions on Ultrasonics, Ferroelectrics, and Frequency Control*, 42(3):429–442, 1995.

[106] Manoj Karmakar, Xiang Li, Jiawei Li, Xavier Sala-Blanch, Admir Hadzic, and Tony Gin. Three-dimensional/four-dimensional volumetric ultrasound imaging of the sciatic nerve. *Regional Anesthesia and Pain Medicine*, 37(1):60–66, 2012.

[107] MK Karmakar, X Li, AM-H Ho, WH Kwok, and PT Chui. Real-time ultrasound-guided paramedian epidural access: evaluation of a novel in-plane technique. *British Journal of Anaesthesia*, 102(6):845–854, 2009.

[108] Takakazu Kawamata, Hiroshi Iseki, Takao Shibasaki, and Tomokatsu Hori. Endoscopic augmented reality navigation system for endonasal transsphenoidal surgery to treat pituitary tumors. *Neurosurgery*, 50(6):1393–1397, 2002.

[109] Siavash Khallaghi, Parvin Mousavi, Ren Hui Gong, Sean Gill, Jonathan Boisvert, Gabor Fichtinger, David Pichora, Dan Borschneck, and Purang Abolmaesumi. Registration of

a statistical shape model of the lumbar spine to 3D ultrasound images. In *International Conference on Medical Image Computing and Computer-Assisted Intervention*, pages 68–75. Springer, 2010.

[110] Ali Khamene and Frank Sauer. A novel phantom-less spatial and temporal ultrasound calibration method. In *International Conference on Medical Image Computing and Computer-Assisted Intervention*, pages 65–72. 2005.

[111] Yaariv Khaykin, Ofer Klemm, and Atul Verma. First human experience with real-time integration of intracardiac echocardiography and 3D electroanatomical imaging to guide right free wall accessory pathway ablation. *Europace*, 10(1):116–117, 2007.

[112] Won Hwa Kim, Jung Min Chang, Choye Kim, Jongho Park, Yangmo Yoo, Woo Kyung Moon, Nariya Cho, and Byung Ihn Choi. Synthetic aperture imaging in breast ultrasound: A preliminary clinical study. *Academic Radiology*, 19(8):923 – 929, 2012.

[113] David Kirsh. A few thoughts on cognitive overload. 2000.

[114] Daniel S Kopac, Jerry Chen, Raymond Tang, Andrew Sawka, and Himat Vaghadia. Comparison of a novel real-time SonixGPS needle-tracking ultrasound technique with traditional ultrasound for vascular access in a phantom gel model. *Journal of Vascular Surgery*, 58(3):735–741, 2013.

[115] Mert Koroglu, Mehmet Demir, Batikan K Koroglu, Mehmet T. Sezer, Okan Akhan, Hasan Yildiz, Lufti Yavuz, Bahar Baykal, and Orhan Oyar. Percutaneous Placement of Central Venous Catheters: Comparing the Anatomical Landmark Method with the Radiologically Guided Technique for Central Venous Catheterization Through the Internal Jugular Vein in Emergent Hemodialysis Patients. *Acta Radiologica*, 47(1):43–47, 2006.

[116] Jacob Kortbek, J Arendt Jensen, and K Løkke Gammelmark. Sequential beamforming for synthetic aperture imaging. *Ultrasonics*, 53(1):1–16, 2013.

[117] Sanghamithra Korukonda and Marvin M Doyley. Visualizing the radial and circumferential strain distribution within vessel phantoms using synthetic-aperture ultrasound elastography. *IEEE Transactions on Ultrasonics, Ferroelectrics, and Frequency Control*, 59(8):1639–1653, 2012.

[118] Jaroslaw Krejza, Michal Arkuszewski, Scott E Kasner, John Weigele, Andrzej Ustymowicz, Robert W Hurst, Brett L Cucchiara, and Steven R Messe. Carotid artery diameter in men and women and the relation to body and neck size. *Stroke*, 37(4):1103–1105, 2006.

[119] Pablo Lamata, Wajid Ali, Alicia Cano, Jordi Cornella, Jerome Declerck, Ole J Elle, Adinda Freudenthal, Hugo Furtado, Denis Kalkofen, Edvard Naerum, et al. Augmented reality for minimally invasive surgery: overview and some recent advances. In *Augmented Reality*. InTech, 2010.

[120] Andrew Lang, Parvin Mousavi, Sean Gill, Gabor Fichtinger, and Purang Abolmaesumi. Multi-modal registration of speckle-tracked freehand 3D ultrasound to CT in the lumbar spine. *Medical Image Analysis*, 16(3):675–686, 2012.

[121] Andras Lasso, Tamas Heffter, Adam Rankin, Csaba Pinter, Tamas Ungi, and Gabor Fichtinger. Plus: open-source toolkit for ultrasound-guided intervention systems. *IEEE Transactions on Biomedical Engineering*, 61(10):2527–2537, 2014.

[122] Andras Lasso, Tamas Heffter, Adam Rankin, Csaba Pinter, Tamas Ungi, and Gabor Fichtinger. Plus: open-source toolkit for ultrasound-guided intervention systems. *IEEE Transactions on Biomedical Engineering*, 61(10):2527–2537, 2014.

[123] Po-Yang Lee, Chih-Chung Huang, and Huihua K Chiang. Implementation of a novel high frequency ultrasound device for guiding epidural anesthesia-in vivo animal study. In *Ultrasonics Symposium (IUS), 2013 IEEE International*, pages 2049–2052. IEEE, 2013.

[124] Julie Leung, Martin Duffy, and Andrew Finckh. Real-Time Ultrasonographically-Guided Internal Jugular Vein Catheterization in the Emergency Department Increases Success Rates and Reduces Complications: A Randomized, Prospective Study. *Annals of Emergency Medicine*, 48(5):540–547, 2006.

[125] Cristian A Linte, Katherine P Davenport, Kevin Cleary, Craig Peters, Kirby G Vosburgh, Nassir Navab, Pierre Jannin, Terry M Peters, David R Holmes, and Richard A Robb. On mixed reality environments for minimally invasive therapy guidance: Systems architecture, successes and challenges in their implementation from laboratory to clinic. *Computerized Medical Imaging and Graphics*, 37(2):83–97, 2013.

[126] Cristian A Linte, John Moore, and Terry M Peters. How accurate is accurate enough? a brief overview on accuracy considerations in image-guided cardiac interventions. In *Engineering in Medicine and Biology Society (EMBC), 2010 Annual International Conference of the IEEE*, pages 2313–2316. IEEE, 2010.

[127] Cristian A Linte, John Moore, Andrew D Wiles, Chris Wedlake, and Terry M Peters. Virtual reality-enhanced ultrasound guidance: A novel technique for intracardiac interventions. *Computer Aided Surgery*, 13(2):82–94, 2008.

[128] Burton Ma, Mehdi H Moghari, Randy E Ellis, and Purang Abolmaesumi. Estimation of optimal fiducial target registration error in the presence of heteroscedastic noise. *Medical Imaging, IEEE Transactions on*, 29(3):708–723, 2010.

[129] Feroze Mahmood, Robina Matyal, Nikolaos Skubas, Mario Montealegre-Gallegos, Madhav Swaminathan, Andre Denault, Roman Sniecinski, John D Mitchell, Mark Taylor, Stephen Haskins, et al. Perioperative ultrasound training in anesthesiology: a call to action. *Anesthesia & Analgesia*, 122(6):1794–1804, 2016.

[130] Hanke E Marcus, Egfried Bonkat, Oguzhan Dagtekin, Robert Schier, Frank Petzke, Jens Wippermann, Bernd W Böttiger, and Peter Teschendorf. The impact of trendelenburg

position and positive end-expiratory pressure on the internal jugular cross-sectional area. *Anesthesia & Analgesia*, 111(2):432–436, 2010.

[131] D Marhofer, MK Karmakar, P Marhofer, SC Kettner, M Weber, and M Zeitlinger. Does circumferential spread of local anaesthetic improve the success of peripheral nerve block? *British Journal of Anaesthesia*, 113(1):177–185, 2014.

[132] Claude Martin, Beatrice Eon, Jean-pierre Auffray, Pierre Saux, and FranÇois Gouin. Axillary or internal jugular central venous catheterization. *Critical Care Medicine*, 18(4):400–402, 1990.

[133] David C McGee and Michael K Gould. Preventing complications of central venous catheterization. *New England Journal of Medicine*, 348(12):1123–1133, 2003.

[134] Martin McHugh, Fergal McCaffery, and Valentine Casey. Barriers to adopting agile practices when developing medical device software. In *International Conference on Software Process Improvement and Capability Determination*, pages 141–147. Springer, 2012.

[135] Martin McHugh, Fergal McCaffery, Brian Fitzgerald, Klaas-Jan Stol, Valentine Casey, and Garret Coady. Balancing agility and discipline in a medical device software organisation. In *International Conference on Software Process Improvement and Capability Determination*, pages 199–210. Springer, 2013.

[136] Jason McVicar, Ahtsham U Niazi, Harry Murgatroyd, Ki Jinn Chin, and Vincent W Chan. Novice performance of ultrasound-guided needling skills: effect of a needle guidance system. *Regional Anesthesia and Pain Medicine*, 40(2):150–153, 2015.

[137] Verena Constanze Meiser, Helene Kreysa, Orlando Guntinas-Lichius, and Gerd Fabian Volk. Comparison of in-plane and out-of-plane needle insertion with vs. without needle guidance. *European Archives of Oto-Rhino-Laryngology*, 273(9):2697–2705, 2016.

[138] Cécilia Menacé, Olivier Choquet, Bertrand Abbal, Sophie Bringuier, and Xavier Capdevila. Comparison of a gps needle-tracking system, multiplanar imaging and 2D imaging for real-time ultrasound-guided epidural anaesthesia: a randomized, comparative, observer-blinded study on phantoms. *Anaesthesia Critical Care & Pain Medicine*, 36(2):83–89, 2017.

[139] Antonio Meola, Fabrizio Cutolo, Marina Carbone, Federico Cagnazzo, Mauro Ferrari, and Vincenzo Ferrari. Augmented reality in neurosurgery: a systematic review. *Neurosurgical Review*, pages 1–12, 2016.

[140] Laurence Mercier, Thomas Langø, Frank Lindseth, and Louis D Collins. A review of calibration techniques for freehand 3-D ultrasound systems. *Ultrasound in Medicine & biology*, 31(2):143–165, 2005.

[141] Ralph Metson. Image-guided sinus surgery: lessons learned from the first 1000 cases. *Otolaryngology-Head and Neck Surgery*, 128(1):8–13, 2003.

[142] Paul Milgram, Haruo Takemura, Akira Utsumi, and Fumio Kishino. Augmented reality: A class of displays on the reality-virtuality continuum. In *Telemanipulator and telepresence technologies*, volume 2351, pages 282–292, 1994.

[143] Truman J Milling, John Rose, William M Briggs, Robert Birkhahn, Theodore J Gaeta, Joseph J Bove, and Lawrence A Melniker. Randomized, controlled clinical trial of point-of-care limited ultrasonography assistance of central venous cannulation: the Third Sonography Outcomes Assessment Program (SOAP-3) Trial. *Critical Care Medicine*, 33(8):1764–1769, 2005.

[144] Andres Missair, Robyn S Weisman, Maria Rene Suarez, Relin Yang, and Ralf E Gebhard. A 3-dimensional ultrasound study of local anesthetic spread during lateral popliteal nerve block: what is the ideal end point for needle tip position? *Regional Anesthesia and Pain Medicine*, 37(6):627–632, 2012.

[145] Gabriel Montaldo, Mickaël Tanter, Jérémy Bercoff, Nicolas Benech, and Mathias Fink. Coherent plane-wave compounding for very high frame rate ultrasonography and transient elastography. *IEEE Transactions on Ultrasonics, Ferroelectrics, and Frequency Control*, 56(3):489–506, 2009.

[146] Christopher L Moore and Joshua A Copel. Point-of-care ultrasonography. *New England Journal of Medicine*, 364(8):749–757, 2011.

[147] John T Moore, Michael WA Chu, Bob Kiaii, Daniel Bainbridge, Gerrard Guiraudon, Chris Wedlake, Maria Currie, Martin Rajchl, Rajni Patel, and Terry M Peters. A navigation platform for guidance of beating heart transapical mitral valve repair. *IEEE Transactions on Biomedical Engineering*, 60(4):1034–1040, April 2013.

[148] G Edward Morgan, Maged S Mikhail, Michael J Murray, Wayne Kleinman, Gary J Nitti, Joseph T Nitti, Julio Raya, Robert F Bedford, Julian F Bion, John Butterworth, et al. *Clinical anesthesiology*, volume 1. McGraw-hill New York, 2002.

[149] Mohammad Reza Movahed. Ultrasound-guided internal jugular vein cannulation. *The New England Journal of Medicine*, 363(8):796; author reply 796–797, 2010.

[150] Jay Mung, Francois Vignon, Ramon Erkamp, Doug Stanton, and Ameet Jain. Ultrasonically marked instruments for ultrasound-guided interventions. In *Ultrasonics Symposium (IUS), 2013 IEEE International*, pages 2053–2056. IEEE, 2013.

[151] Jay Mung, Francois Vignon, and Ameet Jain. A non-disruptive technology for robust 3d tool tracking for ultrasound-guided interventions. In *International Conference on Medical Image Computing and Computer-Assisted Intervention*, pages 153–160. Springer, 2011.

[152] Simrin Nagpal, Purang Abolmaesumi, Abtin Rasoulian, Tamas Ungi, Ilker Hacihaliloglu, Jill Osborn, Dan P Borschneck, Victoria A Lessoway, Robert N Rohling, and

Parvin Mousavi. CT to US registration of the lumbar spine: a clinical feasibility study. In *International Conference on Information Processing in Computer-Assisted Interventions*, pages 108–117. Springer, 2014.

[153] David Napolitano, Ching-Hua Chou, Glen W McLaughlin, Derek DeBusschere, Larry YL Mo, and Ting-Lan Ji. Zone-based B-mode imaging. In *Ultrasonics, 2003 IEEE Symposium on*, volume 1, pages 25–28. IEEE, 2003.

[154] AU Niazi, KJ Chin, R Jin, and VW Chan. Real-time ultrasound-guided spinal anesthesia using the SonixGPS ultrasound guidance system: a feasibility study. *Acta Anaesthesiologica Scandinavica*, 58(7):875–881, 2014.

[155] PKT Nichols and E Major. Central venous cannulation. *Current Anaesthesia & Critical Care*, 1(1):54–60, 1989.

[156] RWD Nickalls and MS Kokri. The width of the posterior epidural space in obstetric patients. *Anaesthesia*, 41(4):432–433, 1986.

[157] S Ivanov Nikolov and J Arendt Jensen. Investigation of the feasibility of 3D synthetic aperture imaging. In *IEEE Symposium on Ultrasonics*, volume 2, pages 1903–1906 Vol.2, Oct 2003.

[158] Paul M Novotny, Jeff A Stoll, Nikolay V Vasilyev, J Pedro, Pierre E Dupont, Todd E Zickler, and Robert D Howe. GPU based real-time instrument tracking with three-dimensional ultrasound. *Medical Image Analysis*, 11(5):458–464, 2007.

[159] David P Odasso. Internal jugular vein and carotid artery anatomic relation as determined by ultrasonography. *Anesthesiology*, 85(1.1111):35–8, 1996.

[160] Matthew O'Donnell and Yao Wang. Coded excitation for synthetic aperture ultrasound imaging. *IEEE Transactions on Ultrasonics, Ferroelectrics, and Frequency Control*, 52(2):171–176, 2005.

[161] Nobuyuki Otsu. A threshold selection method from gray-level histograms. *Automatica*, 11(285-296):23–27, 1975.

[162] Catherine M Otto. *The practice of clinical echocardiography*. Elsevier Health Sciences, 2012.

[163] Luis C Paschoarelli, Ana B de Oliveira, and Helenice JCG Coury. Assessment of the ergonomic design of diagnostic ultrasound transducers through wrist movements and subjective evaluation. *International Journal of Industrial Ergonomics*, 38(11):999–1006, 2008.

[164] Richard G Paul and Susanna Price. Central venous cannulation. *Medicine*, 42(8):473–474, 2014.

[165] Mark C Paulk. On empirical research into scrum adoption. *Institute for Software Research, Carnegie Mellon University*, 2011.

[166] Tina H Pedersen, Jonas Meuli, Eike J Plazikowski, Maximilian Buttenberg, Maren Kleine-Brueggeney, Christian Seidl, Lorenz Theiler, and Robert Greif. Loss of resistance: A randomised controlled trial assessing four low-fidelity epidural puncture simulators. *European Journal of Anaesthesiology (EJA)*, 34(9):602–608, 2017.

[167] Brett W Pelham. *Intermediate statistics: A conceptual course*. Sage, 2012.

[168] Anahi Perlas, Luis E Chaparro, and Ki Jinn Chin. Lumbar neuraxial ultrasound for spinal and epidural anesthesia: a systematic review and meta-analysis. *Regional Anesthesia and Pain Medicine*, 41(2):251–260, 2016.

[169] Terry Peters and Kevin Cleary. *Image-guided interventions: technology and applications*. Springer, 2008.

[170] Terry M Peters and Cristian A Linte. Image-guided interventions and computer-integrated therapy: Quo vadis? *Medical Image Analysis*, 33:56–63, 2016.

[171] Richard W Prager, RN Rohling, AH Gee, and Laurence Berman. Rapid calibration for 3-D freehand ultrasound. *Ultrasound in Medicine & biology*, 24(6):855–869, 1998.

[172] Claudio Pratola, Elisa Baldo, Paolo Artale, Lina Marcantoni, Tiziano Toselli, Gianfranco Percoco, Biagio Sassone, and Roberto Ferrari. Different image integration modalities to guide af ablation: impact on procedural and fluoroscopy times. *Pacing and Clinical Electrophysiology*, 34(4):422–430, 2011.

[173] Morten Fischer Rasmussen and Jørgen Arendt Jensen. Comparison of 3-D synthetic aperture phased-array ultrasound imaging and parallel beamforming. *IEEE transactions on Ultrasonics, Ferroelectrics, and Frequency Control*, 61(10):1638–1650, 2014.

[174] F Reynolds. Logic in the safe practice of spinal anaesthesia. *Anaesthesia*, 55(11):1045–1046, 2000.

[175] David W Roberts, John W Strohbehn, John F Hatch, William Murray, and Hans Kettenberger. A frameless stereotaxic integration of computerized tomographic imaging and the operating microscope. *Journal of neurosurgery*, 65(4):545–549, 1986.

[176] Lauryn R Rochlen, Robert Levine, and Alan R Tait. First-person point-of-viewaugmented reality for central line insertion training. *Simulation in Healthcare: The Journal of the Society for Simulation in Healthcare*, 12(1):1, 2016.

[177] Michael Rosenthal, Andrei State, Joohi Lee, Gentaro Hirota, Jeremy Ackerman, Kurtis Keller, Etta D Pisano, Michael Jiroutek, Keith Muller, and Henry Fuchs. Augmented reality guidance for needle biopsies: an initial randomized, controlled trial in phantoms. *Medical Image Analysis*, 6(3):313–320, 2002.

[178] Pieter Adriaan Rottier and Victor Rodrigues. Agile development in a medical device company. In *Agile, 2008. AGILE'08. Conference*, pages 218–223. IEEE, 2008.

[179] Colin F Royse, David J Canty, John Faris, Darsim L Haji, Michael Veltman, and Alistair Royse. Core review: physician-performed ultrasound: the time has come for routine use in acute care medicine. *Anesthesia & Analgesia*, 115(5):1007–1028, 2012.

[180] Peter Rust, Derek Flood, and Fergal McCaffery. Creation of an IEC 62304 compliant software development plan. *Journal of Software: Evolution and Process*, 28(11):1005–1010, 2016.

[181] Peter Rust, Derek Flood, and Fergal McCaffery. Software process improvement roadmaps–using design patterns to aid SMEs developing medical device software in the implementation of IEC 62304. In *International Conference on Software Process Improvement and Capability Determination*, pages 43–56. Springer, 2016.

[182] MD Salahadin Abdi, MD Sukdeb Datta, and M Trescot Andrea. Epidural steroids in the management of chronic spinal pain: a systematic review. *Pain Physician*, 10:185–212, 2007.

[183] David Sander, Volker Schick, Hannes Ecker, Falko Lindacher, Moritz Felsch, Oliver Spelten, Robert Schier, Jochen Hinkelbein, and Stephan A Padosch. Novel navigated ultrasound compared with conventional ultrasound for vascular accessa prospective study in a gel phantom model. *Journal of Cardiothoracic and Vascular Anesthesia*, 29(5):1261–1265, 2015.

[184] Frank Sauer, Sebastian Vogt, and Ali Khamene. Augmented reality. In Terry Peters and Kevin Cleary, editors, *Image-Guided Interventions: technology and applications*, pages 81–119. Springer Science & Business Media, 2008.

[185] Volker Schick, David Sander, Marc Boensch, Moritz Hahn, Wolfgang A Wetsch, and Robert Schier. Real-time needle-tracking ultrasound facilitates needle placement in a phantom gel model: A randomised crossover trial. *European Journal of Anaesthesiology (EJA)*, 32(9):659–661, 2015.

[186] Gregory A Schmidt, Julien Maizel, and Michel Slama. Ultrasound-guided central venous access: what's new? *Intensive Care Medicine*, 41(4):705–707, 2015.

[187] HJ Scholten, A Pourtaherian, N Mihajlovic, HHM Korsten, and R A Bouwman. Improving needle tip identification during ultrasound-guided procedures in anaesthetic practice. *Anaesthesia*, 2017.

[188] Peter H Schönemann. A generalized solution of the orthogonal procrustes problem. *Psychometrika*, 31(1):1–10, 1966.

[189] Tormod Selbekk, Asgeir Store Jakola, Ole Solheim, Tonni Franke Johansen, Frank Lindseth, Ingerid Reinertsen, and Geirmund Unsgård. Ultrasound imaging in neurosurgery: approaches to minimize surgically induced image artefacts for improved resection control. *Acta Neurochirurgica*, 155(6):973–980, 2013.

[190] AR Selfridge, GS Kino, and BT Khuri-Yakub. A theory for the radiation pattern of a narrow-strip acoustic transducer. *Applied Physics Letters*, 37(1):35–36, 1980.

[191] P G Shekelle, R M Wachter, P J Pronovost, K Schoelles, K M McDonald, S M Dy, K Shojania, J Reston, Z Berger, B Johnsen, J W Larkin, S Lucas, K Martinez, a Motala, S J Newberry, M Noble, E Pfoh, S R Ranji, S Rennke, E Schmidt, R Shanman, N Sullivan, F Sun, K Tipton, J R Treadwell, a Tsou, M E Vaiana, S J Weaver, R Wilson, and B D Winters. Making health care safer II: an updated critical analysis of the evidence for patient safety practices. *Evidence Report/technology Assessment*, (211):1–945, 2013.

[192] George Stetten, Aaron Cois, Wilson Chang, Damion Shelton, Robert Tamburo, John Castellucci, and Olaf von Ramm. C-mode real-time tomographic reflection for a matrix array ultrasound sonic flashlight. *Academic Radiology*, 12(5):535–543, 2005.

[193] George D Stetten and Vikram S Chib. Overlaying ultrasonographic images on direct vision. *Journal of Ultrasound in Medicine*, 20(3):235–240, 2001.

[194] Philipp J Stolka, Pezhman Foroughi, Matthew Rendina, Clifford R Weiss, Gregory D Hager, and Emad M Boctor. Needle guidance using handheld stereo vision and projection for ultrasound-based interventions. In *International Conference on Medical Image Computing and Computer-Assisted Intervention*, pages 684–691. Springer, 2014.

[195] Robert J Stone. Human factors guidelines for interactive 3D and games-based training systems design. *Human Factors Integration Defence Technology Centre Publication*, 2008.

[196] Molly Follette Story. The FDA perspective on human factors in medical device software development. *IQPC Software Design for Medical Devices Europe*, 2012.

[197] Kathleen J M Surry, Heather JB Austin, Aaron Fenster, and Terry M Peters. Poly(vinyl alcohol) cryogel phantoms for use in ultrasound and MR imaging. *Physics in Medicine and Biology*, 49(24):5529–5546, 2004.

[198] Qinggong Tang, Chia-Pin Liang, Kyle Wu, Anthony Sandler, and Yu Chen. Real-time epidural anesthesia guidance using optical coherence tomography needle probe. In *CLEO: Applications and Technology*, pages AM2O–3. Optical Society of America, 2014.

[199] Déborah Tartière, Philippe Seguin, Charlotte Juhel, Bruno Laviolle, and Yannick Mallédant. Estimation of the diameter and cross-sectional area of the internal jugular veins in adult patients. *Critical care*, 13(6):R197, 2009.

[200] Yuriy Tasinkevych, Ihor Trots, Andrzej Nowicki, and Peter A Lewin. Modified synthetic transmit aperture algorithm for ultrasound imaging. *Ultrasonics*, 52(2):333–342, February 2012.

[201] Daniel Theodoro, Missy Krauss, Marin Kollef, and Bradley Evanoff. Risk factors for acute adverse events during ultrasound-guided central venous cannulation in the emergency department. *Academic Emergency Medicine*, 17(10):1055–1061, 2010.

[202] Karl Thiele, James Jago, Robert Entrekin, and Roy Peterson. Exploring nsight imaging-
a totally new architecture for premium ultrasound. *White paper, Koninklijke Philips NV*,
2013.

[203] Joho Tokumine, Alan T Lefor, A Yonei, A Kagaya, K Iwasaki, and Y Fukuda. Three-
step method for ultrasound-guided central vein catheterization. *British Journal of Anaes-
thesia*, 110(3):368–373, 2013.

[204] Kristine E Torske and Doris H Dyson. Epidural analgesia and anesthesia. *Veterinary
Clinics: Small Animal Practice*, 30(4):859–874, 2000.

[205] Gregg E Trahey and Levin F Nock. Synthetic receive aperture imaging with phase cor-
rection for motion and for tissue inhomogeneities. ii. effects of and correction for motion.
IEEE Transactions on Ultrasonics, Ferroelectrics, and Frequency Control, 39(4):496–
501, 1992.

[206] Christopher A. Troianos, Gregg S. Hartman, Kathryn E. Glas, Nikolaos J. Skubas,
Robert T. Eberhardt, Jennifer D. Walker, and Scott T. Reeves. Guidelines for performing
ultrasound guided vascular cannulation: Recommendations of the american society of
echocardiography and the society of cardiovascular anesthesiologists. *Anesthesia and
Analgesia*, 114(1):46–72, 2012.

[207] Geirmund Unsgaard, OM Rygh, Tormod Selbekk, Tomm B Müller, Frode Kolstad,
Frank Lindseth, and TA Nagelhus Hernes. Intra-operative 3D ultrasound in neuro-
surgery. *Acta Neurochirurgica*, 148(3):235–253, 2006.

[208] Manuel C Vallejo, Amy L Phelps, Suckdip Singh, Steven L Orebaugh, and Neera Sah.
Ultrasound decreases the failed labor epidural rate in resident trainees. *International
Journal of Obstetric Anesthesia*, 19(4):373–378, 2010.

[209] DWF van Krevelen and Ronald Poelman. A survey of augmented reality technologies,
applications and limitations. *International Journal of Virtual Reality*, 9(2):1, 2010.

[210] Francisco Vasconcelos, Donald Peebles, Sebastien Ourselin, and Danail Stoyanov. Similarity registration problems for 2D/3D ultrasound calibration. In *European Conference on Computer Vision*, pages 171–187. Springer, 2016.

[211] Ryan Walsh, Marie Soehl, Adam Rankin, Andras Lasso, and Gabor Fichtinger. Design of a tracked ultrasound calibration phantom made of lego bricks. In *SPIE Medical Imaging*, pages 90362C–90362C. International Society for Optics and Photonics, 2014.

[212] David Wang, Nikhil Amesur, Gaurav Shukla, Angela Bayless, David Weiser, Adam Scharl, Derek Mockel, Christopher Banks, Bernadette Mandella, Roberta Klatzky, et al. Peripherally inserted central catheter placement with the sonic flashlight. *Journal of Ultrasound in Medicine*, 28(5):651–656, 2009.

[213] Zhouping Wei, Gang Wan, Lori Gardi, Gregory Mills, Donal Downey, and Aaron Fenster. Robot-assisted 3D-TRUS guided prostate brachytherapy: system integration and validation. *Medical Physics*, 31(3):539–548, 2004.

[214] Wolfgang Wein, Shelby Brunke, Ali Khamene, Matthew R Callstrom, and Nassir Navab. Automatic CT-ultrasound registration for diagnostic imaging and image-guided intervention. *Medical Image Analysis*, 12(5):577–585, 2008.

[215] Menachem M Weiner, Paul Geldard, and Alexander JC Mittnacht. Ultrasound-guided vascular access: a comprehensive review. *Journal of Cardiothoracic and Vascular Anesthesia*, 27(2):345–360, 2013.

[216] Andrew D Wiles, Alexander Likholyot, Donald D Frantz, and Terry M Peters. A statistical model for point-based target registration error with anisotropic fiducial localizer error. *Medical Imaging, IEEE Transactions on*, 27(3):378–390, 2008.

[217] Harald Willschke, Peter Marhofer, Adrian Bösenberg, S Johnston, Oliver Wanzel, Christian Sitzwohl, Stephan C Kettner, and Stephan Kapral. Epidural catheter placement in

children: comparing a novel approach using ultrasound guidance and a standard loss-of-resistance technique. *BJA: British Journal of Anaesthesia*, 97(2):200–207, 2006.

[218] Jennifer G Wilson and Kristine EW Breyer. Critical care ultrasound: a review for practicing nephrologists. *Advances in Chronic Kidney Disease*, 23(3):141–145, 2016.

[219] Susanne Winter, Bernhard Brendel, Ioannis Pechlivanis, Kirsten Schmieder, and Christian Igel. Registration of CT and intraoperative 3-D ultrasound images of the spine using evolutionary and gradient-based methods. *IEEE Transactions on Evolutionary Computation*, 12(3):284–296, 2008.

[220] Simon W Wong, Ahtsham U Niazi, Ki J Chin, and Vincent W Chan. Real-time ultrasound-guided spinal anesthesia using the SonixGPS$^{\circledR}$ needle tracking system: a case report. *Canadian Journal of Anesthesia/Journal canadien d'anesthésie*, 60(1):50–53, 2013.

[221] Hsin-Kai Wu, Silvia Wen-Yu Lee, Hsin-Yi Chang, and Jyh-Chong Liang. Current status, opportunities and challenges of augmented reality in education. *Computers & Education*, 62:41–49, 2013.

[222] Wenfeng Xia, Simeon J West, Malcolm C Finlay, Jean-Martial Mari, Sebastien Ourselin, Anna L David, and Adrien E Desjardins. Looking beyond the imaging plane: 3D needle tracking with a linear array ultrasound probe. *Scientific Reports*, 7(1):3674, 2017.

[223] Ziv Yaniv and Cristian A Linte. Applications of augmented reality in the operating room. In Woodrow Barfield, editor, *Fundamentals of Wearable Computers and Augmented Reality*, pages 485–518. CRC Press, 2016.

[224] Caitlin T Yeo, Tamas Ungi, U Paweena, Andras Lasso, Robert C McGraw, and Gabor Fichtinger. The effect of augmented reality training on percutaneous needle placement in spinal facet joint injections. *IEEE Transactions on Biomedical Engineering*, 58(7):2031–2037, 2011.

Appendix A. Copyright Transfers and

Reprint Permissions

For the chapters that were adapted from previously published articles, permission to reprint was obtained.

This Agreement between Robarts Research Institute -- Golafsoun Ameri ("You") and Springer Nature ("Springer Nature") consists of your license details and the terms and conditions provided by Springer Nature and Copyright Clearance Center.

License Number	4258730070621
License date	Dec 30, 2017
Licensed Content Publisher	Springer Nature
Licensed Content Publication	Springer eBook
Licensed Content Title	Augmented Reality Ultrasound Guidance for Central Line Procedures: Preliminary Results
Licensed Content Author	Golafsoun Ameri, John S. H. Baxter, A. Jonathan McLeod et al
Licensed Content Date	Jan 1, 2015
Type of Use	Thesis/Dissertation
Requestor type	academic/university or research institute
Format	print and electronic
Portion	full article/chapter
Will you be translating?	no
Circulation/distribution	<501
Author of this Springer Nature content	yes
Title	Ms
Instructor name	Golafsoun Ameri
Institution name	Robarts Research Institute
Expected presentation date	Dec 2017
Portions	A variation of the full article will be used in a dissertation.
Requestor Location	Robarts Research Institute 1151 Richmond Street North London, ON N6A 5B7 Canada Attn: Robarts Research Institute
Billing Type	Invoice
Billing Address	Robarts Research Institute 1151 Richmond Street North London, ON N6A 5B7 Canada Attn: Robarts Research Institute
Total	0.00 CAD

Terms and Conditions

SPIE.
CONNECTING MINDS.
ADVANCING LIGHT.

January 2, 2018

Dear Mr. Ameri,

     Thank you for seeking permission from SPIE to reprint material from our publications. As author, SPIE shares the copyright with you, so you retain the right to reproduce your paper in part or in whole.
     Publisher's permission is hereby granted under the following conditions:
(1) the material to be used has appeared in our publication without credit or acknowledgment to another source; and
(2) you credit the original SPIE publication. Include the authors' names, title of paper, volume title, SPIE volume number, and year of publication in your credit statement.

Regards,

Nicole Harris
Administrative Editor, SPIE Publications
1000 20th St.
Bellingham, WA 98225
+1 360 685 5586 (office)
nicoleh@spie.org

SPIE is the international society for optics and photonics. http://SPIE.org

    SPIE   Publisher's permission is hereby granted under the following conditions: (1) you obtain permission of the author(s); (2) the material to be used has appeared in our publication without credit or acknowledgment to another source; and (3) you credit the original SPIE publication. Include the authors' names, title of paper, volume title, SPIE volume number, and year of publication in your credit statement.

Director of Publications
SPIE
PO Box 10, Bellingham, WA 98227-0010 USA
360/676-3290 (Pacific Time) eric@spie.org

SPIE.ORG
help@spie.org

Mail: PO Box 10
Bellingham, WA
98227-0010 USA

Eric Pepper, Director of Publications   Date 1/2/18

Ship: 1000 20th St.
Bellingham, WA
98225-6705 USA

Tel: +1 360 676 3290
Fax: +1 360 647 1445

SPIE IS THE INTERNATIONAL SOCIETY
FOR OPTICS AND PHOTONICS.

This Agreement between Robarts Research Institute -- Golafsoun Ameri ("You") and Springer Nature ("Springer Nature") consists of your license details and the terms and conditions provided by Springer Nature and Copyright Clearance Center.

License Number	4256730316605
License date	Dec 26, 2017
Licensed Content Publisher	Springer Nature
Licensed Content Publication	International Journal of Computer Assisted Radiology and Surgery
Licensed Content Title	Mixed reality ultrasound guidance system: a case study in system development and a cautionary tale
Licensed Content Author	Golafsoun Ameri, John S. H. Baxter, Daniel Bainbridge et al
Licensed Content Date	Jan 1, 2017
Type of Use	Thesis/Dissertation
Requestor type	academic/university or research institute
Format	print and electronic
Portion	full article/chapter
Will you be translating?	no
Circulation/distribution	<501
Author of this Springer Nature content	yes
Title	Ms
Instructor name	Golafsoun Ameri
Institution name	Robarts Research Institute
Expected presentation date	Dec 2017
Portions	Full article including all figures and tables.
Requestor Location	Robarts Research Institute 1151 Richmond Street North London, ON N6A 5B7 Canada Attn: Robarts Research Institute
Billing Type	Invoice
Billing Address	Robarts Research Institute 1151 Richmond Street North London, ON N6A 5B7 Canada Attn: Robarts Research Institute
Total	0.00 CAD

Terms and Conditions

Appendix B. Research Ethics Approval

Ethics approval was obtained from the Health Sciences Research Ethics Board at Western University, London, Canada, for the studies presented in Chapter 4.

Western Research

Western University Health Science Research Ethics Board
HSREB Delegated Initial Approval Notice

Principal Investigator: Dr. Elvis Chen
Department & Institution: Schulich School of Medicine and Dentistry, Robarts Research Institute

Review Type: Delegated
HSREB File Number: 107254
Study Title: Validation of an augmented reality guidance system for needle placement in a phantom of the internal jugular vein
Sponsor: Canadian Institutes of Health Research

HSREB Initial Approval Date: January 13, 2016
HSREB Expiry Date: January 13, 2017

Documents Approved and/or Received for Information:

Document Name	Comments	Version Date
Letter of Information & Consent	Letter of Information & Consent, revised/clean version	2015/12/01
Western University Protocol	Western Protocol, revised and clean version	2015/12/01

The Western University Health Science Research Ethics Board (HSREB) has reviewed and approved the above named study, as of the HSREB Initial Approval Date noted above.

HSREB approval for this study remains valid until the HSREB Expiry Date noted above, conditional to timely submission and acceptance of HSREB Continuing Ethics Review.

The Western University HSREB operates in compliance with the Tri-Council Policy Statement Ethical Conduct for Research Involving Humans (TCPS2), the International Conference on Harmonization of Technical Requirements for Registration of Pharmaceuticals for Human Use Guideline for Good Clinical Practice Practices (ICH E6 R1), the Ontario Personal Health Information Protection Act (PHIPA, 2004), Part 4 of the Natural Health Product Regulations, Health Canada Medical Device Regulations and Part C, Division 5, of the Food and Drug Regulations of Health Canada.

Members of the HSREB who are named as Investigators in research studies do not participate in discussions related to, nor vote on such studies when they are presented to the REB.

The HSREB is registered with the U.S. Department of Health & Human Services under the IRB registration number IRB 00000940.

Ethics Officer, on behalf of Dr. Marcelo Kremenchutzky, HSREB Vice Chair

Ethics Officer to Contact for Further Information: Erika Basile ___ Nicole Kaniki ___ Grace Kelly ___ Mina Mekhail ___ Vikki Tran ___

This is an official document. Please retain the original in your files

Curriculum Vitae

Name: Golafsoun Ameri

Post-Secondary   Master of Science, Biomedical Physics
Education and   Ryerson University, Toronto, Ontario
Degrees: 2009 - 2011

                     Bachelor of Engineering (Hon), Electrical Engineering
                     Ryerson University, Toronto, Ontario
                     2005 - 2009

Related Work   Teaching Assistant
Experience: The University of Western Ontario
                     2012-2016

                     Research Intern
                     Philips Research North America, Briarcliff Manor, NY
                     Sept-Dec 2013

Journal Manuscripts: (* - primary author)

Ameri, G.*, Rankin, A., Ganapathy, S., Peters, T.M. & Chen, E.C.S., Integration of A-mode and B-mode Ultrasound in an Augmented Reality Guidance System for Epidural Anesthesia: Preliminary Results. *IEEE Transactions on Biomedical Engineering* (In preparation).

Ameri, G.*, Bainbridge, D., Peters, T.M., Chen, E.C.S., Quantitative analysis of needle navigation under ultrasound guidance in a simulated central line procedure. *Ultrasound in Medicine*

& Biology (Under review).

Ameri, G.*, Baxter, J.S.H.,* Bainbridge, D., Peters, T.M. & Chen, E.C.S., Mixed Reality Ultrasound Guidance System: a Case Study in System Development and a Cautionary Tale. *International Journal of Computer Assisted Radiology and Surgery*, 1-11, 2017.

Ameri, G.*, Baxter, J.S.H., McLeod, A.J., Peters, T.M. & Chen, E.C.S., Effects of Line Fiducial Parameters and Beamforming on Ultrasound Calibration. *Journal of Medical Imaging*, 4(1):015002, 2017.

McLeod, A.J.*, Baxter, J.S.H., **Ameri, G.**, Ganapathy, S., Peters, T.M., & Chen, E.C.S. Detection and Visualization of Dural Pulsation for Spine Needle Interventions. *International Journal of Computer Assisted Radiology*, 10(6):947-956, 2015.

Conference Proceedings: (* - primary author)

Ameri, G.*, Baxter, J.S.H.*, Bainbridge, D., Peters, T.M., & Chen E.C.S. A Case Study on the Development of an Augmented Reality Ultrasound Guidance System. *International Conference of Computer Assisted Radiology and Surgery*, Spain, 2017. (Podium presentation)

Ameri, G.*, Son, J., Liang, J., Foster, F.S. & Peters, T.M. Development of a high frequency single-element ultrasound needle transducer for anesthesia delivery. *Society of Photographic Instrumentation Engineers Proceedings in Medical Imaging*, FL, USA, 2017. (Podium presentation)

Ameri, G.*, Baxter, J.S.H., McLeod, A.J., Peters, T.M. & Chen, E.C.S. Augmented Reality Ultrasound Guidance for Central Line Procedures: Preliminary Results. *MICCAI Workshop*

in Augmented Environments for Computer-Assisted Interventions, Germany, 2015. (Podium presentation)

Ameri, G.*, McLeod, A.J., Baxter, J.S.H., Chen, E.C.S., & Peters, T.M., Line fiducial material and thickness considerations for ultrasound calibration. *Society of Photographic Instrumentation Engineers Proceedings in Medical Imaging*, CA, USA, 2015. (Poster presentation)

Ameri, G.*, Baxter, J.S.H., McLeod, A.J., Jayaranthe, U.L., Chen, E.C.S., & Peters, T.M. Synthetic aperture imaging in ultrasound calibration. *Society of Photographic Instrumentation Engineers Proceedings in Medical Imaging*, CA, USA, 2014. (Podium presentation)

Chen, E.C.S.*, **Ameri, G.**, Li, H., Sondekoppam, R.V., Ganapathy, S. & Peters, T.M. Navigated simulator for spinal needle interventions. *Medicine Meets Virtual Reality*, CA, USA, 2014.

Research Abstracts: (* - primary author)

Ameri, G.*, Bainbridge, D., Peters, T.M., Chen, E.C.S., An analysis of needle navigation under real-time ultrasound guidance for central line insertion: a phantom study. *Canadian Anesthesiologists' Society Annual Meeting*, Niagara Falls, ON, 2017. (Podium presentation)

Ameri, G.*, Son, J., Liang, J., Foster, F.S., Peters, T.M. Development of a single-element ultrasound needle transducer for anesthesia delivery. *Imaging Network Ontario*, London, ON, 2017. (Poster presentation)

Ameri, G.*, Bainbridge, D., Peters, T.M., Chen, E.C.S. Augmented reality for improved ultrasound guidance in central venous access. *Imaging Network Ontario*, Toronto, ON, 2016. (Podium presentation)

Ameri, G.*, Bainbridge, D., Peters, T.M., Chen, E.C.S. Augmented reality ultrasound guidance for internal jugular vein cannulation: preliminary results. *London Health Research Day*, London, ON, 2016. (Podium presentation)

Ameri, G.*, Baxter, J.S.H., McLeod, A.J., Peters, T.M., Chen, E.C.S. The effect of phantom material on accuracy in ultrasound calibration. *London Health Research Day*, London, ON, 2015. (Podium presentation)

McLeod, A.J., Baxter, J.S.H., **Ameri, G.***, Ganapathy, S., Peters, T.M. and Chen, E.C.S. Automatically identifying dural pulsation in ultrasound video of the lumbar spine. *London Health Research Day*, London, ON, 2015. (Poster presentation)

Ameri, G.*, Chen, E.C.S., Peters, T.M. Ultrasound-guided spinal injections. *London Health Research Day*, London, ON, 2013. (Poster presentation)

Ameri, G.*, Yang, V.X.D., Kumaradas, J.C. Synthetic aperture imaging in acoustic microscopy. *CIHR Symposium on Novel Cancer Therapies and Innovations in Treatment Monitoring*, Toronto, ON, 2011. (Poster presentation)

Ameri, G.*, Yang, V.X.D., Kumaradas, J.C. Synthetic aperture imaging in acoustic microscopy- a preliminary study. *Fields-Mitacs Conf. on Mathematics of Medical Imaging*, Toronto, ON, 2011. (Poster presentation)

Ameri, G.*, Nayebi, N., Yang, V.X.D., and Kumaradas, J.C. Synthetic aperture ultrasound imaging. *Canadian Association of Physicists Conf.*, Toronto, ON, 2010. (Poster presentation)

Ameri, G.*, Naghshineh, S., Zereshki, M., Abdoli-Eramaki, M., and Krishnan, S. 3D virtual real time upper body link segment modeling. *Ontario Biomechanics Conf.*, Barrie, ON, 2009. (Poster presentation)

Invited Lectures:

"Goals, guidelines, and best practices: a framework for designing augmented reality ultrasound guidance systems; or if you build it, will they come?" Presented at Computer Assisted Radiology and Surgery Congress, Berlin, June 2018. Invited by Dr. Heinz U. Lemke.

"Human-computer interface design challenges for surgical applications," Presented in a graduate course entitled: Software Engineering for Human-Computer Interface Design, Electrical Engineering Department, Western University, ON, July 2017. Invited by Dr. Roy Eagleson.

Honours and Awards:	Best Paper in Education and Simulation- Nominee Canadian Anesthesiologists Society Annual Meeting, Niagara Falls, ON, 2017
	Best Paper Award, 3rd Place (International) Workshop on Augmented Environments for Computer Assisted Interventions, Munich, 2015
	Western Graduate Research Scholarship (Institutional) Western University, London, ON, 2012-present
	Honorable Mention (International) SPIE, Medical Imaging, San Diego, CA, 2015

NSERC-CREATE (Institutional)

Computer-Assisted Medical Intervention Program

Western University, London, ON, 2013-2015

Nominee of the Learning and Teaching Office TA/GA Awards (Institutional)

Ryerson University, Toronto, ON, 2011

Best Graduate Teaching Assistant Award (Departmental)

Department of Physics, Ryerson University, Toronto, ON, 2010

Ryerson Graduate Award (Institutional)

Ryerson University, Toronto, ON, 2009-2011

Natural Sciences and Engineering Research Council of Canada - Undergraduate Research Award (National), 2009

Natural Sciences and Engineering Research Council of Canada - Undergraduate Research Award (National), 2008

Ryerson In-Program Scholarships Institutional)

Ryerson University, Toronto, ON, 2006-2009

Jack Roy Longstaffe Memorial Scholarship for Academic Excellence (Institutional)

Ryerson University, Toronto, ON, 2007

Deans Honor List (Institutional)

Ryerson University, Toronto, ON, 2006-2009

Leadership/	Volunteer Activities
Volunteer	Chair
Activities:	The IEEE Engineering in Medicine and Biology Society Student Chapter
	Western University, London, ON
	2016-2018

Speaker at over 6 sessions

Discovery Day in Health Sciences; The Canadian Medical Hall of Fame

Robarts Research Institute, London, ON

2016-2017

Co- Chair

The IEEE Engineering in Medicine and Biology Society Student Chapter

Western University, London, ON

2012-2015